Spring 2014

COMPARISON OF A SIERPINSKI GASKET MONOPOLE ANTENNA TO BOW-TIE ANTENNAS BASED OFF THE FRACTAL ITERATIVE SHAPES

Kyle Nathan Murg
Purdue University

Graduate School ETD Form 9
(Revised 01/14)

PURDUE UNIVERSITY
GRADUATE SCHOOL
Thesis/Dissertation Acceptance

This is to certify that the thesis/dissertation prepared

By Kyle Nathan Murg

Entitled
COMPARISON OF A SIERPINSKI FRACTAL ANTENNA TO BOW-TIE ANTENNAS BASED OFF THE FRACTAL ITERATIVE SHAPE

For the degree of Master of Science

Is approved by the final examining committee:

John Denton

Helen McNally

Kevin Webb

To the best of my knowledge and as understood by the student in the *Thesis/Dissertation Agreement. Publication Delay, and Certification/Disclaimer (Graduate School Form 32)*, this thesis/dissertation adheres to the provisions of Purdue University's "Policy on Integrity in Research" and the use of copyrighted material.

John Denton

Approved by Major Professor(s): _____

_____

Approved by: James Mohler 4/17/2014

Head of the Department Graduate Program Date

COMPARISON OF A SIERPINSKI GASKET MONOPOLE ANTENNA TO BOW-TIE ANTENNAS BASED OFF THE FRACTAL ITERATIVE SHAPES

A Thesis

Submitted to the Faculty

of

Purdue University

by

Kyle Murg

In Partial Fulfillment of the

Requirements for the Degree

of

Master of Science

May 2014

Purdue University

West Lafayette, Indiana

TABLE OF CONTENTS

Page

Page

LIST OF TABLES

Table Page

LIST OF FIGURES

Figure Page

Figure Page

Figure Page

ABSTRACT

Murg, Kyle N. M.S., Purdue University, May 2014. Comparison of a Sierpinski Gasket Monopole Antenna to Bow-tie Antennas based off the Fractal Iterative Shape.
Major Professor: John Denton.

Antennas are an integral part of mobile devices. Recently, the demand for smaller phones has increased requiring smaller components within the device. This leads to problems with performance and limitations of RF systems within mobile devices including antennas which have been affected by the size thus affected frequency output. In this thesis, fractal theory will be utilized to compare the performance of the Sierpinski Gasket Monopole antenna to single band antennas to see if this is a viable substitute in mobile applications. By utilizing simulations and physical antennas, the performance will be observed at each frequency band and compared.

CHAPTER 1. INTRODUCTION

1.1 Introduction

Antennas are an integral part of our everyday lives. People are provided with communication media such as voice communication and internet by the antennas that are in each cell phone and laptop. Antennas are part of satellite assemblies that provide data transfer for the telecommunication industry and global positioning systems. As wireless communication continues to increase, so does the dependence of antennas in our lives.

An antenna is a frequency-dependent device that is used to transfer electromagnetic waves (signals) to radiating waves in an unbounded medium, usually free space or air, in either the transmitting or receiving mode of operation (Kishk, 2009). Antennas are designed to operate over a single narrow designated frequency band. To achieve a wider frequency range, antennas have evolved from single frequency resonators to arrays of antennas that can output at many frequency bands.

1.2 Background

Since the early 1990's mobile device usage has increased to the point where 86.7% of the world's population has a cell phone or has access to one (Table 1.1). Communications is a customer driven industry. Customers demand communications that deliver good voice quality, higher data transfer rates, and longer battery life (Matsumori,

2011). The demand of wireless handset use has created a problem with the availability of frequency bands which limits the amount of data that is transferred in populous areas. The creation of new hardware designs can help increase the reliability and expectations the customers expect out of their phones (Ali, Hayes, Sadler, & Hwang, 2003).

Table 1.1 *Worldwide Cell Access by Population Percentage ("Key Global Telecom Indicators for the World Telecommunication Service Sector," 2012)*

	Global	Developed Nations	Developing Nations	Africa	Arab States	Asia & Pacific	CIS	Europe	The Americas
Mobile cellular subscriptions (millions)	5981	1461	4520	433	349	2897	399	741	969
Per 100 people (%)	86.7	117.8	78.8	53	96.7	73.9	143	119.5	103.3
Fixed telephone (millions)	1159	494	665	12	35	511	74	242	268
Per 100 people (%)	16.6	39.8	11.6	1.4	9.7	13	26.3	39.1	28.5
Active mobile broadband subscriptions (millions)	1186	701	484	31	48	421	42	336	286
Per 100 people (%)	17	56.5	8.5	3.8	13.3	10.7	14.9	54.1	30.5
Fixed mobile broadband subscriptions (millions)	591	319	272	1	8	243	27	160	145
Per 100 people (%)	8.5	25.7	4.8	0.2	2.2	6.2	9.6	25.8	15.5

Just 20 years ago, wireless communication was new, technically difficult and not widely used by the public. The first experiment that led to the discovery of wire antennas occurred in 1842 by Joseph Henry, the inventor of wire telegraphy. Henry found that by

adding a current to a wire it would affect a circuit 30 feet away by magnetizing needles. He later revised his design by adding a wire to the roof of his house to detect lightning flashes up to 8 miles away (Ramsay, 1981). In 1886, Heinrich Hertz conducted research on the relation between electromagnetic forces and dielectric polarization by creating the first balanced half-wave dipole antenna and square loop antenna transmitter/receiver system. By using this combination, Hertz was able to usher in a new era of radio communication while expanding his experiments to demonstrate the reflection, refraction, and polarization of electromagnetic waves. By 1901, trans-Atlantic communication occurred with Guglielmo Marconi's 15kW system that transmitted an 820kHz signal from Cornwall, England to St. John's, Newfoundland. Marconi's system of a fan monopole antenna on each side of the Atlantic Ocean introduced directive communications (Ramsay, 1981). The global communication era began and the desire to communicate wirelessly increased.

Innovations that occurred after Marconi's Trans-Atlantic transmission were exponential. Antenna testing through both World Wars I and II led to a trend of utilizing VHF (Very High Frequencies) for radar. This radar technology ushered in new antenna theories such as reflectors, waveguides, and horn radiators that helped increase frequency ranges and accuracy in transmission. By the late 1950's wideband antennas, like the helical antenna, were being tested at frequencies as high as 4GHz (Kraus, 1985). The 1980's brought planar antenna theory along with numerical-electromagnetic microwave circuit design (Visser, 2012). In recent years (since 1979), the invention of mobile devices that transferred data wirelessly increased the demand for multiband antennas that met the expectations of the consumer. The task for present and future engineers is to

design more efficient antennas that can output multiple frequency bands (Ciais, Staraj, Kossiavas, & Luxey, 2004a).

To understand the complexity of today's mobile device, one only has to only look at the wireless system in the device. Today, an average 4G mobile phone contains 4 – 6 antennas supporting 8-12 frequency bands or more (Matsumori, 2011). This includes two or more antennas used for transferring data throughout the cellular network. 3G or LTE/4G coverage is used by most carriers depending on the phone technology and region. The newest models are expected to have coverage for LTE networks with a 3G failback feature when 4G cellular services are not available. The antennas for this feature need to operate in the 700MHz to 2.7GHz frequency bands (Technologies, 2010). One or more antennas need to be added for Wi-Fi data transfer. Having the phone utilize a local network, like 802.11 Wi-Fi, alleviates the cellular networks due to less data being transferred on the network. Another antenna needs to be added for the Global Positioning System feature mobile phones have today.

These antennas have a fixed physical size plus the isolation required for transmission/reception, thus could create a large phone that is not ideal for the customer. Consolidating the antennas into one or two multi-band antennas, phone size can be reduced or used for other needs such as more memory or larger batteries. Efficient antennas also allow for less network capacity meaning the mobile phone carriers do not need to invest in more split cells (Matsumori, 2011). The question is how antennas can be consolidated to solve these problems. The recent trends show that wideband and multiband antennas can be utilized to consolidate the antennas in a mobile phone. There

are many types of wideband and multiband antennas that have been designed for the telecommunication industry.

Wideband antennas are antennas that have wide frequency bandwidths with good performance among the whole spectrum. Antennas that have a bandwidth of less than 500MHz are known as wideband antennas but antennas with a bandwidth larger than 500MHz are known as Ultra-wideband antennas (UWB) ("Ultra-wideband antenna," 2005). Unlike single band antennas, UWB antennas for mobile applications can transmit/ receive frequencies from bandwidths as large as 7GHz. Wideband and UWB antennas are attractive in the mobile phone industry due to the coverage of the required frequencies for present cell phones while having a simple design that radiates in an omnidirectional radiation pattern (Chung, Kim, & Choi, 2005). UWB antennas are also used outside of the mobile environment with stunning performance. In laboratory testing, Utra-wideband horn antennas have been able to transmit/receive signals in a frequency bandwidth of 17GHz from 1GHz – 18GHz (Davies & Holliday, 2005).

The problem with wideband antennas is the wireless interference that can occur by having too many devices using UWB antennas at the same time. For this reason, the FCC limited the power output of UWB antennas. This limitation means that a device with a UWB antenna would only be able to transmit/receive over small distances (up to 10m). Many mobile applications today can utilize UWB antennas to wirelessly transfer personal files or data to other devices close to user ("Ultra-wideband antenna," 2005).

Unlike wideband antennas, multiband antennas do not operate along a large frequency bandwidth. Multiband antennas are designed to transmit/receive at multiple small bandwidth frequency ranges. These antennas are ideal for mobile devices by

focusing on the required bandwidths that are required to communicate with multiple networks. Quad-band antennas, antennas that operate on four different frequency bands, are already being used in phones while dual-band antennas are being used for local networks, like WLAN systems (Ciais, Staraj, Kossiavas, & Luxey, 2004b). Multiband antennas have not been designed yet to operate on all of the required network frequency bandwidths at once. Due to this limitation, mobile phones that do use multiband antennas usually will have more than one in the device to operate on all the required frequencies.

A promising antenna type for multi-band and antenna design is the fractal antenna. Pantoja et al. stated, "Fractal antennas use pre-fractal geometries, an extension of Euclidian geometry, that are built with a finite number of iterations due to their intricate and convoluted configurations" (Pantoja et al., 2003, p. 238). Fractal patterns are repeating shapes that are scaled down with each iteration. This can be seen in nature such as snowflakes (Figure 1.1) and nautical shells (Figure 1.2). In a practical environment, the iterations in fractal antennas are limited reflecting the amount of frequency bands or bandwidth the antenna will operate on. In mobile phone applications, the fractal antenna essentially has the shape folded over itself making it a rather long antenna that fills a small space. This feature allows it to operate well in multiband and wideband applications. The Sierpinski Gasket Monopole antenna (Figure 1.3), also called the Sierpinski fractal antenna, is a common antenna for fractal research (Werner & Gangul, 2003). This design is explained in more detail in the next chapter.

Figure 1.1 Snowflake with a fractal pattern (Bentley, 1922)

This work will look in depth into how fractal theory can be implemented into antenna designs for mobile devices. The tests conducted in this work will show how the Sierpinski Fractal antenna compares to single band bow-tie antennas designed to perform at the same frequencies.

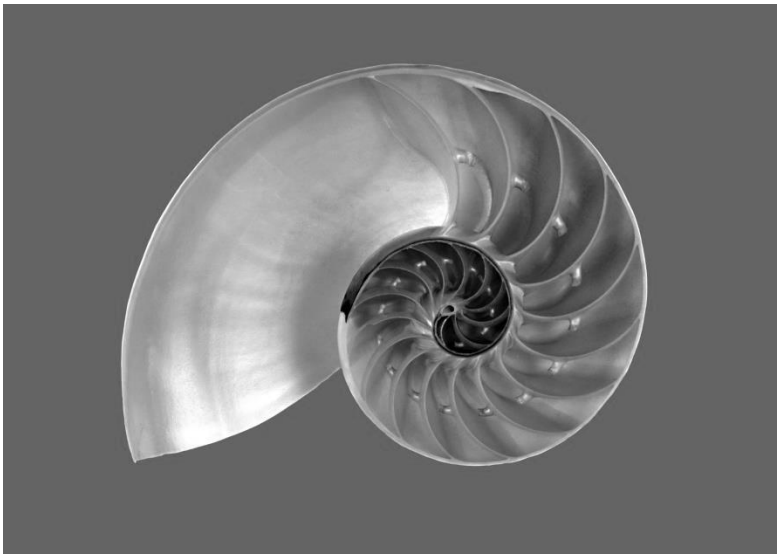

Figure 1.2 Nautilus Shell displaying a fractal pattern (Matz, 2003)

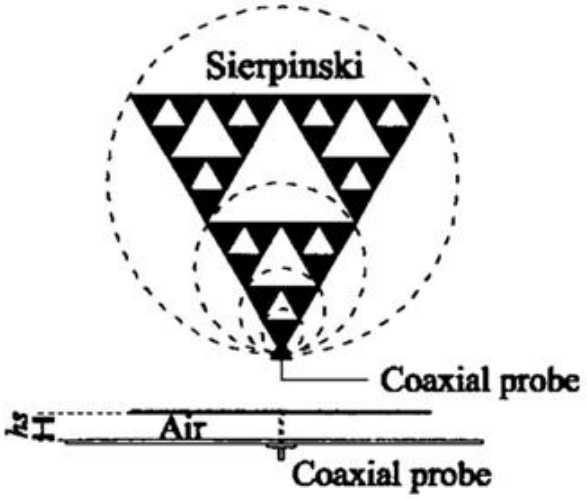

Figure 1.3 Generic Sierpinski Gasket Monopole Antenna (Borja & Romeu, 2000)

CHAPTER 2. LITERATURE REVIEW

2.1 Introduction

Many topics and theories need to be understood in order to correctly design the antennas that will be used in this work. This chapter will discuss the theories that focus on electromagnetics and RF theory.

2.2 Introduction into Electromagnetic Spectrum

Frequency is the most important and basic concept in RF systems. Frequency measures how fast a wave is oscillating. Waves can be in the form of everything from water, light, or sound. Antennas function by radiating electromagnetic waves to send signals through space. An electromagnetic wave is a basic wave that consists of an electric wave with an associated magnetic field. These basic waves are sinusoidal and vary in space and time. To measure how many oscillations occur over a certain time period, the speed of light (3.0×10^8 m/s) is divided by the wavelength of the signal (λ) (Eqn. 2.1). This can also be calculated by taking the inverse of the signal's period. The period is the amount of time it takes to complete one full oscillation or cycle. The common unit for frequency is the Hertz. Hertz describes the amount of oscillations that occur in one second.

$$f = \frac{c}{\lambda} \quad \text{(Eqn. 2.1)}$$

Where;

f = Frequency (Hz)
c = Speed of light (3 x10^8m/s)
λ = Wavelength (m)

Each electromagnetic wave is part of the electromagnetic spectrum. The electromagnetic spectrum is the range of all possible electromagnetic waves by the oscillation frequency or Hertz (Hz). The spectrum consists of 7 regions (Figure 2.1). The regions are radio waves, microwaves, infrared waves, visible waves, ultraviolet waves, X-ray waves, and Gamma Ray waves. Gamma Rays are ionizing radiation causing harm to biological samples, having frequencies that are 30EHz (10^{18} Hz) and above (Molinaro, 2006). X-Rays frequencies are the region below Gamma Rays, having frequencies between 30PHz (10^{15} Hz) and 30EHz (10nm to 10pm wavelength) (Molinaro, 2006). Ultraviolet light is made up of frequencies that are not visible to humans but can be seen by some animals. UV has frequencies between 790THz and 30PHz (380nm to 10nm wavelength) (Molinaro, 2006). Ultraviolet Light is emitted from the sun and can cause sunburn to humans.

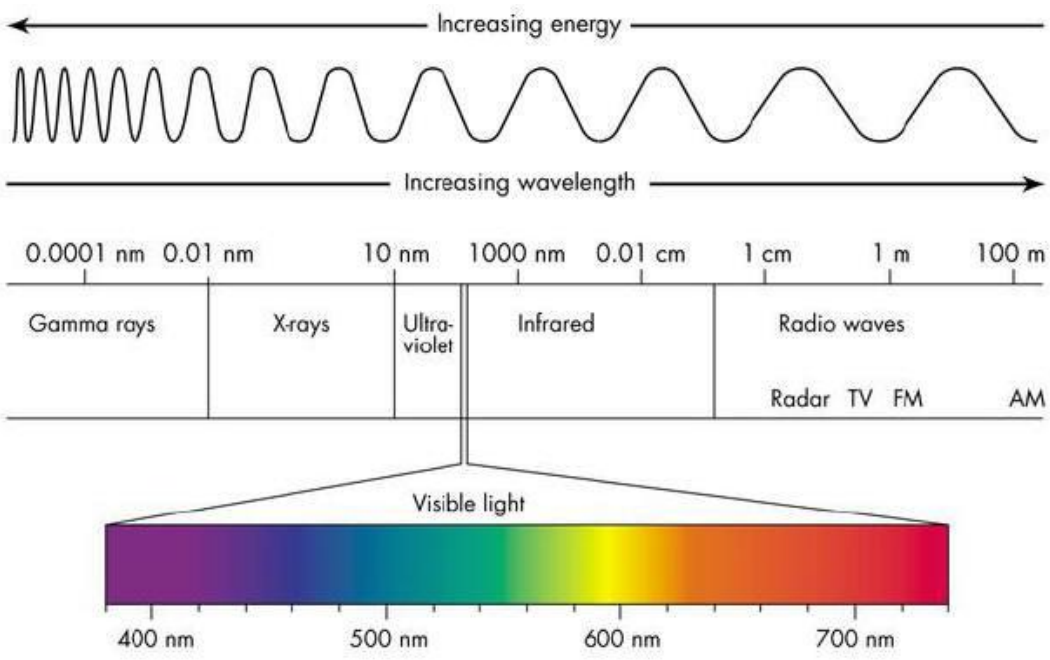

Figure 2.1 Electromagnetic Spectrum (Fordham, 2012)

Visible light is all the wavelengths in the spectrum that can be seen by the human eye. The frequencies within the visible spectrum are between 400 THz to 790 THz (750nm to 380nm wavelength)(Molinaro, 2006). The visible spectrum is the most important spectrum to people because it allows for observations of the world through optics. After visible spectrum comes infrared radiation. Infrared radiation is contains frequencies between 300GHz and 400THz (1mm to 750nm wavelength)(Molinaro, 2006). Infrared commonly used in thermal infrared imaging.

Microwaves and radio waves are next on the spectrum. These two spectrums make up the frequencies that used in wireless communication in today's devices. Microwaves consist of frequencies between 3GHz and 300GHz (10cm to 1mm wavelength)(Molinaro, 2006). The microwave frequencies can be used for point-to-point communications in the TV, telephone, and spacecraft communication. Radio

frequencies are also in the same region but also occur at lower frequencies. Radio frequencies are between 100kHz and 3GHz (3km to 1dm wavelength)(Molinaro, 2006). Like microwaves, radio waves are used to transmit data for television, mobile phones, wireless networking, and radio stations. Radio and microwave frequencies will be discussed in more detail since this paper is focused on mobile devices and their operational frequencies.

The frequencies commonly used by mobile devices today are between 30kHz and 30Ghz. AM radio device utilize the low end of the spectrum (between 30kHz and 300kHz). This spectrum is called the Low Frequency Band (LF). The High Frequency Band is used for shortwave radio that can utilize the Earth's ionosphere to transmit signals extremely long distances. The Very High Frequency (VHF) band is a popular for transmitting signals. FM radios utilize the VHF band between 30MHz and 300MHz to transmit data. The last important frequency ranges with mobile devices are the Ultra High Frequency band (UHF) and Super High Frequency band (SHF). The UHF band consists of frequencies between 300MHz and 3GHz. The SHF band consists of frequencies between 3GHz and 30GHz. At these frequencies most mobile phones and GPS devices transmit data.

Each industry has allocated frequency bands that the devices use. This allows for less interference between devices. Television companies broadcast at 54MHz to 216MHz. FM radios in the United States broadcast between 87.5MHz to 108MHz. These ranges in frequencies are known as the bandwidth of the signal. US FM radios have a bandwidth of 20.5MHz (108MHz – 87.5MHz = 20.5MHz). Bandwidth use is very important in the mobile industry due to the use of many frequency bands.

Cellular carriers in the United States utilize multiple frequency bandwidths to transfer data at different speeds (Table 2.1).

Table 2.1 *Frequency Bands Utilized in Mobile Devices*

Application	Band (MHz)	Frequency Range (MHz)
3G Network	850	824.2 - 849
	1900	1850.2 - 1910
4G network	700	689 - 806
	1700	1710 - 1755
	2100	2110 - 2155
GPS	1550	1525 - 1559
Wi-Fi/ Bluetooth (ISM Band)	2400	2400 - 2480
	5800	5725 - 5875

Industrial, scientific, and medical bands (ISM) were originally designed to be used for applications other than communications like microwave ovens. These frequencies were isolated due to the power emission that radiated from the device that could interfere with other signals. Lately, ISM bands have been used for short range wireless communication applications to get around the problem of signal interference. The most widely used ISM bands are the 433MHz, 915MHz, 2.4GHz, and 5.8GHz bands.

2.3 Antenna Parameters

In order to utilize the frequencies, the correct antenna has to be used based on the application. All antennas have common parameters that characterize its performance. These parameters allow for a better understanding on how types of antennas differ from each other. It also allows for easier antenna designing by comparing performances to the criteria required for the application. The most common parameters are impedance, gain, efficiency, radiation patterns and directivity.

2.3.1 Impedance

The input impedance of an antenna is the ratio of the voltage to current at the input of the antenna (Kishk, 2009; Kraus & Marhefka, 2001). The impedance partly determines the maximum power ideally transferred from the antenna. The impedance of a sinusoidal wave consists of a real and imaginary part. The real part represents the radiated power of the antenna. The imaginary part of the impedance is non-radiated power that is stored in the near field of the antenna (Bevelacqua, 2011a).

In low frequency applications, the impedance of the wires and components matter in the performance of the antenna. If there is much more resistance at the source than at the antenna there will be little power transferred to the antenna. This also occurs when the antenna has much more resistance than the source impedance. To allow for the best performance the impedance at the antenna need to match the impedance at the source (Wentworth, 2007a).

In high frequency applications changes occur in the behavior of the antenna system. In theory, a short circuit will have a resistance of zero ohms but in a high frequency system that same short circuit measured at the end of a quarter wavelength transmission line can have a large impedance (Wentworth, 2007a). When finding the input impedance of a high frequency system the measurement is performed at the end of a transmission line with a predetermined length and characteristic impedance. The characteristic impedance (Z_0) is the ratio of the voltage and current of the signal along the transmission line (Wentworth, 2007a). By knowing the characteristic impedance, antenna impedance and the length of the transmission line the input impedance can be calculated (Eqn. 2.2).

$$Z_{in} = Z_0 \left(\frac{Z_L + jZ_0 * \tan\left(\frac{2\pi f}{c} L\right)}{Z_0 + jZ_L * \tan\left(\frac{2\pi f}{c} L\right)} \right) \quad \text{(Eqn. 2.2)}$$

Where;

Z_{in} = Input Impedance
Z_0 = Characteristic Impedance
Z_L = Load impedance
L = Transmission Line Length
f = frequency (Hz)
c = Speed of light (3×10^8 m/s)

Antenna impedance relates the voltage to the current at the input to the antenna. The impedance of the antenna is determined by the type of antenna. Matching the antenna to the system is a very important part of a properly working antenna. Having the antenna impedance match the characteristic impedance allows for maximum power transfer to the antennas. If the antenna and system are not matched an impedance mismatch will occur (Bevelacqua, 2011a; Kishk, 2009). Impedance mismatch is when signal loss occurs along the transmission line as the signal reflects back to the source. The superposition of the incident wave and reflected waves in the transmission line can set up a standing wave pattern.

A standing wave ratio is the ratio of the amplitude at the maximum and minimum points of a standing wave. The standing wave ratio is defined as a ratio (Wentworth, 2007b). The Voltage Standing Wave Ratio (VSWR) method helps determine whether the antenna is properly matched to the transmission line or source. The VSWR is a ratio of the mismatch loss in the system (Kishk, 2009). A value of "1" means that there is no mismatch loss. Anything value greater than 1 indicates a mismatch loss is the system. A VSWR value under 2 is generally considered suitable for most antenna applications.

2.3.2 Gain and Efficiency

Antenna gain is a very important parameter that directly shows the performance of the antenna based on the strength of the signal radiating off of the conductor (Kishk, 2009). Antenna gain, measured in dBi, is defined as the amount of power that is transmitted in the direction of peak radiation compared to that of an isotropic source. An isotropic radiator is an ideal theoretical point source that radiates the same intensity of a signal in all directions (Wentworth, 2007a). Gain of an antenna can be calculated by multiplying the antenna efficiency by the directivity of the antenna (Eqn. 2.4).

$$\varepsilon_R = \frac{P_{radiated}}{P_{input}} \quad \text{(Eqn. 2.3)}$$

$$G = \varepsilon_R * D \quad \text{(Eqn. 2.4)}$$

Where;

G = Antenna Gain
ε_R = Antenna Efficiency
D = Directivity

The antenna efficiency is the ratio of power transmitted to the power inputted to the antenna (Eqn. 2.3). The higher the efficiency means less power is lost from the antenna. Low efficiencies can occur due to impedance mismatch, poor conduction and dielectric losses. Directivity is the measurement of how directional the radiation pattern of an antenna is (Eqn. 2.5) (Bevelacqua, 2011b). An antenna that radiates from all directions, like an isotropic antenna, will have a directivity of 1 (Bevelacqua, 2011b; Kishk, 2009). A higher directivity value indicates a more focused radiation pattern. A more unidirectional antenna, like a horn antenna, can have a directivity as high as 100.

$$D = \frac{1}{\frac{1}{4\pi}\int_0^{2\pi}\int_0^{\pi}|F(\theta,\phi)|^2 sin\theta d\theta d\phi} \quad \text{(Eqn. 2.5)}$$

2.3.3 Radiation Pattern

Directivity also pertains to the radiation pattern. The radiation pattern of an antenna is the variation of power radiated in all directions away of the antenna (Figure 2.2) (Wentworth, 2007c). This pattern shows the characteristics of the antenna fields. There are three fields that surround the antenna (Figure 2.3) which are the Reactive Near Field, Radiating Near Field (Fresnel Region), and the Far Field (Fraunhofer Region) (Bevelacqua, 2011c). The Reactive Near field is in the closest region of the antenna. This field consists of reactive fields that have the Electric (E) and Magnetic (H) fields out of phase by 90 degrees (Wentworth, 2007c). Having the fields out of phase causes the antenna not to radiate power at this distance. The Radiating Near field is located between the Reactive Near field and Far field. This region starts to propagate a maturing signal as the E and H fields start to move in phase with each other. The last, and most important, field that surrounds the antenna is the Far field. The far field represents the region that radiates the strongest signals (Eqn. 2.6). This region is also important because most wireless applications transmit signals long distances and at this point the radiation pattern has an established shape without near field interference. This region dictates which antenna will be used for a certain application based on the Far field radiation pattern.

$$R_f = \frac{2D^2}{\lambda} \quad \text{(Eqn. 2.6)}$$

Where:

R_f = Far Field distance (Fraunhofer Distance)
D = Largest length on Antenna (m)
λ = Wavelength of signal (m)

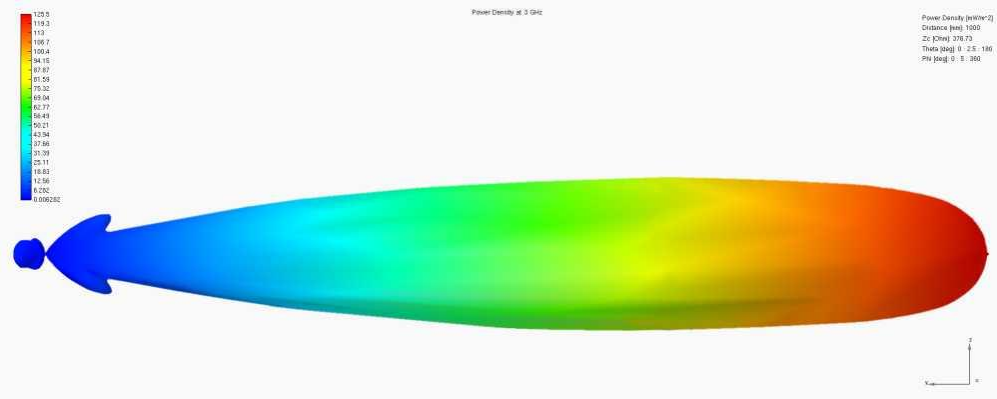

Figure 2.2 Finite Analysis of Radiation output from an Antenna (Wolff, n.d.)

There are two common types of radiation patterns, omnidirectional and directional. Omnidirectional antennas have a radiation pattern that is symmetrical on all sides. Many mobile device applications utilize an omnidirectional antenna because it allows for signals to be transmitted and received from all directions. A directional antenna with have a focused radiation pattern that is not symmetrical. Unlike the omnidirectional pattern, the focused radiation pattern allows for a stronger signal to radiate but only a certain direction. Directional patterns consist of a main lobe and side lobes (Kishk, 2009). The main lobe(s) is the located in the direction of where the signal is at its maximum radiation (Figure 2.4). When designing an antenna the main lobe should be located in the desired direction of the application. Usually, at the 45° and 135° points on either side of the main beam there are side lobes. Side lobes are weak

unwanted signals that exist in all non-ideal scenarios (Kishk, 2009). Side lobes cannot be totally eliminated but can be minimized with a proper design.

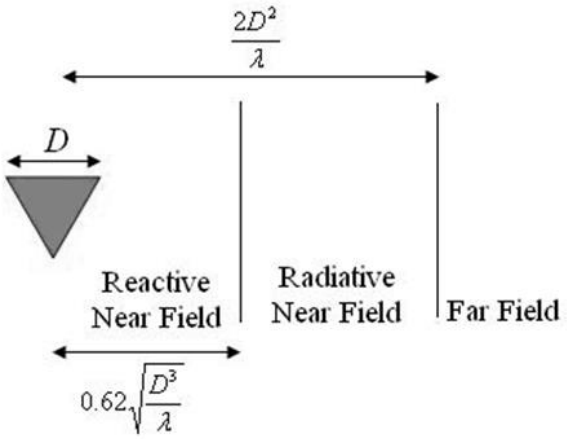

Figure 2.3 Diagram showing the three forms of Radiation fields (Bevelacqua, 2011d)

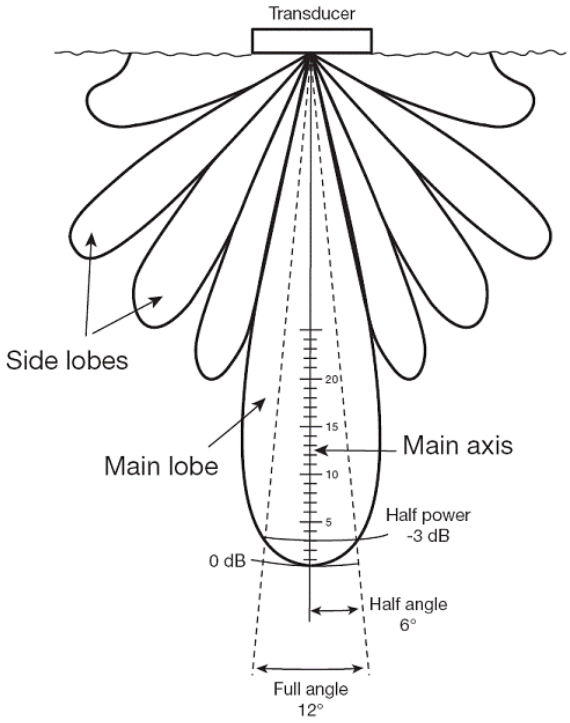

Figure 2.4 Main lobe and Side lobes emitting from a transducer (Johannesson & Mitson, 1983)

2.4 Friis Equation

Knowing the antenna parameters allows for designs to be implemented for certain applications based on the performance characteristics. The amount of power transmitted from one antenna and received by another over any distance can be determined by Friis Transmission equation (Wentworth, 2007c). To implement the equation, the gain of both antennas, transmitter and receiver, need to be known as well as the distance between the two antennas and the frequency of the signal being transmitted (Eqn. 2.7). The equation can also be revised to reflect gain directivity and the aperture of the antenna. Friis equation is useful to measure the gain of an antenna by finding the ratio of received to transmitted power for given antenna gains, distance and wavelength under ideal conditions.

$$\frac{P_R}{P_T} = G_T G_R \left(\frac{\lambda}{4\pi d}\right)^2 \qquad \text{(Eqn. 2.7)}$$

Where;

P_R = power received (Watts)
P_T = power transmitted (Watts)
G_T = Transmitter Antenna Gain
G_R = Receiver Antenna Gain
λ = Signal wavelength (m)
d = Distance between antennas (m)

2.5 Types of Antennas.

There are many types of antenna, such as dipoles, parabolic, microstrip, and traveling wave antennas. Each is designed for a certain applications and situation.

2.5.1 Dipole Antenna

Wire antennas are the simplest of all antennas. The most basic antenna in this category is the dipole antenna (Figure 2.5). A dipole antenna consists of two symmetrical conductors. The dipole conductors are both connected to the feedline of the transmitter/receiver. Dipole antennas are resonant antenna which means the standing wave of the signal current flows between both ends of the antenna conductors (Croswell, Christiansen, Alexander, & Jurgen, 2004). This antenna characteristic means that the length and the dipole conductors are directly related to the wavelength that is be radiated (Bevelacqua, 2011e).

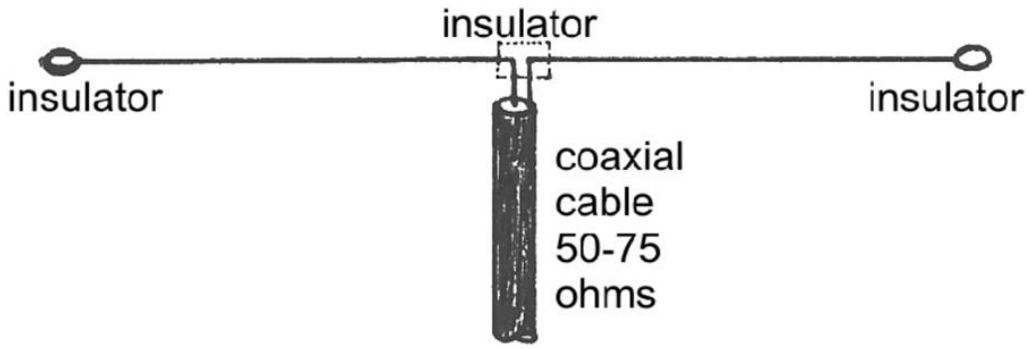

Figure 2.5 Dipole Antenna (Segalstad, 1972)

There are few types of dipole design that are used to achieve different performances. The first and most commonly used variation is the half-wave dipole (Figure 2.6). The half-wave dipole consists of two quarter-wave conductors that form a half-wavelength when put together on the antenna. The half-wave dipole antenna has the largest voltage differential out of all the dipoles. This is due the signal voltage being its largest positive value at one end of the dipole antenna while the other end has the largest

negative voltage. The large voltage differential allows for more current. An ideal half-wave dipole antenna in free space has an impedance of 73+j42.5Ω (Wentworth, 2007c). It should be noted that as the dipole wavelength increases so does the impedance (both real and imaginary). At about 0.46λ the reactance is zero making the antenna resonate. Wavelengths shorter than 0.46λ have a capacitive reactance while wavelengths larger than 0.46λ have an inductive reactance (Bevelacqua, 2011e). The directivity of an ideal half-wave dipole antenna is 1.64 which yields a gain of 2.17 dBi (Silver, 1984).

Another variation of the dipole antenna is a quarter-wave dipole antenna. The quarter-wave dipole antenna is the same as the half-wave dipole antenna except there is only a single element (Figure 2.7). The quarter wave conductor behaves as a half-wave dipole due to a quarter-wave conductive reflector tied to ground. This grounding plane acts as a mirror for the quarter-wave conductor creating a pseudo half-wave antenna (Croswell et al., 2004). Since there is only one conductor, the impedance is divided by two making the impedance of an ideal quarter-wave antenna 36+j21Ω (Wentworth, 2007c). This allows for higher gain because the same signal is being transmitted with less resistance and elements. An ideal gain is about 5.14 dBi.

The folded dipole antenna is a closed loop design that follows the same theories of a dipole antenna (Figure 2.8). The folded dipole antenna's impedance is dependent on the length and impedance of the folded conductor. Since the transmission line is folded back onto itself the currents reinforce each other instead of cancelling out. This also makes the antenna naturally have a higher impedance than a normal dipole. Standard equations for dipole antennas show that the folded dipole will have an impedance four times the impedance of a half-wave dipole antenna (Bevelacqua, 2011e; Nikolova, 2012).

This makes the folded dipole antenna a popular choice for applications that require antennas with larger impedances.

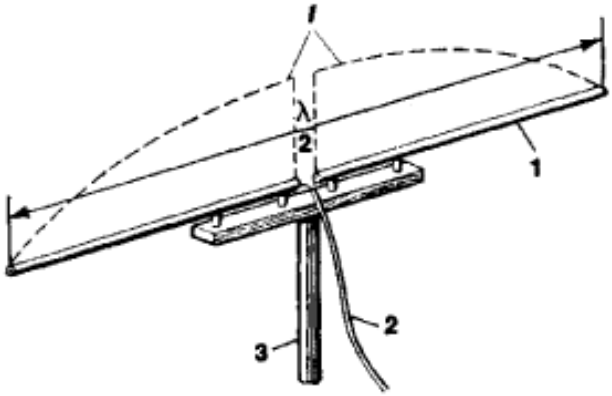

Figure 2.6 Half-wave Dipole Antenna (The Great Soviet Encyclopedia, 1970)

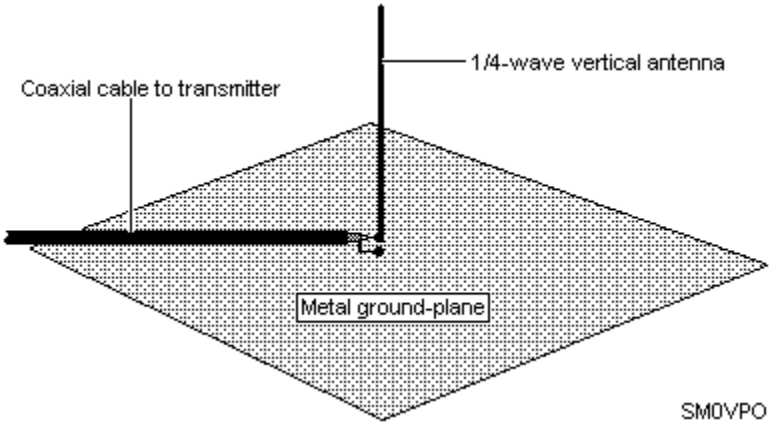

Figure 2.7 Quarter-wave Dipole Antenna (Lythall, n.d.)

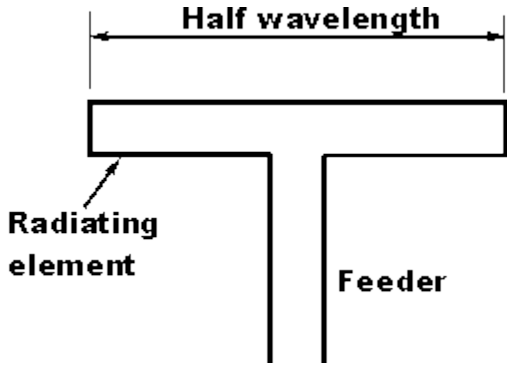

Figure 2.8 Half-wave Folded Dipole Antenna (Poole, n.d.)

2.5.2 Travelling Wave Antenna

A traveling wave antenna works by having the current travel along the antenna. While the current travels across the antenna the phase continuously varies. The phase is important part of the antenna performance because these type of antennas do not radiate naturally. The discontinuities of the continuously changing phase allows for the antenna to radiate. The signal can radiate at the beginning and end of the antenna structure due this propagation technique. This technique also allows for a very focused radiation pattern.

One example of a traveling wave antenna is the helical antenna (Figure 2.10). A helical antenna is a focused antenna where the conductor is in the shape of a helix or corkscrew. The signal propagates in the direction of the helical structure ($+z$). The circumference and length of the helical conductor determines the resonant frequency (Shui, Wang, Huang, Jing-huil, & Jin-xiang, 2010). The helical antenna has a mostly real impedance that can be determined by equation 2.8. The helical structure has a pitch angle that is measured from the base of the antenna to the spiraling conductor (Figure 2.9). An ideal helical antenna has a pitch of 13° or 14°. With this pitch, the helical

antenna can reach gain levels as high as 17.3 dBi (Djordjević, Zajić, & Ilić, 2006).

Helical antennas have a reputation for having excellent wideband performance.

$$Z_{in} = 140\frac{C}{\lambda} \quad \text{(Eqn. 2.8)}$$

Where;

Z_{in} = Input impedance
C = Circumference of helix
λ = Wavelength (m)

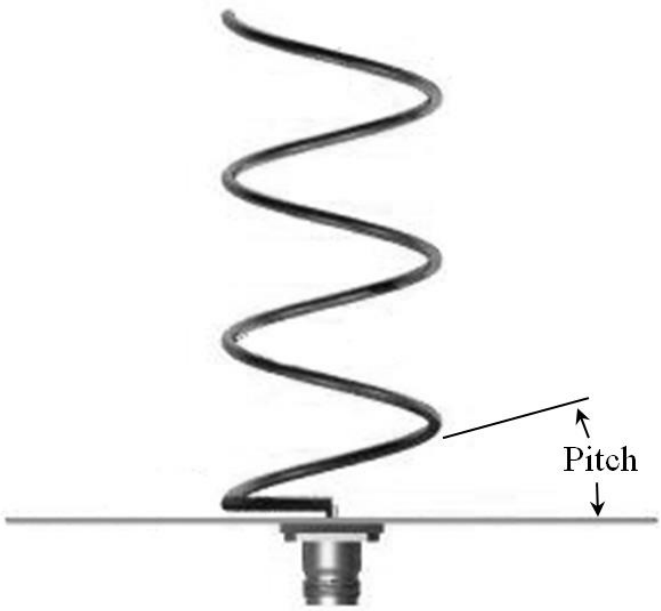

Figure 2.9 Helical Antenna showing the Pitch angle (Coppens, n.d.)

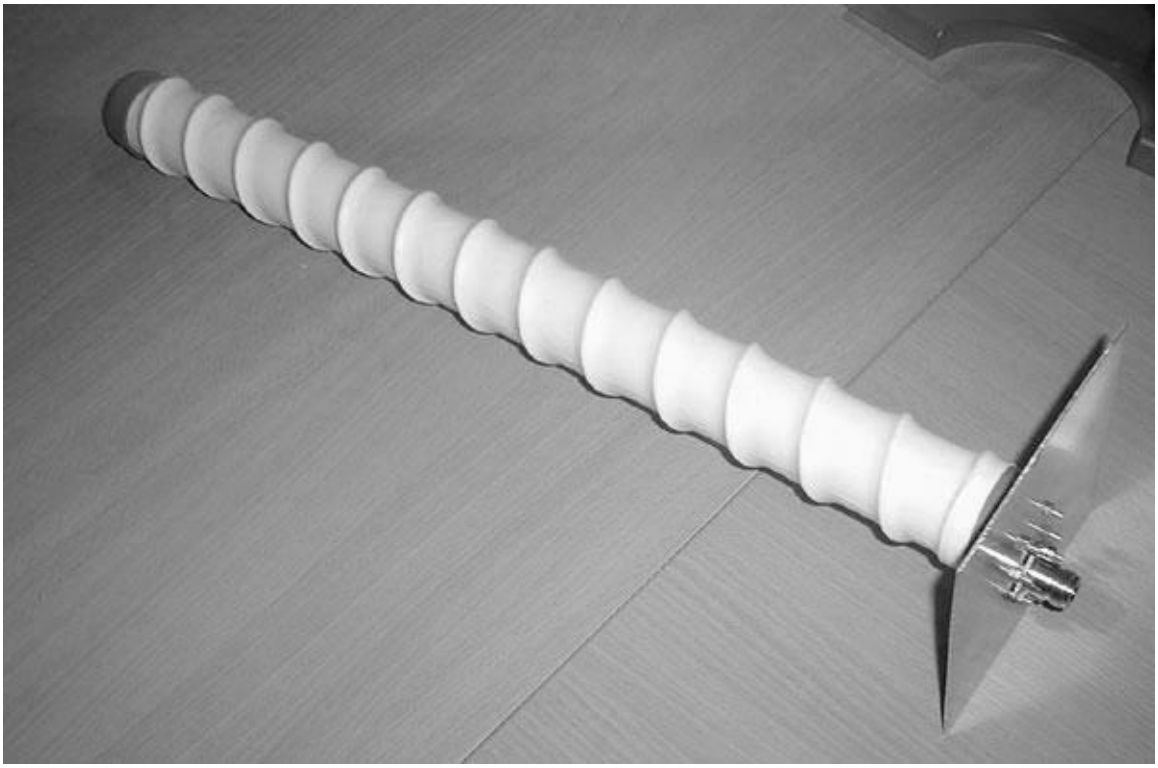

Figure 2.10 Helical Antenna (Jaspers, n.d.)

Another example of a traveling wave antenna is the Yagi-Uda antenna. The Yagi-Uda antenna was design by Shintaro Uda is 1926. The design was later presented by one of Uda's colleagues, Hidetsugu Yagi (Thiele, 1969). Yagi-Uda antennas are highly focused beam antennas with high gain. Unlike the helical antenna, the Yagi-Uda antenna has very a narrow bandwidth to achieve the high gain performance. The antenna works by having a half-wave or folded dipole antenna excited while connected to two or more dipoles that are not excited directly by the feed (Figure 2.11) (Thiele, 1969). The other dipoles reradiate the signal received from the single driven dipole. These are known as parasitic elements to the antenna. One of the parasitic dipoles will be slightly longer than a half- wavelength which allows for the current to lag the phase of the voltage. This is called the reflector. The other parasitic dipole will be slightly shorter than a half-

wavelength. This will allow for the voltage phase to lag behind the current. This is called the director element (Thiele, 1969). Research shows that the first director can increase the gain by 3dBi. A second director can add another 2dBi of gain and a third can add 1.5dBi. As more directors are added the gain increase will be smaller (Bevelacqua, 2011f). Yagi-Uda antennas can achieve gains higher than 10dBi.

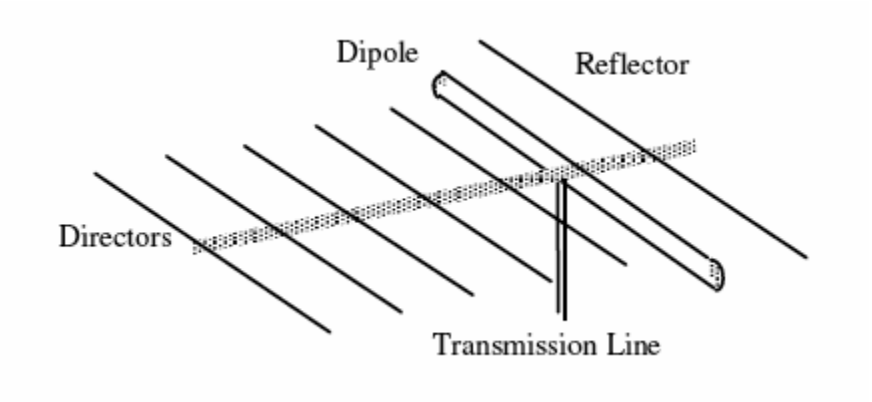

Figure 2.11 Yagi-Uda Antenna (Jugandi, 2001)

2.5.3 Parabolic Antenna

A parabolic reflector antenna reflects the single off a feed antenna. This antenna is commonly known as a satellite dish antenna (Figure 2.12). The dish reflector works by receiving a signal from a feed antenna that is pointed at the reflector. The focal length of the parabola determines how focused the signal beam will be. Unlike the other antenna described before, the reflector for the antenna needs to be multiple wavelengths wide for the antenna to perform correctly. The larger the diameter and the more focused the signal beam allows for a very high gain (greater than 50dBi).

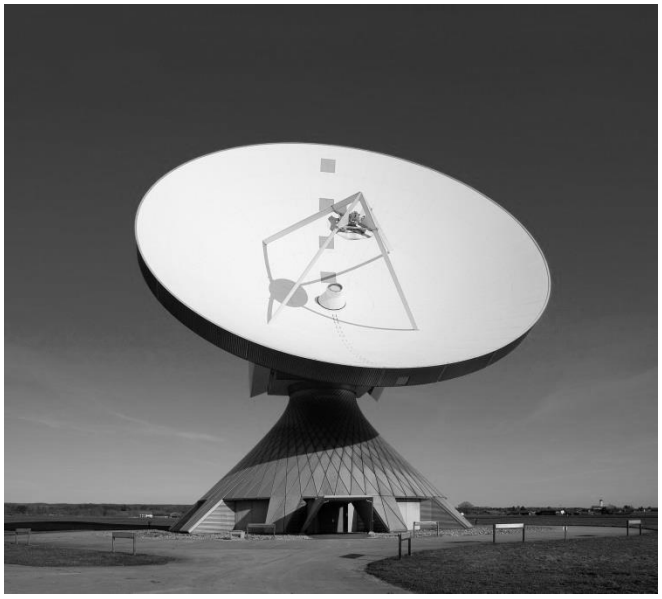

Figure 2.12 Parabolic Antenna (Bartz, 2008)

2.5.4 Microstrip Antennas

Microstrip antennas, commonly known as patch antennas, are fabricated on printed circuit boards (PCB) (Figure 2.13). Patch antennas are cheap and small for the performance achieved (Kishk, 2009; Maci & Gentili, 1997). A few factors determine the characteristics of the antenna. To find the center frequency of the antenna the length and width of the microstrip patch needs to be known along with the permittivity and height of the dielectric material used as the substrate (Eqn. 2.9). In a rectangular patch antenna, the width of the conductor determines the input impedance and bandwidth. By increasing the width, the impedance will decrease and the bandwidth will increase (Maci & Gentili, 1997). The gain of patch antennas can be as high 9dBi but average around 6dBi (Orban & Moernaut, n.d.).

$$f_c = \frac{1}{2L\sqrt{\varepsilon_0 \varepsilon_r \mu_0}} \quad \text{(Eqn. 2.9)}$$

Where;

f_c = Center frequency (Hz)
L = Length of patch (m)
ε_0 = Permittivity of free space ($8.854*10^{-12}$ F/m)
ε_r = Relative Permittivity
μ_0 = Free space Permeability ($4\pi*10^{-7}$ H/m)

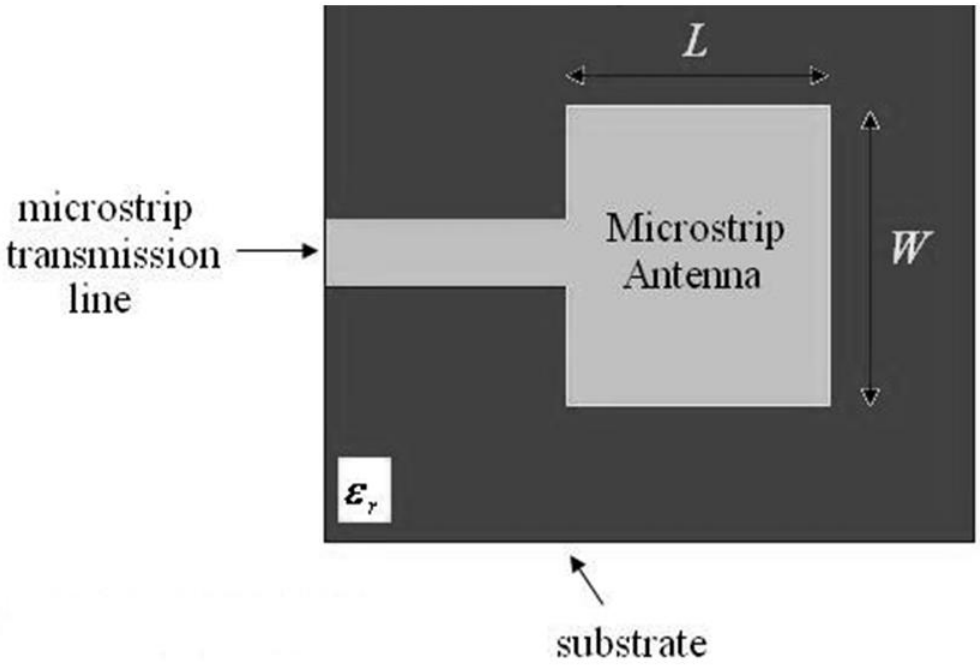

Figure 2.13 Patch Antenna (Bevelacqua, 2011g)

2.5.5 Bow-tie Antenna

Bow-tie antennas are a triangle antenna that resembles a bow-tie shape (Figure 2.14). They are similar to half-wave dipole antennas yet the antenna is dependent on the angles of the shape instead of the length (Shlager, Smith, & Maloney, 1994). This allows for lower frequencies to be radiated with a smaller area. Bow-tie antennas are simple log periodic antennas. Log periodic antennas radiate at all frequencies that are constant

multiples of the primary frequency. The name, log periodic, comes from the rule that if all of the elements grow by a constant multiple then the ratios of the logarithm are constant (Bevelacqua, 2011h). Bow-tie antennas, also known as a biconical or butterfly antenna, have a similar radiation pattern as a dipole antenna but with a larger bandwidth. These antennas can also be formed with a single triangle instead of two like a half-wave dipole and a quarter-wave dipole antenna (Shlager et al., 1994). This antenna design is commonly used on microstrip due to the simplicity of the shape and the wide radiation pattern.

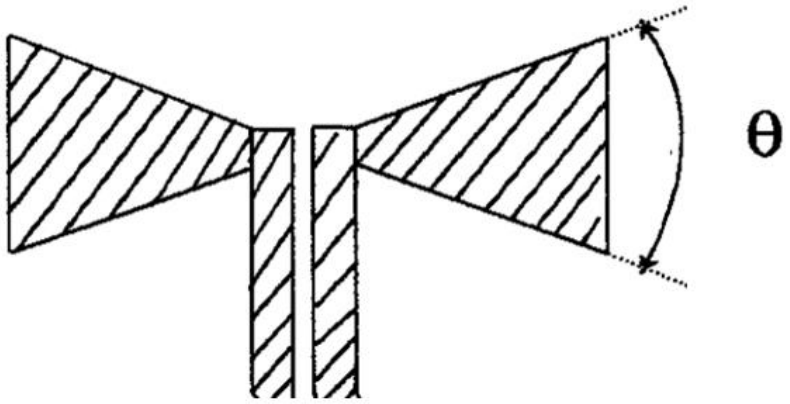

Figure 2.14 Bow-tie Antenna (Lin, 1997)

This work will use microstrip bow tie antennas and Sierpinski Monopole Gasket Antennas fabricated on PCB. To understand the Sierpinski Monopole Gasket antenna one must also understand the basics of fractal theory and how it relates to the design and performance of fractal antennas.

2.6 Introduction to Fractal Theory

Fractal antennas are a growing interest in the mobile industry due to the compact size, low profile, and multiband performance. According to Werner and Gangul, "The term fractal means a family of complex shapes that possess an inherent self-similarity or self-affinity in its geometrical structure" (Werner & Gangul, 2003, p. 38). In theory, these self-similar shapes can be scaled down infinitely through a simple recursive process to form an infinite length or area within a certain boundary (Krzysztofik & Member, 2009). When looking at this theory in terms of mobile antennas, it can be seen that a highly compact antenna with the ability to operate at both low and high frequencies is possible.

2.6.1 Theoretical Background

The most versatile method for generating fractals in a variety of shapes and sizes is with Iterated Function Systems (IFS). A series of affine transformations that calculate the shape's parameters such as scaling, rotation, and translation is shown in Eqn. 2.10. The variables a, b, c, d, e, and f are real numbers where a, b, c, and d control the rotation and scaling. The e and f variables control the linear translation (Werner & Gangul, 2003).

$$w\begin{pmatrix} x \\ y \end{pmatrix} = \begin{pmatrix} a & b \\ c & d \end{pmatrix}\begin{pmatrix} x \\ y \end{pmatrix} + \begin{pmatrix} e \\ f \end{pmatrix} \qquad \text{(Eqn. 2.10)}$$

By applying a set of affine linear transformations ($w_1, w_2, \ldots, w_n$) along with an initial geometrical shape (A), a Hutchinson operator can be used to produce a new geometry (Eqn. 2.10). When the Hutchinson operator is applied to the previous geometry

a fractal pattern will occur (Eqn. 2.11). The physical shape will repeat itself at a fraction of the previous size (Eqn. 2.13) (Figure 2.15). In theory, this operation can occur infinitely (A_∞). An example of this can be seen in equations 2.11 thru 2.13.

$$W(A) = \bigcup_{n=1}^{N} w_n(A) \quad \text{(Eqn. 2.11)}$$

$$A_1 = W(A_0),\ A_2 = W(A_1), \ldots, A_{k+1} = W(A_k) \quad \text{(Eqn. 2.12)}$$

(Eqn. 2.13)

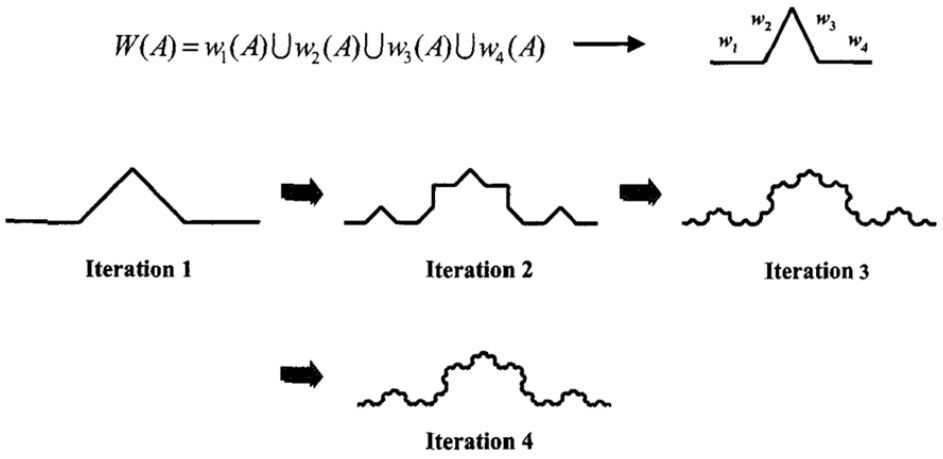

Figure 2.15 Fractal Geometry Process using Hutchinson Operator
(Puent-Baliarda, Romeu, & Cardama, 2000)(Werner & Gangul, 2003)

2.6.2 Koch Geometry

The Iterated Function Systems allows for the formation of fractal patterns for any shape. When designing a fractal antenna there are three frequently used shapes or designs. Koch geometry was introduced by Helge von Koch in 1904 (Li, Zhang, Zhao, Ma, & Li, 2012). A Koch snowflake (Figure 2.15) is constructed by adding decreasing sizes of equilateral triangles to form a pattern. The Koch snowflake is a desired design because the perimeter length increases exponential with respect to the initial shape as

iterations are being added. This allows for antennas utilizing the Koch geometry to transmit/receive lower frequencies while keeping a small area. The Koch geometry can be used on loop antennas or patch antennas depending on the application. Koch fractal antennas are designed by taking three triangles and scaling them by a third of the original size while rotating each of them by 60°. The third iteration involves nine triangles scaled to a third of the size of the second iteration and then rotated 60°. The fourth iteration continues the fractal pattern as more triangles are added (Figure 2.16)(Li et al., 2012)(Werner & Gangul, 2003).

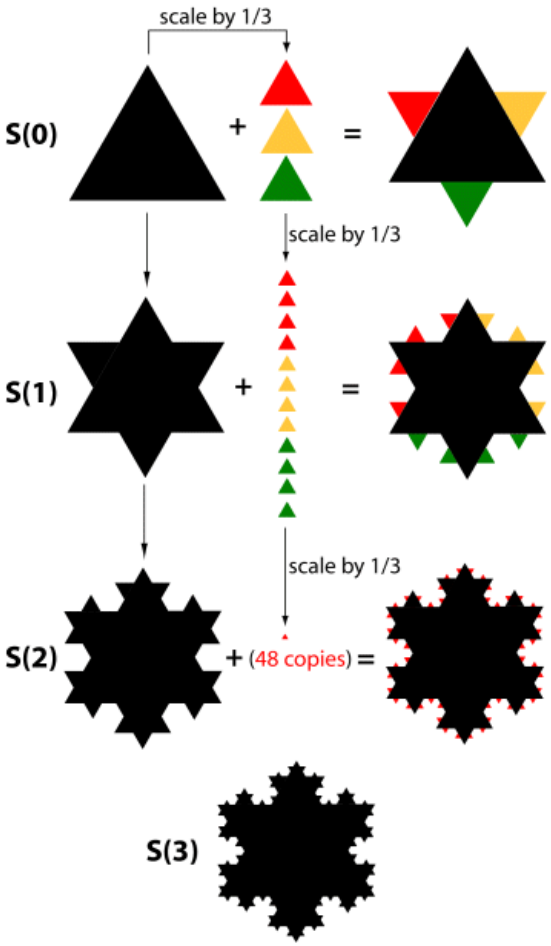

Figure 2.16 Koch Geometry Steps (Riddle, 2014)

2.6.3 Hilbert Curve Geometry

Another fractal design that has been in incorporated into antennas is the Hilbert curve antenna. The Hilbert curve is a space-filling geometrical pattern that was designed by David Hilbert in 1891 (Werner & Gangul, 2003). The pattern is unique in that it does not have any intersection points. Like the Koch fractal, the length increases with each iteration as the shape's area stays the same allowing for antenna performance at lower frequencies. Fractal Hilbert curves are created by adding four copies of the previous iteration together thus replacing the last iteration (Figure 2.17) (Vinoy, Jose, Varadan, & Varadan, 2001). Since the Hilbert curve only consists of one line, the topological dimension of the curve is 1 but the dimension of the fractal curve can be defined by the Multiple Copy Algorithm (Eqn. 2.14) where *n* is the number of iterations in the pattern and *D* represents the Hausdorff Dimension. The Hausdorff Dimension is a real number that represents the dimension of real vector space. The Hausdorff dimension of an n-dimensional space equals n (McMullen, 1984) (Kohavi & Davdovich, 2006). Since the Hilbert curve is a space filling shape on a plane, the Hausdorff Dimension is 2, assuming that n is a very large number. When *n* is small the equation will show that *D* is slowly increasing closer to 2 meaning that the geometry is a still a fractal number. The algorithm also shows that as the iterations increases the dimensions of the fractal curve increases. This length increase allows for the reduction of resonant frequencies and allows for an antenna using this design to operate at lower frequencies with a smaller total area.

$$D = \frac{\log[(4^n-1)/(4^{n-1}-1)]}{\log[(2^n-1)/(2^{n-1}-1)]} \qquad \text{(Eqn. 2.14)}$$

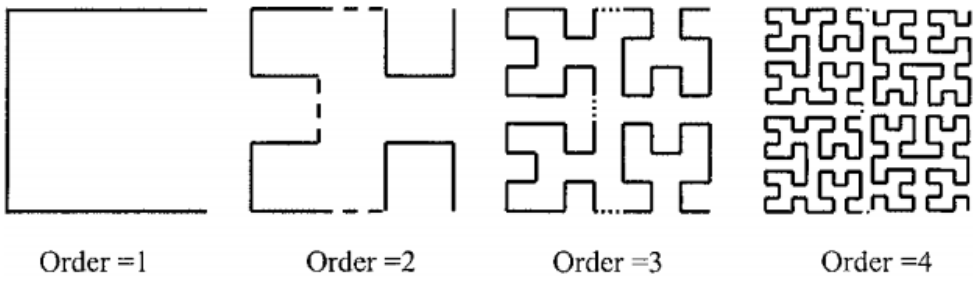

Figure 2.17 Hilbert Curve Fractal Process (Vinoy et al., 2001; Werner & Gangul, 2003)

2.6.4 Sierpinski Triangle Geometry

The last fractal design that is commonly used and will be the focus of this work is the Sierpinski fractal pattern. The Sierpinski pattern was first described in 1916 by Waclaw Sierpinski (Puente-Baliarda, Romeu, Pous, & Cardama, 1998). The pattern scales down iterations of a triangle by using IFS. Unlike the Koch snowflake, the Sierpinski triangle pattern subtracts triangles away from the original shape. This is accomplished by removing the second iteration central triangle with vertices at the midpoints of the original shape. This pattern is repeated with the third iteration triangle being removed with the vertices at the midpoints of the three remaining triangles (Figure 2.18) (Krzysztofik & Member, 2009) (Borja & Romeu, 2000).

2.7 Sierpinski Gasket Monopole

By utilizing this pattern, Puente et. al. created the first Sierpinski Gasket Monopole antenna. The experiment created a multi-band antenna by utilizing a repeating triangle shape. The fractal antenna was compared to a single-band bow-tie antenna that was the same size of the original triangle shape. Since not much was known about how

to design a Sierpinski Gasket Monopole antenna it was assumed that the performance characteristics and equations of the bow-tie antenna would give a good reflection on how the fractal antenna would perform. Like the bow-tie antenna, the current of the Sierpinski fractal antenna flows over the skin of the antenna.

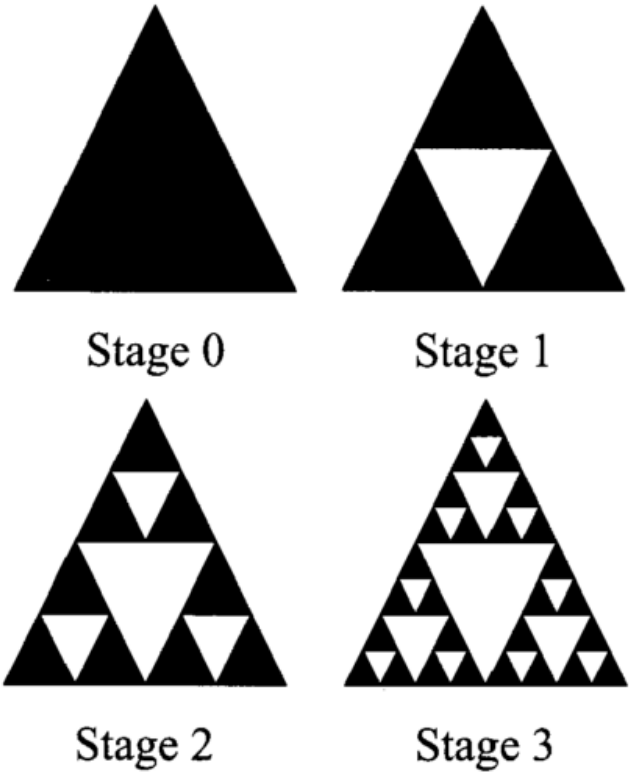

Figure 2.18 Sierpinski Triangle Fractal Process
(Werner & Gangul, 2003)(Krzysztofik & Member, 2009; Puente-Baliarda et al., 1998)

When the current flows from the feed point of the fractal antenna it will concentrate around the region that is comparable in size to the wavelength. Since the Sierpinski Gasket Monopole is comprised of different sized shapes, which can reflect the length of multiple wavelengths, it has a multiband operation (Figure 2.19) (Puente-Baliarda et al., 1998). When designing the antenna, each iteration of the shape was

scaled down by half of the last iteration's size. It was shown that this scaling produced a log-period behavior as opposed to the harmonic behavior of classic monopoles (Puente, Navarro, Romeu, & Pous, 1998). The feed was put at one of the vertices of the triangle. After numerous iterations, the team had a design with a 60° flare angle at the feed with an input impedance of 50Ω.

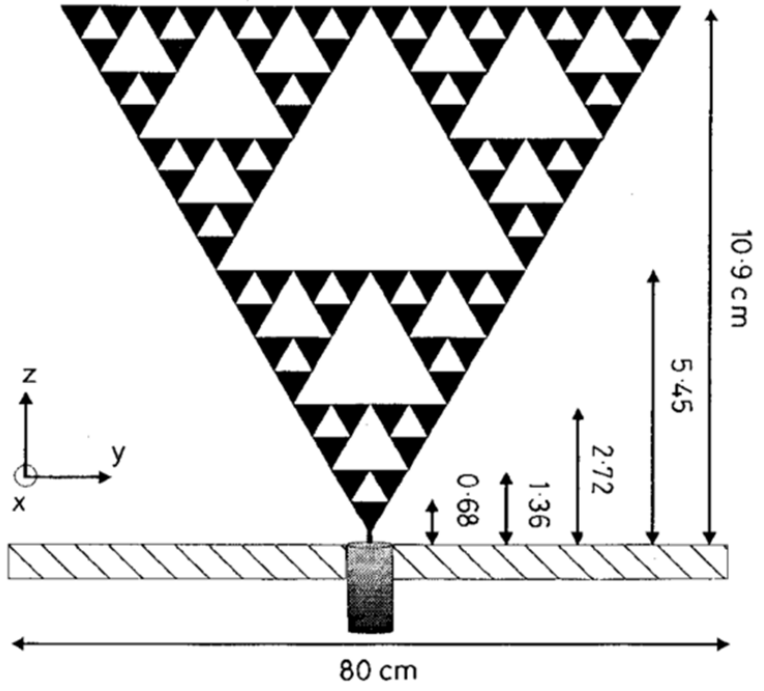

Figure 2.19 Sierpinski Gasket Monopole Created by Puente-Baliarda (C. Puente, Romeu, Pous, Garcia, & Benitez, 1996)

Tests were conducted comparing the Sierpinski Gasket Monopole antenna and the bow-tie antennas. The results showed that fractal antenna behaved similarly to the bow-ties antennas that were being compared to the Sierpinski Gasket Monopole. Each band on the fractal antenna reflected the performance of its single-band bow-tie antenna.

After the tests were completed and the results were affirmed, the team developed an equation to find the resonant frequencies based off the dimensions and characteristics of the fractal (Eqn. 2.15).

$$f_n = k\frac{c}{h}\cos(\alpha/2)\delta^n \qquad \text{(Eqn. 2.15)}$$

Where;

f_n = resonant frequency (Hz)
c = Speed of light (3 x10^8m/s)
h = Height of the monopole (mm)
n = Resonant band number
α = Flare angle at the feed (deg)
δ = Similarity factor
k = Substrate ratio

Puente et. al. proved the Sierpinski Gasket Monopole antenna was a viable solution for multiband applications. However, the study did not show how the flare angle at the feed would affect the fractal antenna's performance characteristics. To delve deeper into the idea, Puente returned to the topic with a new study that focused on comparing Sierpinski Gasket Monopole antennas with different flare angles. To research the topic, flares angles at 30° (SPK-30), 60° (SPK-60), and 90° (SPK-90) were chosen (Puente et al., 1998).

Studies have been conducted on the effects of changing the flare angle of bow-tie antennas (Figure 2.20). It was shown that as the flare angle increased, the impedance and reactance changes were small (Chen & Chia, 2001). Puente et. al. tested the fractal antennas and determined the impedance and resonant frequency changes throughout the three samples. The test data showed at 90°, the frequencies shifted toward longer

wavelengths. As the flare angle decreased to 30° the antenna performance deviated away from the log-period behavior and acted like a classic monopole antenna with a harmonic output (Puente et al., 1998). This was caused by the shorter lengths of the triangle edges which did not allow for proper generation and attenuation of most multiband antennas (Puente et al., 1998). This study showed that the flare angle can change the impedance and resonant frequencies. It also showed that when the angle is small enough it can create a classic monopole antenna.

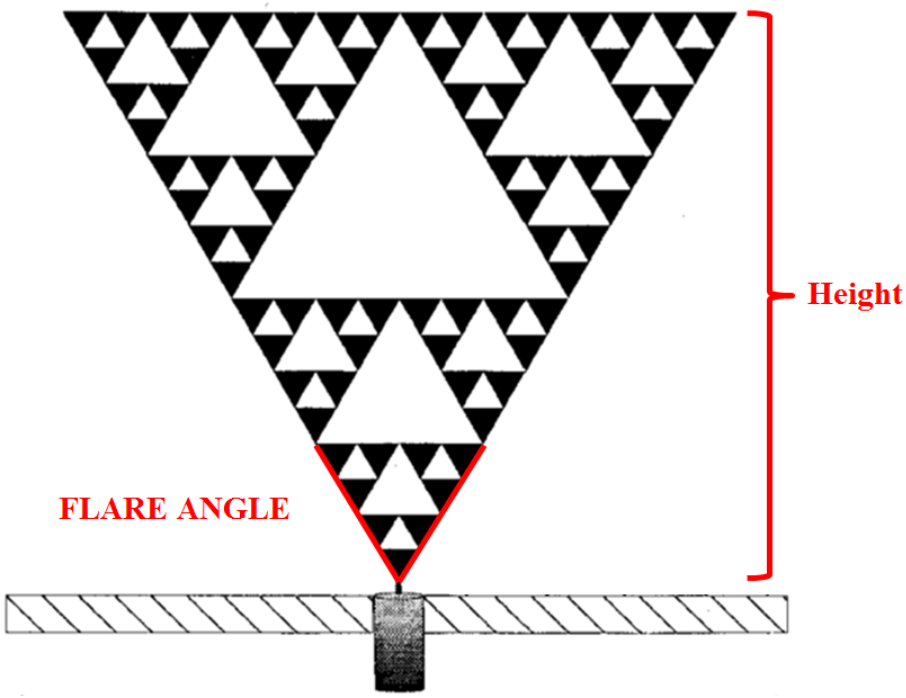

Figure 2.20 Sierpinski Gasket Monopole showing Flare angle and Height (Puente-Baliarda et al., 1998)

2.8 Commonalities

The bow-tie antenna will be compared with the Sierpinski Gasket Monopole antenna and with a flare angle of 90°. This work will investigate the commonalties and differences of the Sierpinski Gasket Monopole and the Bow-tie antenna design and performance. The derived equations and knowledge obtained from the studies performed by Puente et. al. will be taken into consideration. The procedures used by Puente et. al. in their comparison study will be loosely replicated in this study. This will provide a template for the experimental process if problems or errors arise.

2.9 Differences

The study in this thesis will differ from the established work. Different frequencies and substrate materials will be used. Frequencies commonly used in mobile and local wireless applications will be the subject of the study. By changing the flare angle of the Sierpinski Gasket Monopole antenna and the bow-tie antennas, the data will differ from past studies. The desire is to extend the data stated in papers reinforcing that the Sierpinski Gasket Monopole antenna has similar behaviors as the bow-tie antenna.

2.10 Learning Points

There are many learning points to take away from these studies. The Sierpinski Gasket Monopole antenna is still in in the early stages with regards to antenna design. This means that there are features and behaviors that are not yet understood. This study will have to take this into account when analyzing the data collected. Analyzing the data and coming up with solid justifications of the results will play a key role in the study.

2.11 Experiment

For this experiment, two Sierpinski fractal antenna models will be used. One will have a flare angle at 90° and the other will have a flare angle at 60°. This will provide a comparison on how each antenna performs and the effect of the flare angle of the antenna feed. Four Bow-tie antennas will also be made to compare the signal frequency of single band antenna to the multiband antennas. 2.4 GHz and 5 GHz frequencies were the chosen bands to be utilized in the experiment. This will allow for the testing of frequencies that the mobile industry use and show a multiband performance. The goal of the experiment is to observe characteristics of each of antenna by measuring and comparing the performance. Major points in this work will focus on the comparison of the single band versus multiband performance and the comparison of the different flare feeds. Chapter 3 will explain further on the design, construction, testing, and analysis.

CHAPTER 3. PROBLEM STATEMENT AND METHODOLOGY

3.1 Problem Statement

This study is quantitative research that will observe and analyze the multiband behavior of a Sierpinski Gasket Monopole antenna by comparing it to single band bow-tie antennas that have self-similar properties as the fractal antenna. This experiment will implement two fractal antenna designs with a 60° and 90° flare angle while using methods and theories of Carles Puente-Baliarda et al. in the research of fractal antenna behavior with a 60 degree flare (Puente-Baliarda et al., 1998). This research will set itself apart from the past studies by utilizing the unique flare angle and by the approach at designing the fractal antenna. Sierpinski Gasket Monopole antenna's governing operators have not been discussed thoroughly in research outside of Puente's research. This allows for a different approach at designing the antenna where there will be more of an experimental approach to the design instead of a theoretical approach.

3.2 Introduction

Conducting this experiment will investigate whether the Sierpinski Gasket Monopole antenna behaves similarly to multiple single-band bow-tie patch antennas. The results will be determined by the data collected in the test.

Prior to conducting the experiment, a plan needs to be designed and implemented to decrease the probability of errors caused by the constraints of experiment.

A thorough examination of the theoretical background, simulations, construction, and physical testing of the antennas needs to take place.

3.3 Theoretical Background

The first part of the research requires the selection of the resonant frequencies to be tested. These are the operating frequency bands for the fractal and bow-tie antennas. The fractal antenna will have two bands that will be affected by the two largest shapes in the antenna (Figure 3.1). The size of each triangle needs to be half the wavelength of the resonant frequency in the design. The third and fourth iterations are not used due to limitations in measuring the high frequencies that are outputted by both of those iterations (greater than 6GHz). As explained in chapter 2, Puente-Baliarda et. al designed the first Sierpinski Gasket Monopole antenna based off the bow-tie antenna design. When testing the antenna, the Sierpinski Gasket Monopole did perform like a bow-tie antenna. However, the fractal antenna had different current densities at each resonant frequency unlike the bow-tie antennas (Puente-Baliarda et al., 1998). Using the equations from these past studies, the resonant spacing of the fractal antenna will be designed (Eqn. 2.15).

The impedance bandwidths and the gain at each resonant frequency of the fractal antenna and bow-tie antennas need to be taken into account. Microstrip patch antennas, like the ones in this experiment, will usually have a lower bandwidth than most other antennas. This is due to how microstrip patch antennas are implemented. As the patch antenna resonates there will be real impedance over the operating frequency creating bandwidths as low as 5°. This also means that the gain at the design resonant frequency should theoretically have a higher gain than wider band designs.

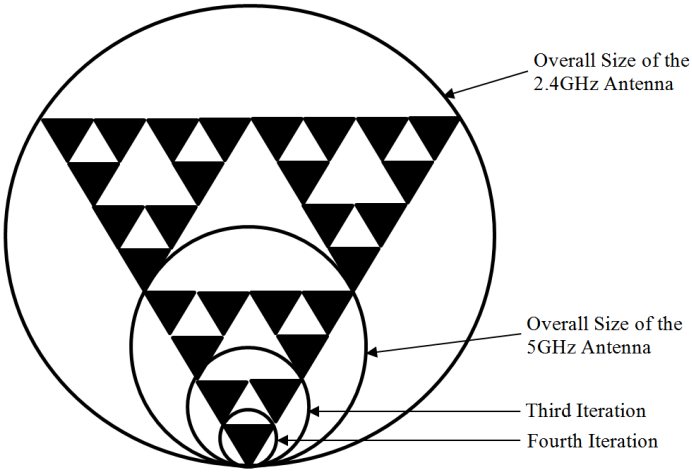

Figure 3.1 Size of each iteration of the Sierpinski Gasket Monopole Antenna

The input impedance of the fractal and bow-tie antennas are calculated to determine if matching networks are required. According to the literature, the input impedance of the Sierpinski Gasket Monopole antenna is determined by the flare angle of the antenna (Chen & Chia, 2001) (Puente et al., 1998). A Sierpinski Gasket Monopole antenna with a flare angle of 60° will have an input impedance of 50Ω (Puente-Baliarda et al., 1998). There is little literature available that includes standard equations for determining the input impedance based on the flare angle. As described in Chapter 2, Puente designed and measured a 90° Sierpinski Gasket Monopole antenna and observed that by using the equation (Eqn. 2.15) the antenna outputted a signal that was shifted off of the ideal frequency. This can be attributed to the change in impedance. The antenna needed to be revised to correct the impedance thus correcting the output frequency.

The last feature that needs to be considered is the radiation pattern of the fractal and bow-tie antennas. It will need to be determined if the patterns of the fractal antenna will differ in the output performance compared to the single-band bow-tie antenna's

radiation pattern. Microstrip patch antennas have uniform omnidirectional output patterns that are ideal for the mobile device applications associated with this study.

3.4 Design and Calculations

Using the methods described in section 2.7, the dimensions of the Sierpinski Gasket Monopole antennas were calculated with Puente's standardized equation. The 2.4GHz and 5GHz frequency bands were chosen to show that the Sierpinski Gasket Monopole is actually outputting two designed frequencies and not just a harmonic of one of the designed frequencies. FR-4 was used as the substrate ($\varepsilon_r = 4.7$) due to its affordability and availability. The similarity factor (ratio) of the two frequencies is 2.08. This allows for easy design as each triangle is about half the size of the larger iteration. There is a 60° flare angle for one of the Sierpinski antennas and 90° flare angle for the second. The substrate ratio was not explained thoroughly in Puente's experiments. For the initial calculations, the value assigned to the variable was 0.15 (the same used by Puente). The substrate ratio will be changed as revisions are performed on the antennas.

While designing for the six antennas it was noted that there is a distinct trade-off with having a multiband antenna instead of only a single band. A single band antenna should output a stronger signal than a multiband antenna but the multiband will be able to output multiple frequencies with moderate signal power transmission. Puente's standardized equation solves for the frequency on the second iteration and greater. To determine out the height of the antenna, the height of the second iteration is calculated and then multiplied by the similarity factor, in this case 2.08. The final height of the antenna is then determined (Table 3.1 and 3.2) (Figure 3.2 and 3.3).

Table 3.1 *Parameters of Sierpinski Gasket Monopole Antenna with 60° Flare Angle*

Antenna Parameters	Value
Similarity factor, δ:	2.08
Height, h:	6.5817 cm
Flare Angle, α	60°
Maximum iterations, N_{max}	4

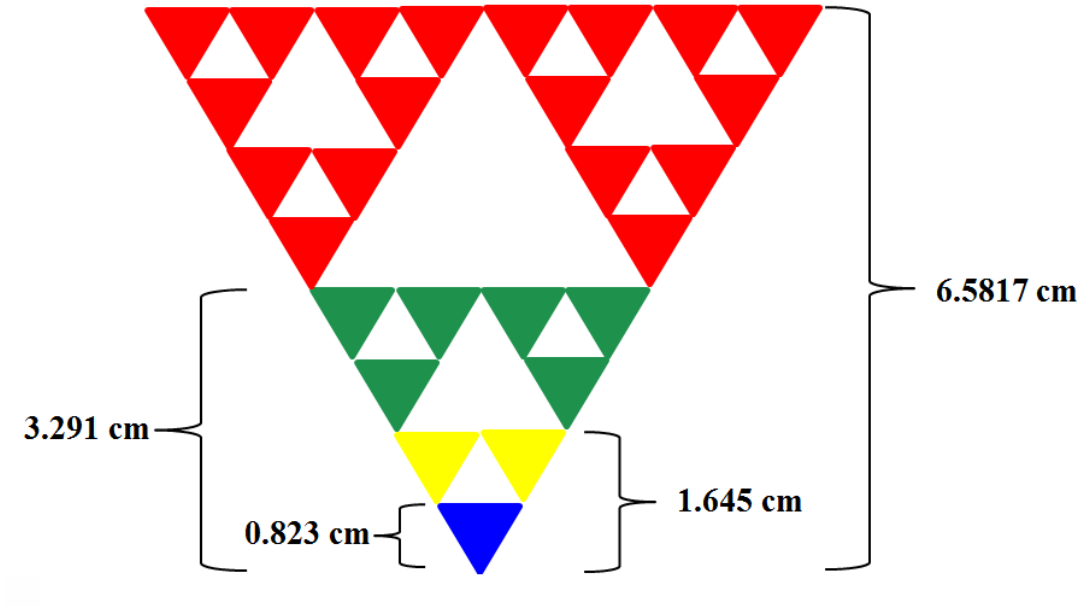

Figure 3.2 Height of Sierpinski Gasket Monopole Antenna with a 60° Flare Angle

Table 3.2 *Parameters of Sierpinski Gasket Monopole Antenna with 90° Flare Angle*

Antenna Parameters	Value
Similarity factor, δ:	2.08
Height, h:	4.9639 cm
Flare Angle, α	90°
Maximum iterations, N_{max}	4

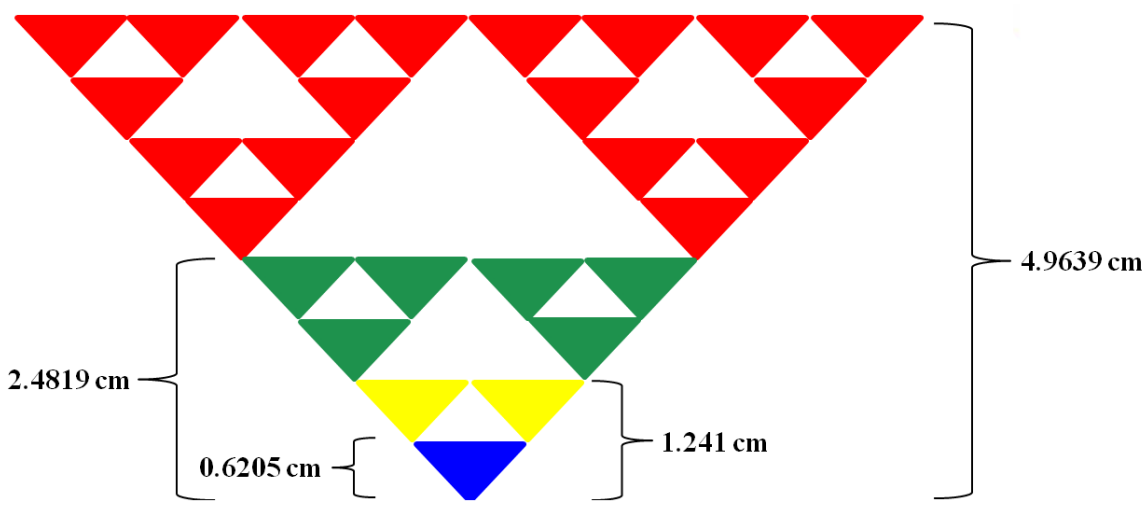

Figure 3.3 Height of Sierpinski Gasket Monopole Antenna with a 90° Flare Angle

The monopole Bow-tie antennas will be copies of the second and third iterations of each of the Sierpinski Gasket Monopole antennas (Figure 3.4 and 3.5). This will allow for the comparison in performance of the bow-tie antenna and how it is affected by the Sierpinski shape when the bow-tie element is inserted into the fractal pattern.

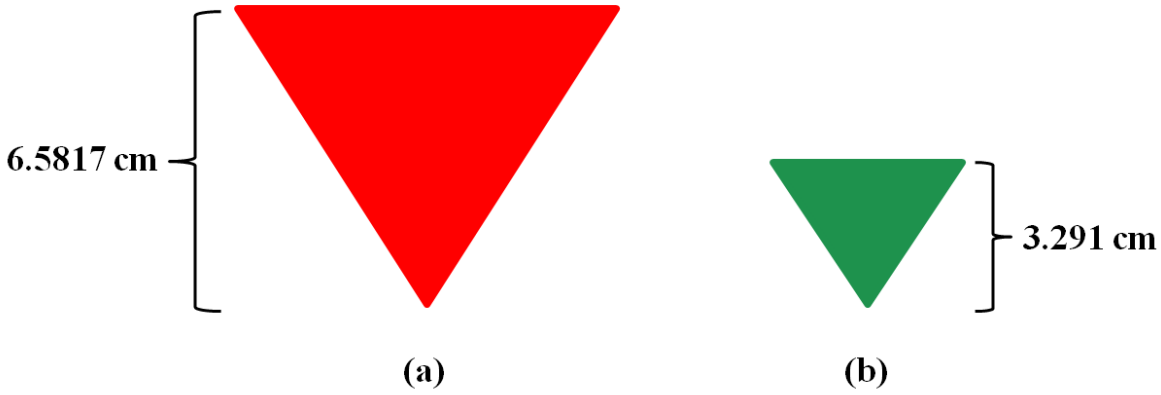

Figure 3.4 Height of Monopole Bow-Tie Antenna with a 60° Flare Angle
a) 2.4 GHz Antenna b) 5 GHz Antenna

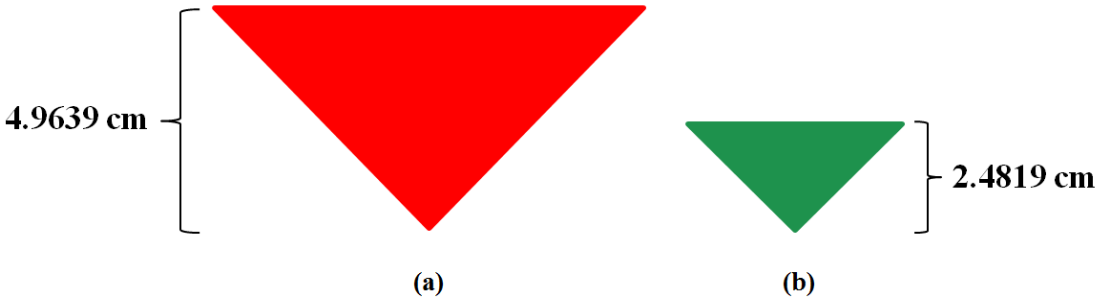

Figure 3.5 Height of Monopole Bow-Tie Antenna with a 90° Flare Angle
a) 2.4 GHz Antenna b) 5 GHz Antenna

3.5 Simulations

When the antennas' dimensions and material characteristics were calculated, the design was then simulated. The point of simulating allows for the user to see the antenna operate prior to construction in an ideal environment with no uncontrolled variables. There are many software suites available for simulating RF systems. For this work simulations were conducted with the Sonnet Suite. Each design was simulated and then the dimensions were revised to meet the required design frequencies. The initial dimensions that were calculated were simulated first. Over the course of a few simulation cycles, the designs of each antenna were finalized by confirming the right output frequencies in the S11 simulation (Figure 3.6, 3.7, 3.8, 3.9, 3.10, and 3.11). The only simulation that looked questionable was the S11 readings for the 90° Sierpinski Gasket Monopole and the 2.4GHz 60° Bow-Tie antenna.

The 2.4GHz band for the fractal antenna had a return loss of -8 dB which means the simulated antenna is only transmitting 85% of the total power of the signal. The 2.4GHz Bow-Tie antenna has a return loss of -7.8 dB which means that the antenna is

transmitting about 84% of the total signal power. While these return loss readings were questioned, the final simulations for all six antennas were within 5% of the design frequencies. The bandwidths for all six antennas were within 200MHz, which is phenomenal when looking for accuracy in the output. After testing the designs, four of the six antennas had their initial sizes modified for fabrication. The two Sierpinski Gasket Monopole Antennas were kept the same size. It should be noted that the designs for the Sierpinski Gasket Monopoles were only simulated and did not have their sizes changed in order to see how the initial design created with Puente's equation would perform in real life. The four Bow-Tie antennas were all modified slightly, which is reflected in the section 3.5. After the antennas had the S11 parameters measured on the VNA, it was decided then if another revision needed to be made. If so, the antennas were modified based on past and present data and then constructed.

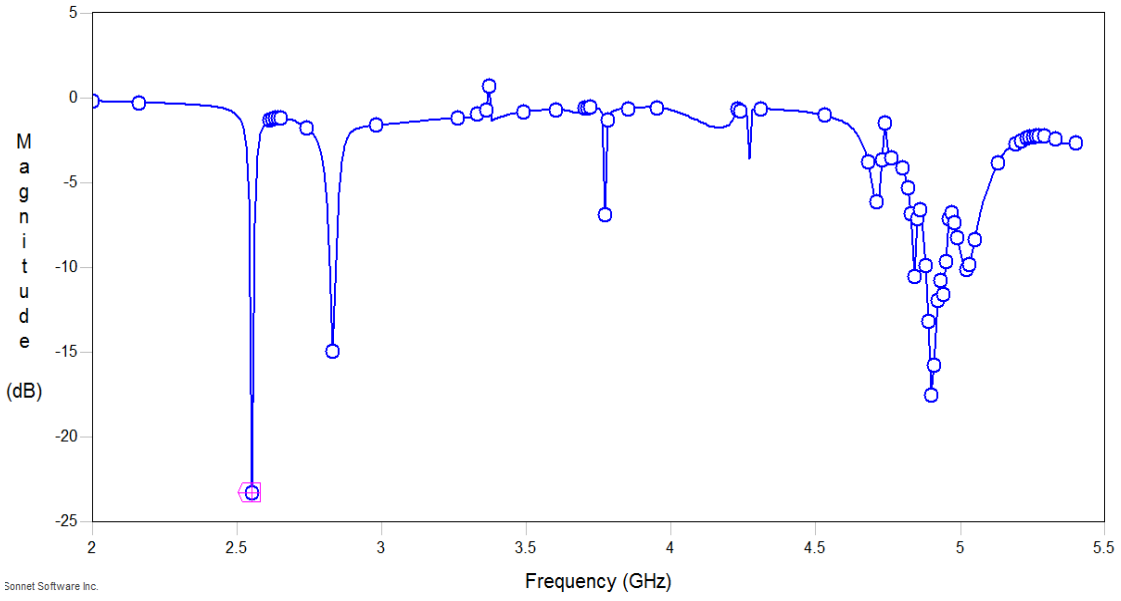

Figure 3.6 60° Sierpinski Gasket Monopole S11 Simulation

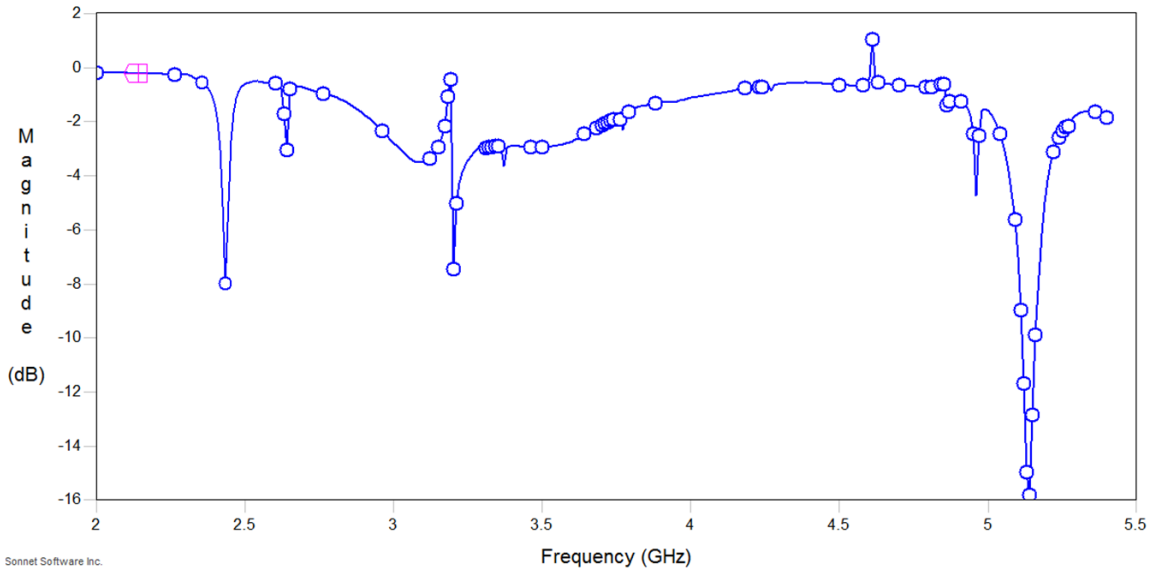

Figure 3.7 90° Sierpinski Gasket Monopole S11 Simulation

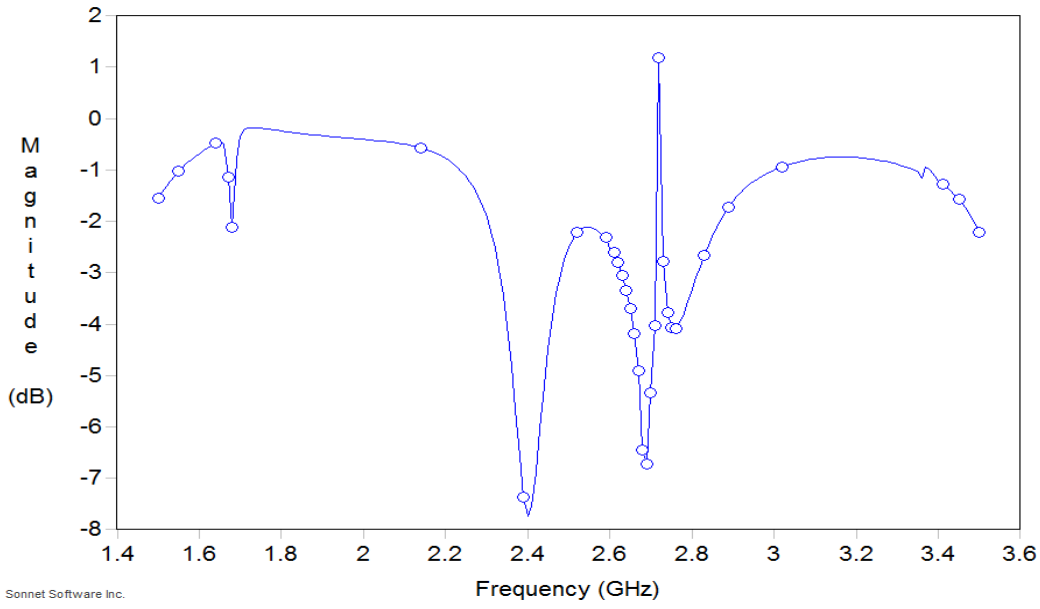

Figure 3.8 60° Bow-Tie Antenna (2.4GHz) S11 Simulation

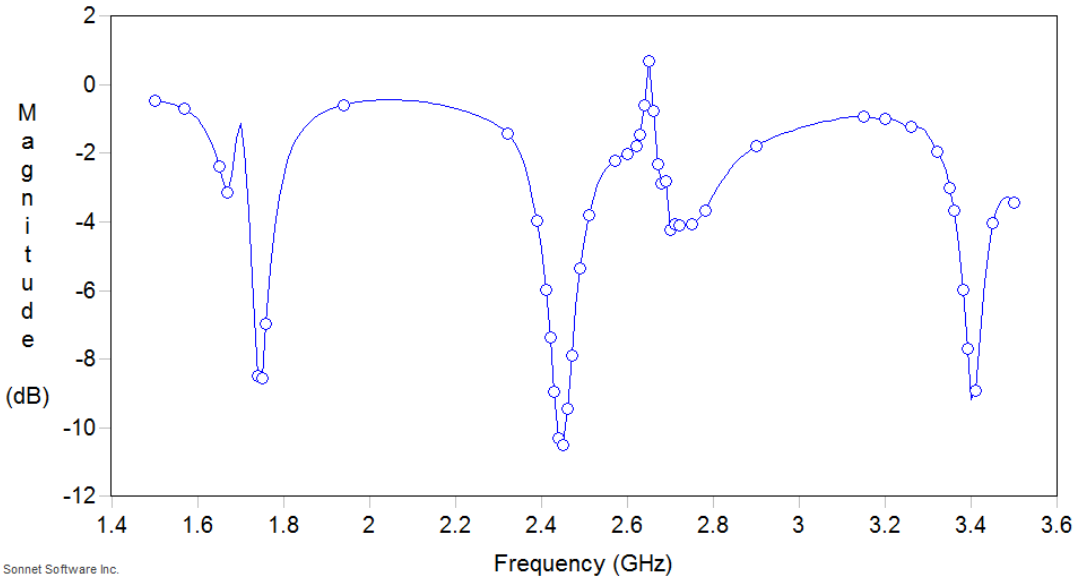

Figure 3.9 90° Bow-Tie Antenna (2.4GHz) S11 Simulation

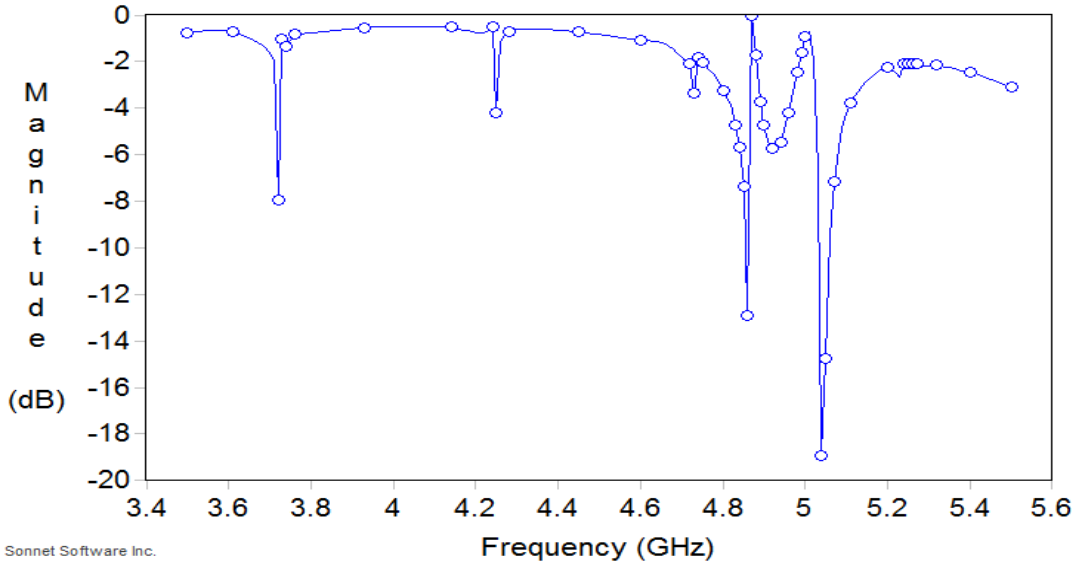

Figure 3.10 60° Bow-Tie Antenna (5GHz) S11 Simulation

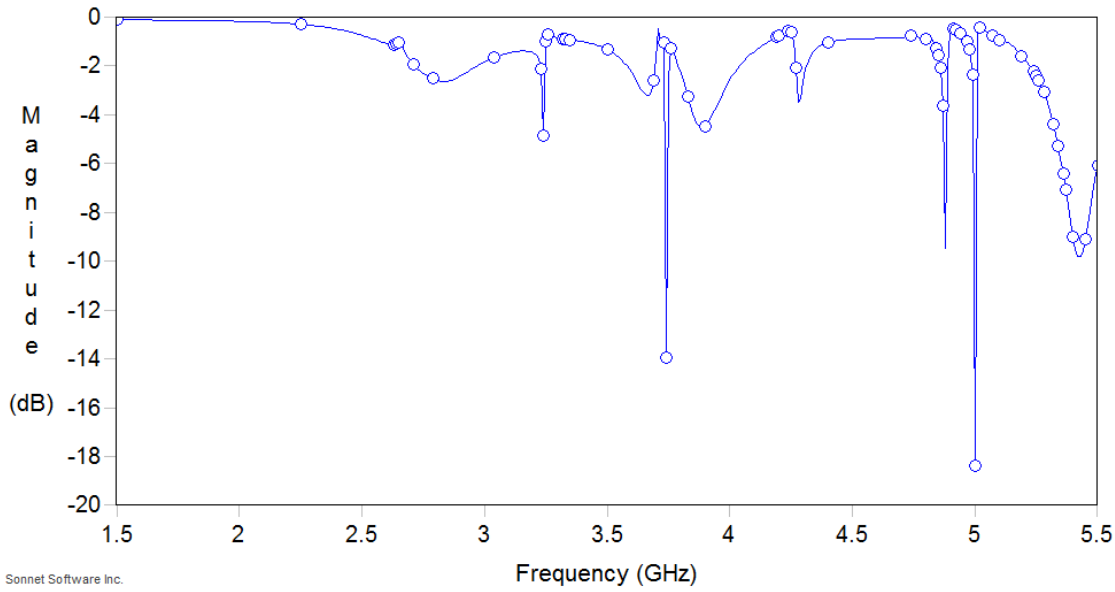

Figure 3.11 90° Bow-Tie Antenna (5GHz) S11 Simulation

3.6 Construction

The construction of the antennas was performed after the simulations yielded an antenna design that met the design specifications. The antennas were designed in a CAD design software called PCB artist, by Advanced Circuits, that specialized in PCB fabrication (Figures 3.12, 3.13, 3.14, 3.15, 3.16, and 3.17). The choice to send the boards off for fabrication instead of making them in the Purdue labs was because of the accuracy that was promised by Advanced Circuits. They were able to meet all of the specifications in resolution and quality that was needed. After the designs were finalized in the CAD program, the board schematics were sent to Advanced Circuits to be fabricated.

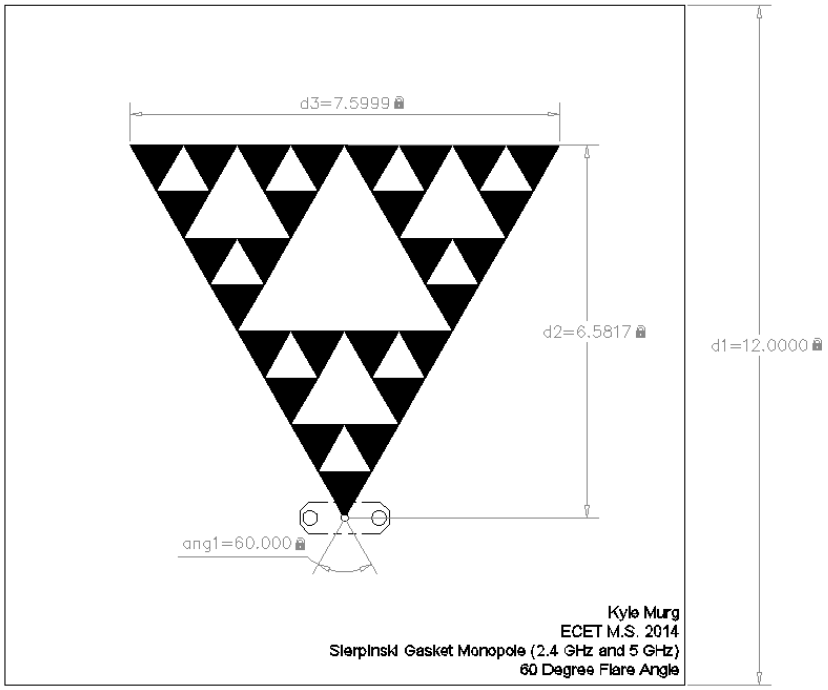

Figure 3.12 Proposed Sierpinski Gasket Monopole with a 60° Flare Angle Layout

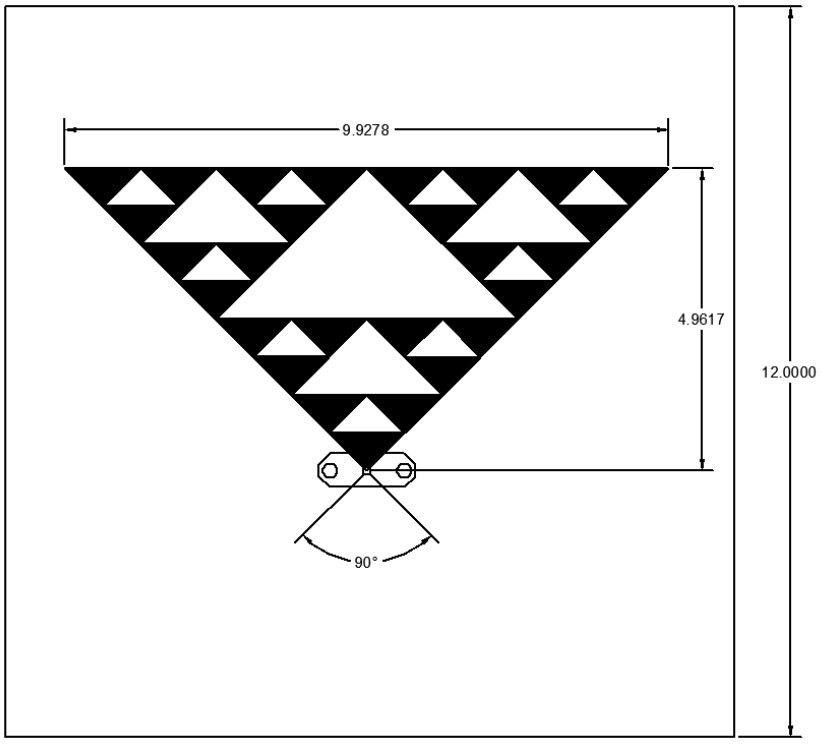

Figure 3.13 Proposed Sierpinski Gasket Monopole with a 90° Flare Angle Layout

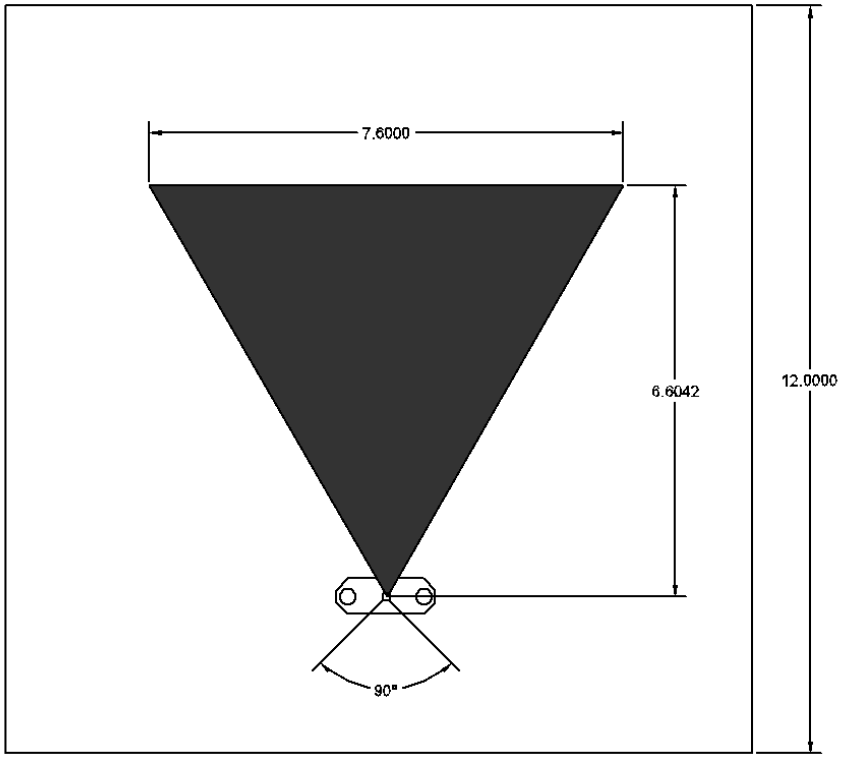

Figure 3.14 Proposed 60° Bow-Tie Antenna (2.4GHz) Board Layout

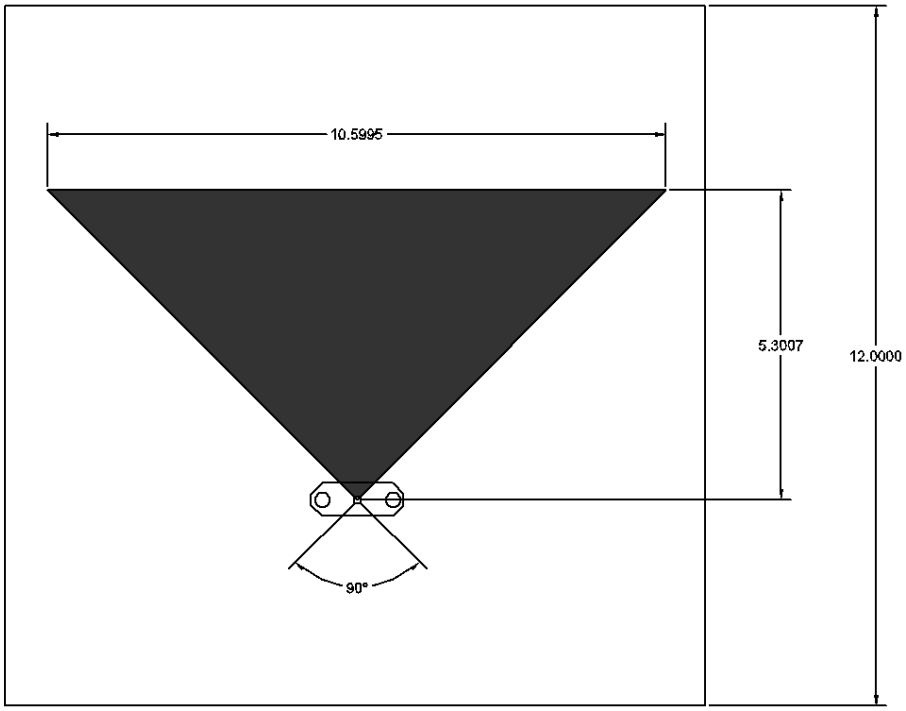

Figure 3.15 Proposed 90° Bow-Tie Antenna (2.4GHz) Board Layout

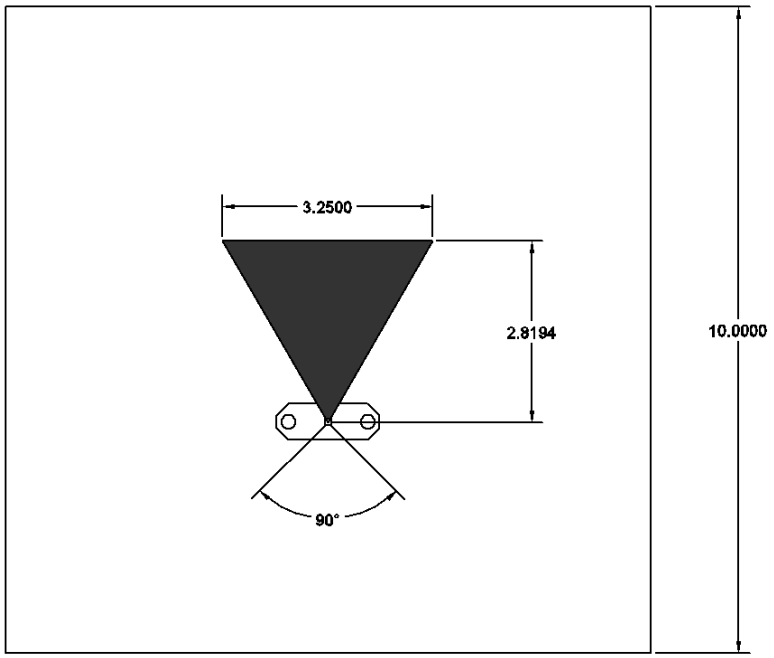

Figure 3.16 Proposed 60° Bow-Tie Antenna (5GHz) Board Layout

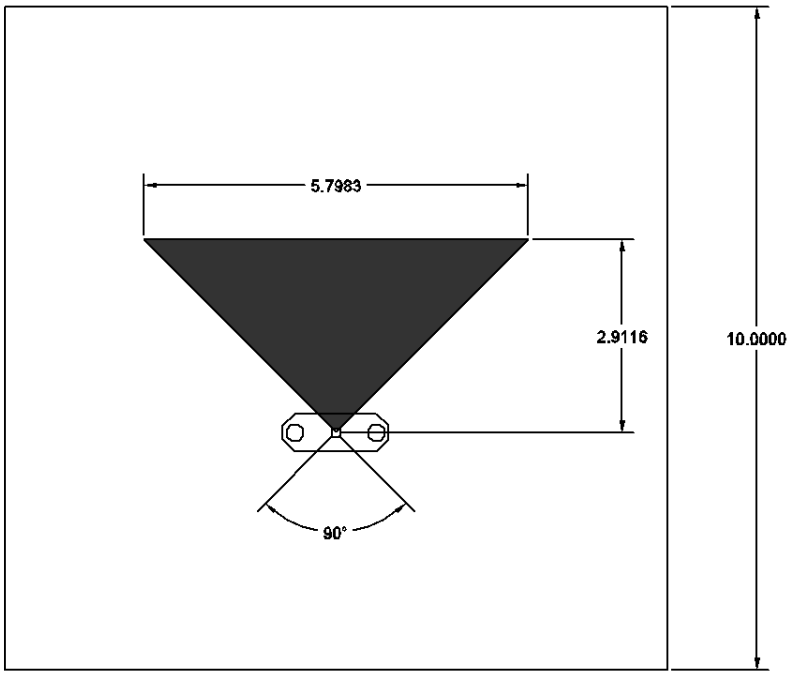

Figure 3.17 Proposed 90° Bow-Tie Antenna (5GHz) Board Layout

3.7 Physical Testing

The antennas were tested on a Vector Network Analyzer (VNA) for resonant characteristics by measuring the S11 and S21 scattering parameters (Sischka, 2002). S11 parameters show the frequency reflections of the antenna (return loss). The frequencies that don't reflect back are radiating from the antenna and thus are resonant frequencies. The VNA also displayed a Smith chart to measure the impedance of the antenna at each frequency in the frequency sweep. The Standing Wave Ratio was also measured.

The S21 parameters show the forward voltage gain of the antenna (Sischka, 2002). While measuring the S21 values, a known wideband antenna was connected to Port 2 of the VNA. The known wideband antenna had a wide spectrum that can measure the required frequency spectrum of this study. The performance characteristics are known for the control antenna which allowed for that data to properly represent the performance of each of the test antennas. The known antenna was connected to port 2 of the vector network analyzer. The test antenna was connected to port 1. The VNA was set to measure the desired frequency range and the two antennas were set at a known distance apart from each other. The S21 data was recorded from the VNA (Figure 3.18). The antenna gain was calculated using Friis Transmission Equation (Eqn. 2.7). The next step in the experiment was to analyze the radiation pattern of the antennas. The antenna was moved around an origin point allowing for all sides of the antenna to be measured and then plotted. In chapter 4, these tests are detailed as to how the antennas performed in a real life scenario.

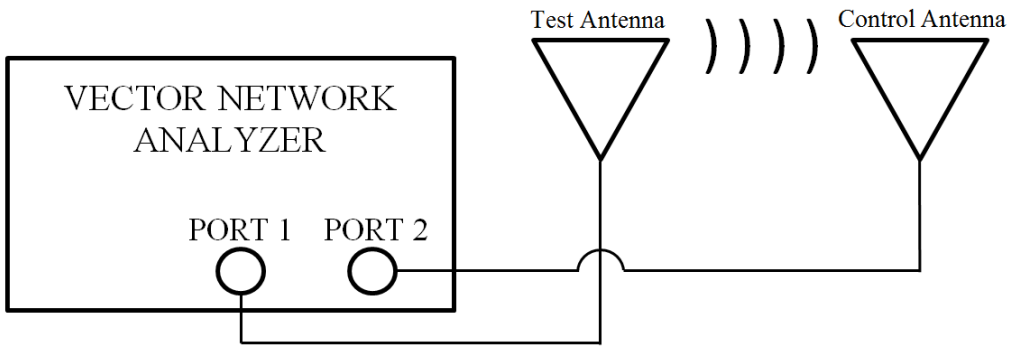

Figure 3.18 Block Diagram of S21 Verification Tests

CHAPTER 4. RESULTS AND EVALUATION

This chapter discusses the testing process and results of the six antennas that were designed for the experiment. As discussed in chapter 3, both a 90° and 60° Sierpinski Gasket Monopole antenna were designed using Puente's equation (Eqn. 2.15). Two iterations for each antenna were also designed to compare the performance of the single band antennas to the multiband fractal antennas. After the initial designs were finalized they were sent off to Advanced Circuits to be manufactured. To prove that the antennas worked correctly a test procedure had to be created. First, the S11 parameters had to be measured. Then, revisions would be made to the antennas until they performed well at the desired frequencies. Next, S21 measurements were conducted to observe the gain of each antenna. Lastly, the radiation patterns were measured and plotted. Conclusions could then be made about how the Sierpinski Gasket Monopole antennas performed against the Single band Bow-Tie antennas.

4.1 S11 Measurements

In order to see if the antennas performed correctly they were connected to the Vector Network Analyzer (VNA) and had the S11 parameter measured. This test was used first to see which frequencies reflected back when transmitting a wide frequency range. The goal is to have the desired frequencies not reflect back thus having a very low measurement (in decibels) at those frequencies. The impedance and VSWR were also measured during the S11 tests (Table 4.1 and 4.2).

The impedance was measured while performing the S11 measurements. The smith chart was brought up on the Vector Network Analyzer display and then the impedance for each frequency band was recorded (Table 4.1). Each antenna was designed to have an impedance of 50Ω.

Table 4.1 *Antenna Impedance at the Design Frequencies*

Antenna Type	Impedance (Ω)
60° Sierpinski (2.4GHz)	42.545-j6.821
60° Sierpinski (5GHz)	34.071+j19.445
90° Sierpinski (2.4GHz)	60.527-j2.631
90° Sierpinski (5GHz)	53.646+j7.249
60° Bow-Tie (2.4GHz)	65.707+j1.75
60° Bow-Tie (5GHz)	52.765-j0.693
90° Bow-Tie (2.4GHz)	60.102+j23.137
90° Bow-Tie (5GHz)	33.318+j0.615

Table 4.2 *Antenna VSWR and Signal Power Measurements*

Antenna Type	Reflected Power (dB)	Reflected Power (%)	Transmitted Power (%)	VSWR
60° Sierpinski (2.4GHz)	-4.758	33.5	66.5	3.75
60° Sierpinski (5GHz)	-10.841	8.2	91.8	1.80
90° Sierpinski (2.4GHz)	-5.0325	31.4	68.6	3.55
90° Sierpinski (5GHz)	-21.721	0.7	99.3	1.18
60° Bow-Tie (2.4GHz)	-19.023	1.2	98.8	1.25
60° Bow-Tie (5GHz)	-34.195	0.04	99.96	1.04
90° Bow-Tie (2.4GHz)	-19.1253	1.2	98.8	1.25
90° Bow-Tie (5GHz)	-14.351	3.6	96.4	1.47

4.1.1 60° Sierpinski Gasket Monopole

The first antenna that was measured was the 60° Sierpinski Gasket Monopole. This was due to the fact that the initial equation was specifically designed for this design and that there were previous examples to compare with the results of this antenna. The initial design for the antenna was 7.6cm on each side of the overall antenna. The first S11 measurements for the 60° Sierpinski Gasket Monopole were very promising. The error of the 2.4GHz frequency measurement was within 2.5% off from the ideal value and the error of the 5GHz band was within 0.67% (Table 4.3). This proved that the equation worked correctly with the design but the 2.4GHz frequency was a little low (2.34GHz). After looking at the measurements it was concluded that the overall Sierpinski antenna was too large.

The second revision was decreased in overall size from 7.6cm to 7.55cm by taking all of the second iterations of the antenna and moving them 0.1cm closer to each other (Figure 4.1). The size of the 5GHz elements (second iteration) (Figure 3.1) were not changed but just moved. This revision, in theory, would affect the output by increasing the 2.4GHz signal band due to the overall size of the antenna decreasing. The S11 parameters were measured on the revised design and the data showed an improvement in the accuracy of antenna (Table 4.3). Like the hypothesis stated, the error at 2.4GHz decreased to 0.04% while the error of the 5GHz band increased slightly to 1.4%.

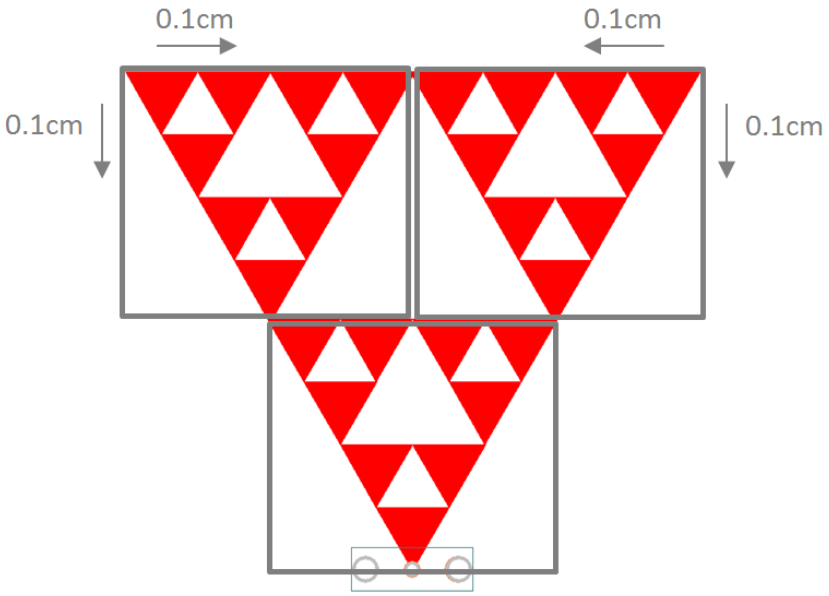

Figure 4.1 Revisions done to the 60° Sierpinski Gasket Monopole

The only area for concern was the level of the reflections at the design frequencies for the 60° Sierpinski Gasket Monopole. While the S11 at the 5GHz band was at -10.124 dB the S11 at the 2.4GHz was -4.758 dB. This means that at 5GHZ the signal was transmitting about 92% of the total signal power while the 2.4GHz band was only transmitting about 67% of the total signal power (Table 4.2). After conducting some research and looking back on Puente's past studies (Anguera, Puente, Borja, & Soler, 2004) it appears that the first iteration on the Fractal antenna seems to have less transmitted power compared to the other iterations in the pattern. A hypothesis can be made that the lack of power can be attributed possibly because the larger iteration has less total area of the conductive layer compared to the smaller iterative shapes. For example, the 2.4GHz element (first iteration) has an overall less percentage of conductive material than the 5GHz element (second iteration).

Overall, the S11 data for the 60° Sierpinski Gasket Monopole showed that the design did work and that the scaling allowed for a multiband performance at 2.4GHz and 5GHz (Figure 4.2).

Table 4.3 *60° Sierpinski Gasket Monopole S11 Measurements*

Rev	Exp Freq (GHz)	Meas Freq (GHz)	Freq Error (%)	Ref Loss (dB)	Exp Freq (GHz)	Meas Freq (GHz)	Freq Error (%)	Ref Loss (dB)
1	2.4	2.3400	2.50	-4.570	5	4.9665	0.67	-10.314
2	2.4	2.4010	0.04	-4.758	5	5.07	1.40	-10.841

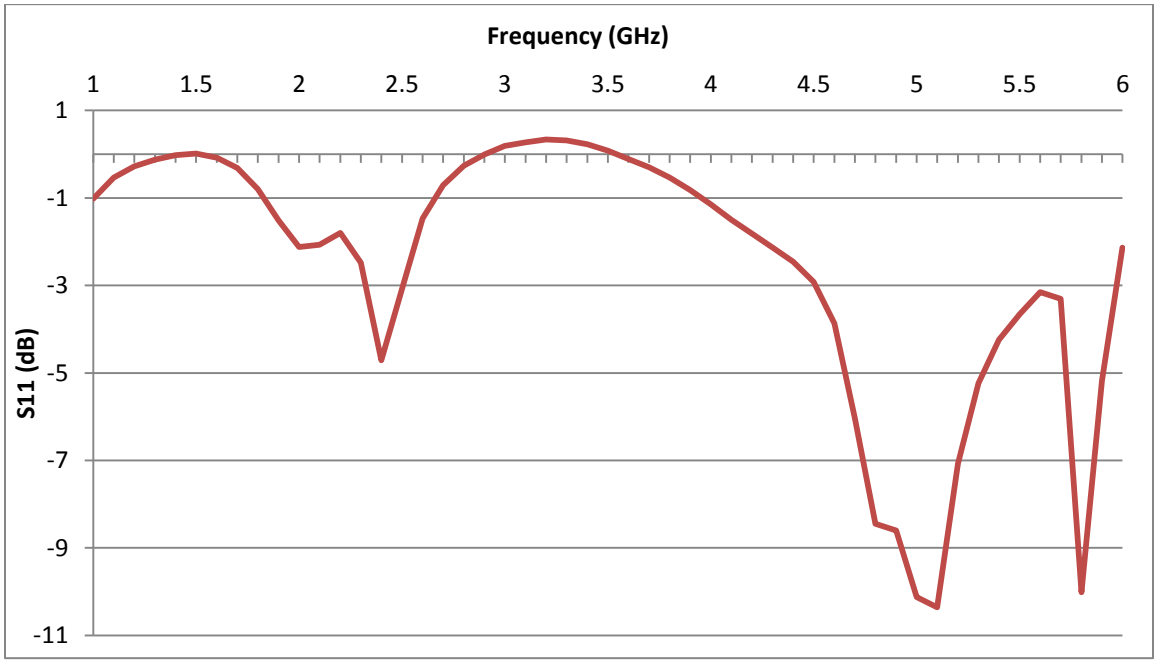

Figure 4.2 S11 Graph - 60° Sierpinski Gasket Monopole

4.1.2 90° Sierpinski Gasket Monopole

The next antenna that had the S11 parameters measured was the 90° Sierpinski Gasket Monopole. The same equation that was used for the 60° Sierpinski Gasket

Monopole was used for the 90° version. While conducting research on how to design the antenna it was mentioned by Puente that as the flare angle of the antenna is increased that the frequency can drift away from the designed frequency (Puente et al., 1998). To combat this problem the first antenna was made just utilizing the equation used previously (Eqn. 2.15). Then, revisions would be made after the original S11 parameters were measured to design an antenna that meets the design requirements.

The original design was 7.02cm on each leg of the antenna's triangular shape. The 5GHz element was 0.8775cm on each leg of the triangle. The antenna was measured and the S11 data showed large errors. Both the 2.4GHz and 5GHz frequency bands were too high with an error of 6.65% at the 2.4GHZ band and 12.07% at the 5GHZ band (Table 4.4). To correct the problem the next revision increased the size from 0.8775cm on each leg to 0.9cm for each fourth iteration element in the antenna (Figure 3.1). This change also increased the total size of the antenna thus increasing the 2.4GHz element to output a lower frequency than what was initially measured. The second revision was measured and showed improvement but the size of the antenna was increased too much. Both frequency bands were 200MHz lower than the desired frequencies. The antenna error decreased to 7.44 % at the 2.4GHz band and 2.51% at the 5GHz band (Table 4.4). This showed progress but the design needed to have errors at least below 5%. The third revision had each fourth iteration element decreased from 0.9cm on each leg of the triangle to 0.89cm which also decreased the overall antenna. This allowed for the antenna to output a signal that was higher than the previous revision's output. The third revision showed significant improvements (Figure 4.3). The error for the antenna was only at 2% at the 2.4GHz band and 2.978% at the 5GHz band. Both of the frequency

bands also had good return loss at the desired frequencies (Table 4.4). The problem with the 2.4GHz return loss from the 60° Sierpinski Gasket Monopole was also visible in the 90° Sierpinski Gasket Monopole. However, the 5GHz return loss was excellent at -21.721 dB. When designing a multiband antenna there is a known trade-off that occurs with the performance when compared to a single band antenna. While they may not output a signal as powerful as a single band antenna the sierpinski gasket monopole can transmit two or more signals at decent levels.

Table 4.4 *90° Sierpinski Gasket Monopole S11 Measurements*

Rev	Exp Freq (GHz)	Meas Freq (GHz)	Freq Error (%)	Ref Loss (dB)	Exp Freq (GHz)	Meas Freq (GHz)	Freq Error (%)	Ref Loss (dB)
1	2.4	2.5595	6.65	-4.988	5	5.6035	12.07	-24.166
2	2.4	2.2215	7.44	-5.035	5	4.8745	2.51	-17.054
3	2.4	2.3519	2.00	-5.0325	5	5.1489	2.978	-21.721

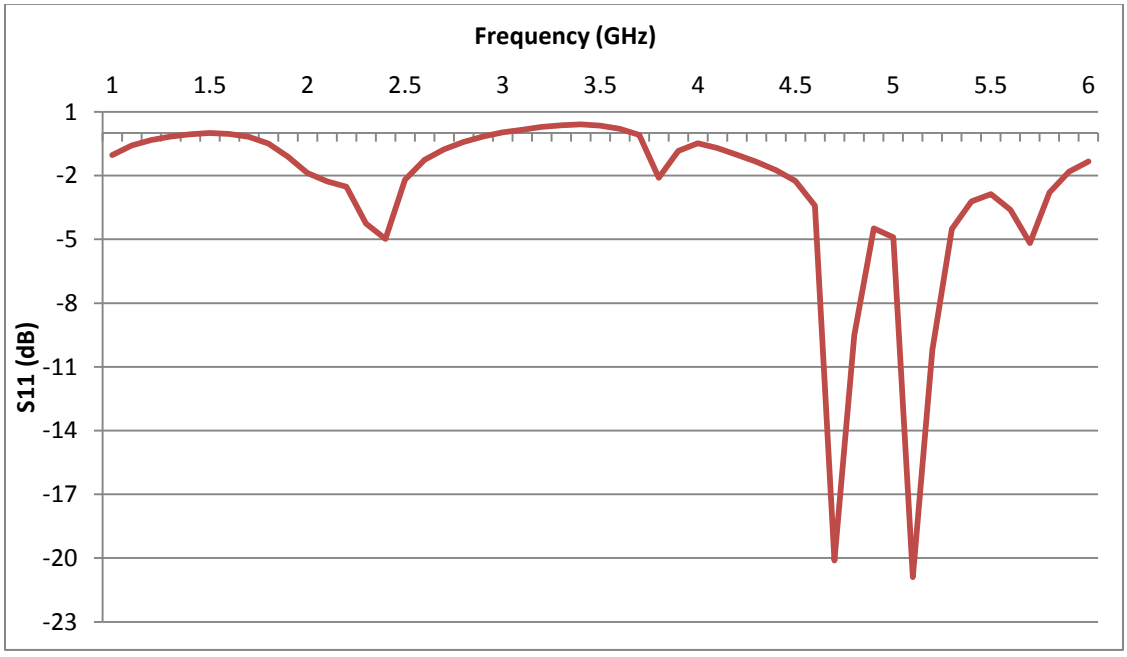

Figure 4.3 S11 Graph - 90° Sierpinski Gasket Monopole

4.1.3 60° Bow-Tie Antennas

The next S11 measurements were conducted on the 60° 2.4 GHz Bow-Tie antenna. The initial design for the bow-tie antennas were derived from each iteration of the initial Sierpinski Gasket Monopole antenna designs. Since the Bow-Tie designs were based off the initial fractal designs the same patterns occurred when measuring. The first Bow-tie antenna was 7.6cm in size. The measured S11 parameter for the antenna outputted a signal frequency that was too low for the designed ideal frequency with an error of 5.34% (Table 4.5). Just like the 60° Sierpinski Gasket Monopole the 60° 2.4GHz Bow-Tie antenna needed to be decreased in size in order to have a higher frequency output. The size of the Bow-Tie antenna was decreased form 7.6cm to 7.575cm. The second revision outputted better results when the S11 parameter was measured (Table 4.5). Since the 60° 2.4GHz Bow-Tie was a single band antenna it was expected to have a good return loss at the desired frequency. This proved true when the VNA showed that at 2.4GHz the antenna had a return loss of -19.023 dB which means that the signal was having more than 98% of its power transmitted (Figure 4.4) (Table 4.2).

Table 4.5 *60° Bow-Ties Antenna (2.4GHz) S11 Measurements*

Rev	Exp Freq (GHz)	Meas Freq (GHz)	Ref Loss (dB)	Freq Error (%)
1	2.4	2.2719	-18.823	5.34
2	2.4	2.3899	-19.023	0.42

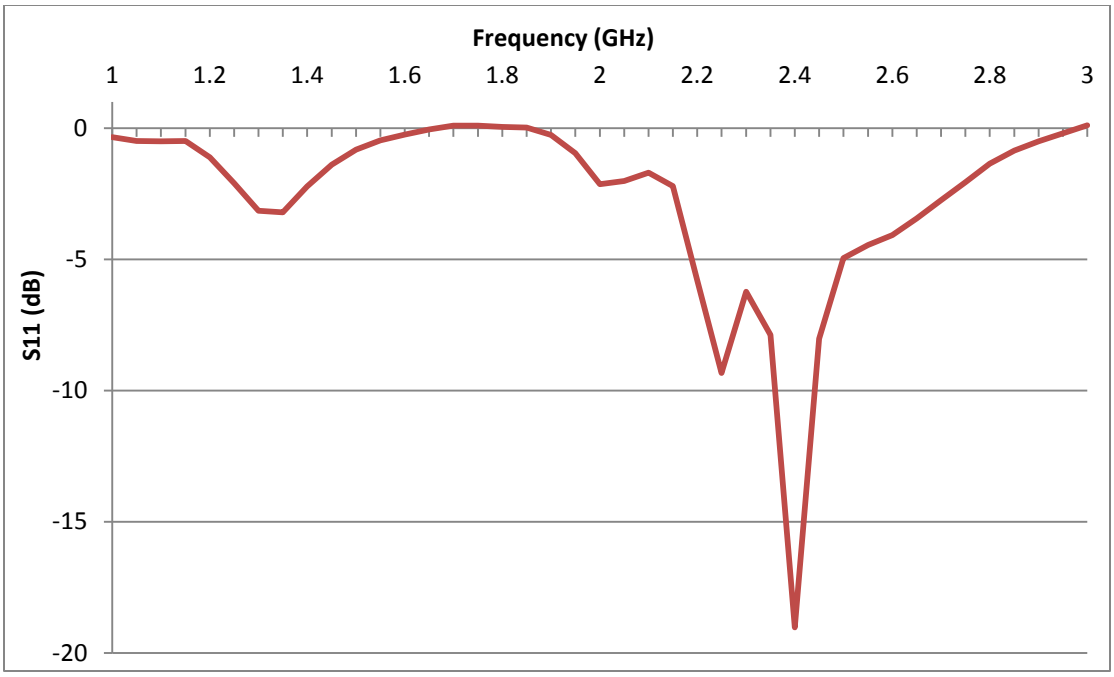

Figure 4.4 S11 Graph - 60° Bow-Tie Antenna (2.4GHz)

The 60° 5GHz Bow-Tie antenna showed the exact opposite pattern of error as the 60° 2.4GHz Bow-Tie antenna. The first design outputted a signal frequency that was higher than what was expected. The first antenna had an error of 2.91% (Table 4.6). The second design was slightly increased in size from 3.25cm to 3.35cm. The S11 parameter was then measured once again. The second revision performed correctly with the signal outputting at the designed frequency (Figure 4.5). The final revision for the 60° 5GHz Bow-Tie antenna had a return loss of -34.195 dB (Table 4.6).

Table 4.6 *60° Bow-Tie Antenna (5GHz) S11 Measurements*

Rev	Exp Freq (GHz)	Meas Freq (GHz)	Ref Loss (dB)	Freq Error (%)
1	5	5.1453	-20.353	2.91
2	5	5.0103	-34.195	0.21

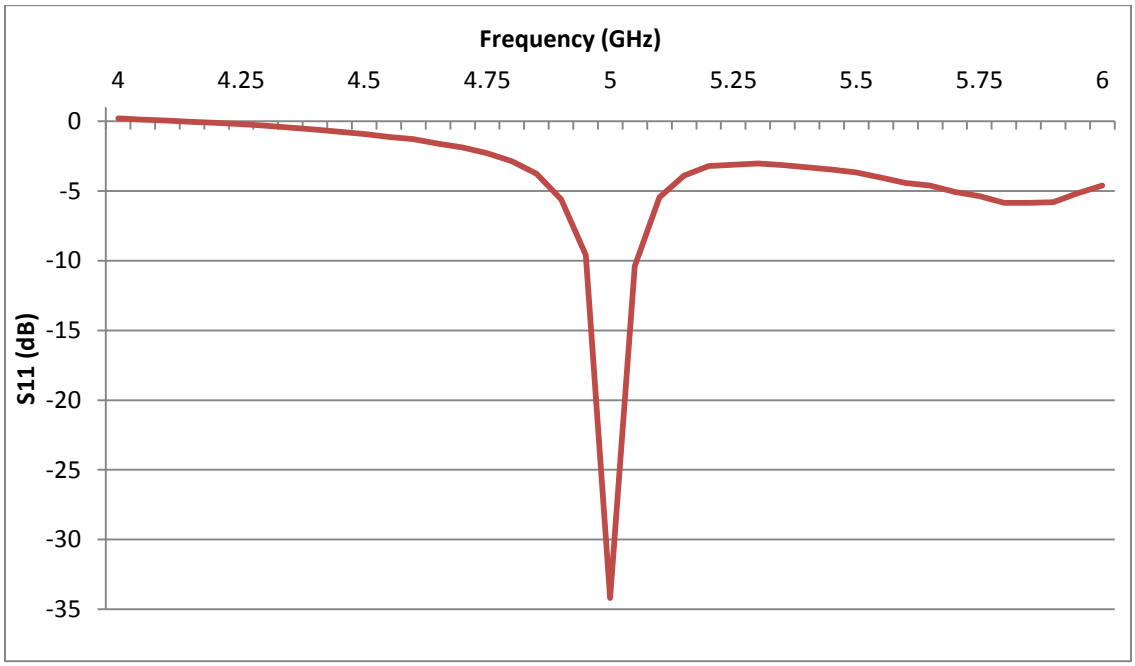

Figure 4.5 S11 Graph - 60° Bow-Tie Antenna (5GHz)

4.1.4 90° Bow-Tie Antennas

The 90° Patch Antennas followed the same error pattern as the 90° Sierpinski Gasket Monopole antenna. The original size of the 90° 2.4GHz Bow-Tie was 7.495cm on each leg of the triangle (sides other than the hypotenuse). When the S11 parameter was measured the results showed the signal was outputted at a lower frequency than what was expected. The 90° 2.4GHz Bow-Tie antenna had an error 10.61% (Table 4.7). The second revision was increased in size from 7.495cm to 7.55cm to decrease the output

frequency of the antenna. When the S11 measurements were conducted the antenna outputted a signal that was lower than what was expected but with a lower error (5.9%). In order to increase the output frequency the third revision was decreased in size from 7.55cm to 7.5cm. This revision was tested and showed good results (Figure 4.6). The 90° 2.4GHz Bow-Tie had an error of only 0.43% with a return loss of -19.153 dB (Table 4.7).

Table 4.7 *90° Bow-Tie Antenna (2.4GHz) S11 Measurements*

Rev	Exp Freq (GHz)	Meas Freq (GHz)	Ref Loss (dB)	Freq Error (%)
1	2.4	2.6546	-9.381	10.61
2	2.4	2.2584	-11.053	5.90
3	2.4	2.4104	-19.153	0.43

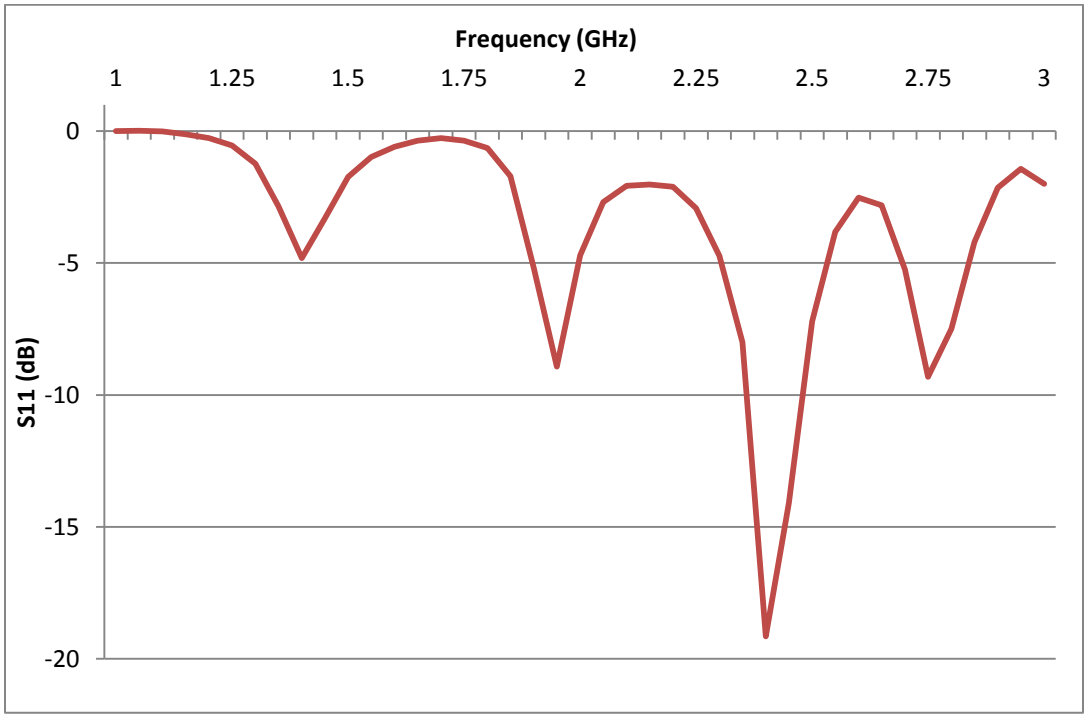

Figure 4.6 S11 Graph - 90° Bow-Tie Antenna (2.4GHz)

The initial 90° 5GHz Bow-Tie antenna design performed decently well. The first revision was 4.1cm long on each leg of the triangle. When the S11 parameter was measured, the 90° 5GHz Bow-Tie only had an error of 2.10% (Table 4.8). A second revision was made to see if the error could be decreased. This was done by decreasing the size of the antenna legs from 4.1cm to 4.0cm. The second revision was measured and performed better than the first design (Figure 4.7). The second revision of the 90° 5GHz Bow-Tie outputted a signal at 5.001GHz with a return loss of -14.351 dB (Table 4.8).

Table 4.8 *90° Bow-Tie Antenna (5GHz) S11 Measurements*

Rev	Exp Freq (GHz)	Meas Freq (GHz)	Ref Loss (dB)	Freq Error (%)
1	5	4.89959	-13.315	2.01
2	5	5.0010	-14.351	0.02

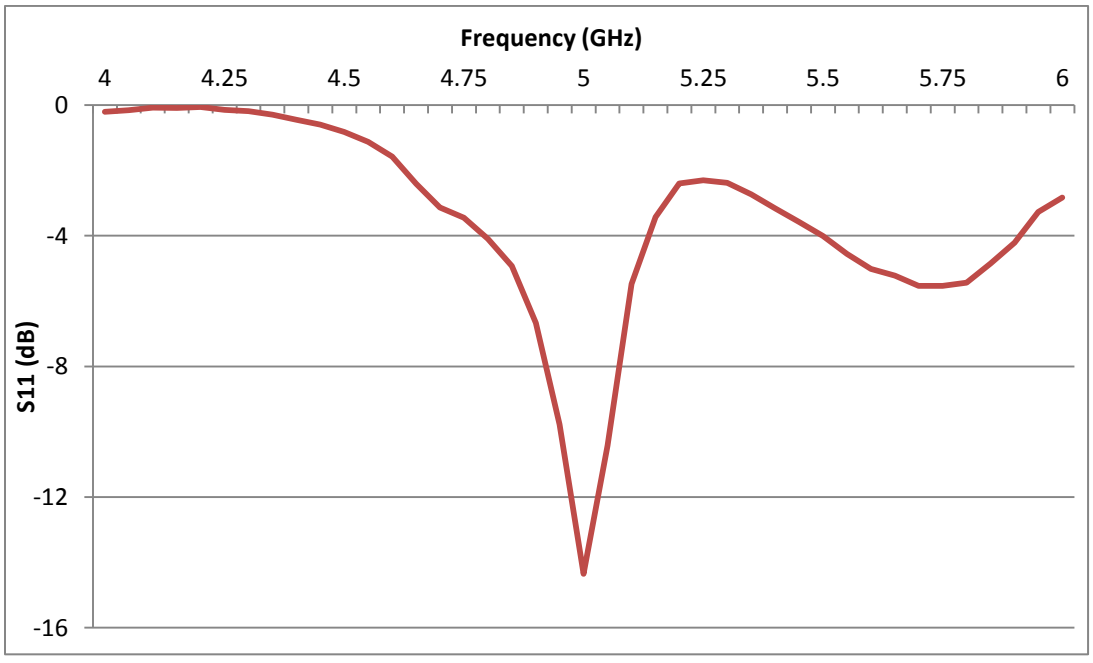

Figure 4.7 S11 Graph - 90° Bow-Tie Antenna (5GHz)

4.2 S21 Measurements and Radiation Patterns

The test antennas had to have the S21 parameter measured in order to figure out the gain of the antenna. To measure the S21 data, a control antenna needed to be used as the receiver antenna. For this experiment, a wide band Yagi-Uda antenna with a frequency range of 850MHz to 6500MHz was used. The data sheet stated the expected gain from the control antenna was about 6dBi. The test set-up consisted of connecting one of the test antennas to Port 1 of the VNA and connecting the control antenna to Port 2 (Figure 3.18). To figure out the distance between the two antennas, the far-field distance was calculated (Eqn. 2.6). After calculating the far-field distance for each antenna, it was determined that the test and control antennas had to be at least 0.38m apart from each other. In this experiment, the antennas were 0.6731m (26.5in) apart from each other. This distance was used later when calculating the gain. Once the S21 measurements were recorded, the Friis transmission equation was used to calculate the gain of each test antenna (Eqn. 2.7).

The expected gain for each of the test antennas was about 2dBi. After looking the S11 data it was apparent that the 2.4GHz bands for the Sierpinski antennas would probably not meet the goal of 2dBi due to having only around 67% of the signal power being transmitted.

After each of the S21 measurements were observed the radiation pattern was recorded for each antenna. This was performed by keeping the antenna at the same distance that was used for both the S11 and S21 measurements. The antenna was then rotated in 15° intervals until a complete circle was completed. At each interval the S21

level was measured and then the gain was calculated. Finally, all of the gains were normalized to 0 dB and then plotted.

4.2.1 60° Bow-Tie Antennas

The first antenna that was measured was the 60° Bow-Tie Antenna (2.4GHz) antenna. At the 2.4GHz band, the S21 was measured at -29.506 dB (Figure 4.8 and 4.9). The Friis Transmission equation calculated the gain of the antenna to be 1.078 dBi (Table 4.9). While the gain was not as high as the expected gain it was still good. This data point also showed that the other Bow-tie antennas should output similar gains due to the similar S11 levels each of the antennas shared.

Table 4.9 *60° Bow-Tie Antenna (2.4GHz) S21 Measurements and Gain Calculation*

Parameter	Value
Distance (m)	0.6731
λ (m)	0.12491
Receiver Antenna Gain (dBi)	6
S21 (dB)	-29.506
Transmitter Antenna Gain (dBi)	1.1078

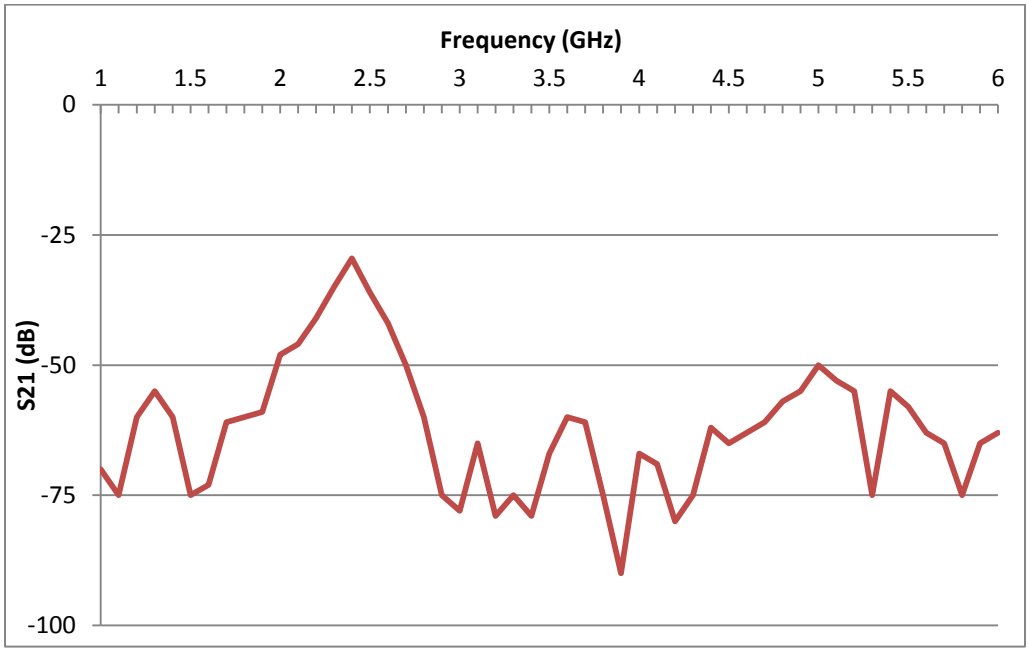

Figure 4.8 S21 Graph - 60° Bow-Tie Antenna (2.4GHz)

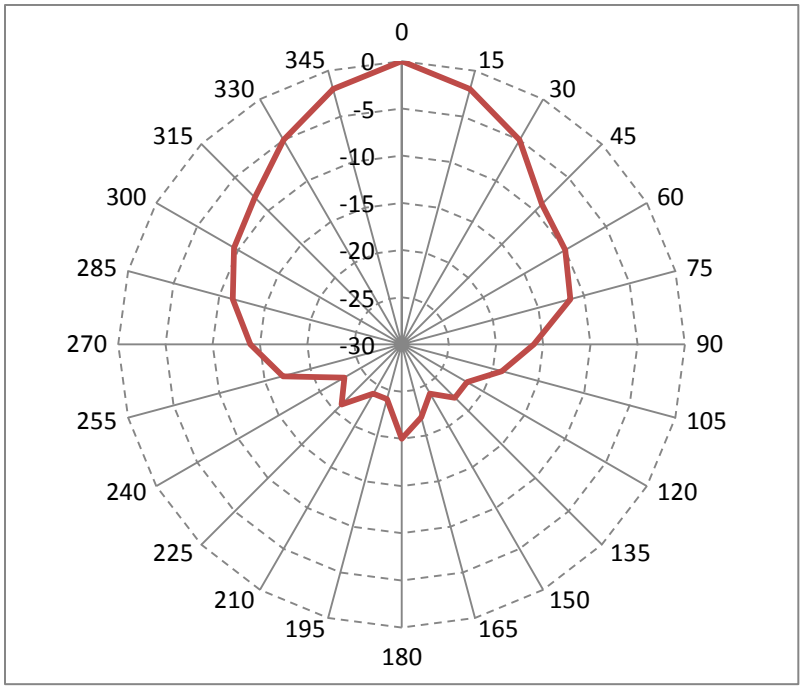

Figure 4.9 60° Bow-Tie Antenna (2.4GHz) Radiation Pattern

The next antenna that was measure was the 60° Bow-Tie Antenna (5GHz). The S21 parameter was measured at -35.259 dB (Figure 4.10 and 4.11). This was a lower S21 level than the 2.4GHz antenna but because the frequency has a shorter wavelength the gain of the antenna came out to be higher at 1.3896 dB (Table 4.10).

Table 4.10 *60° Bow-Tie Antenna (5GHz) S21 Measurements and Gain Calculation*

Parameter	Value
Distance (m)	0.6731
λ (m)	0.06
Receiver Antenna Gain (dBi)	6
S21 (dB)	-35.259
Transmitter Antenna Gain (dBi)	1.3896

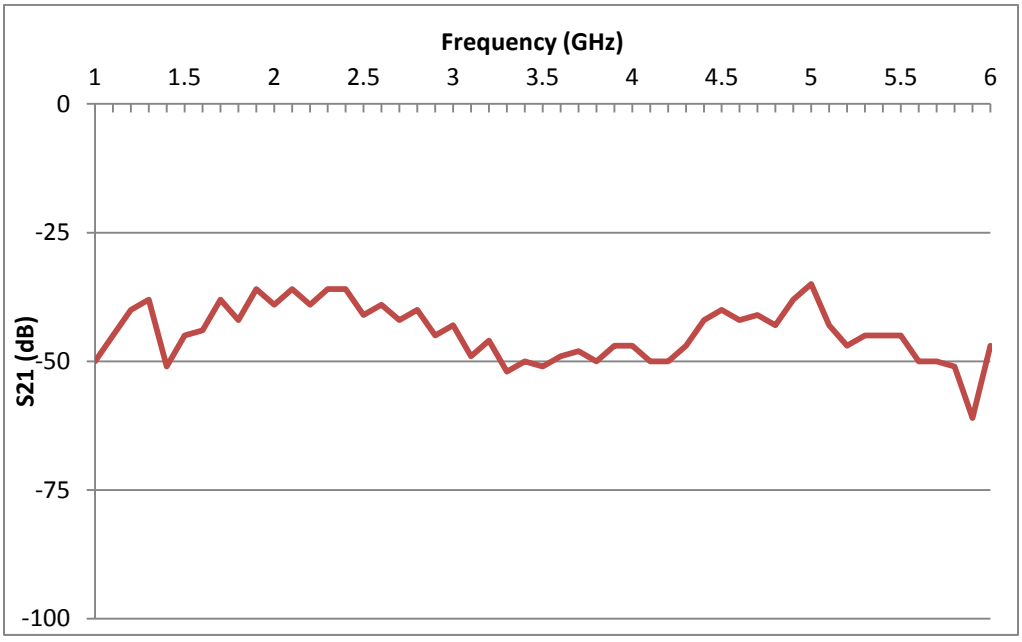

Figure 4.10 S21 Graph - 60° Bow-Tie Antenna (5GHz)

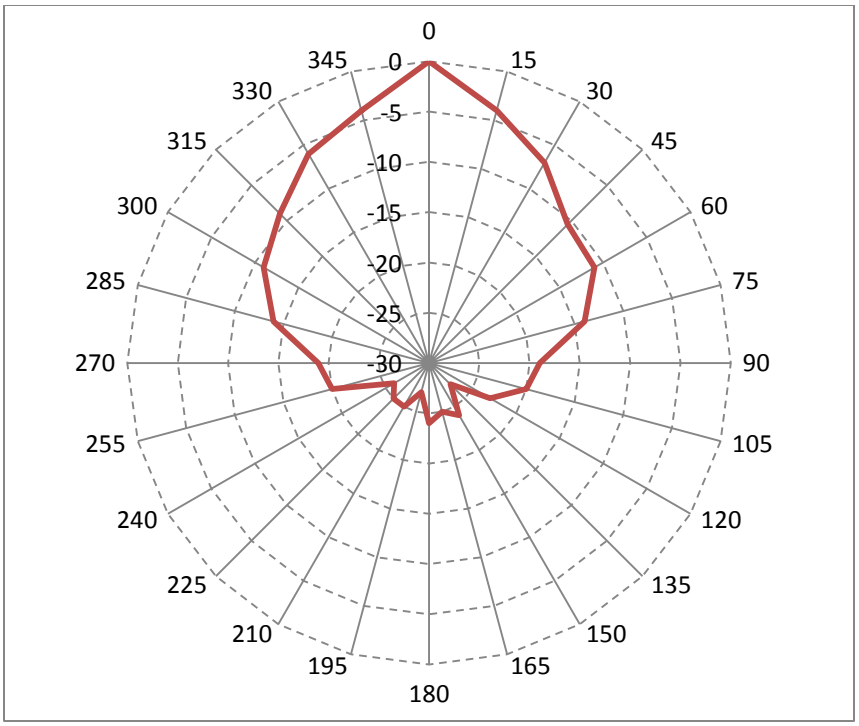

Figure 4.11 60° Bow-Tie Antenna (5GHz) Radiation Pattern

4.2.2 90° Bow-Tie Antennas

The 90° Bow-Tie Antenna (2.4GHz) had the S21 parameter measured next. Just like the 60° Bow-Tie Antenna, the 90° version also had about a -29.5 dB level (Figure 4.12 and 4.13). After calculations, the gain came out to be 1.0888 dB (Table 4.11).

Table 4.11 *90° Bow-Tie Antenna (2.4GHz) S21 Measurements and Gain Calculation*

Parameter	Value
Distance (m)	0.6731
λ (m)	0.12491
Receiver Antenna Gain (dBi)	6
S21 (dB)	-29.525
Transmitter Antenna Gain (dBi)	1.0888

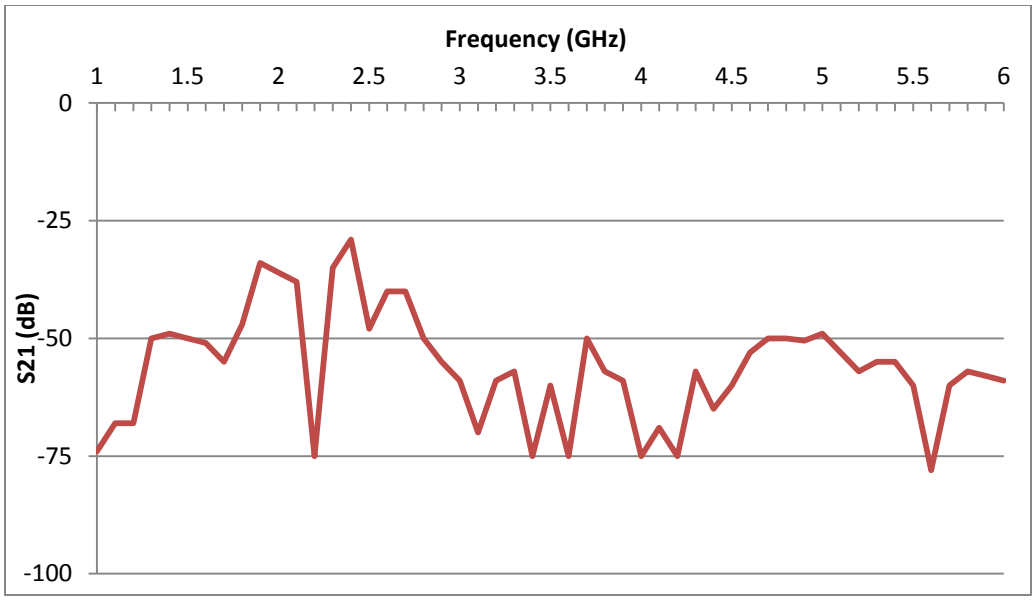

Figure 4.12 S21 Graph - 90° Bow-Tie Antenna (2.4GHz)

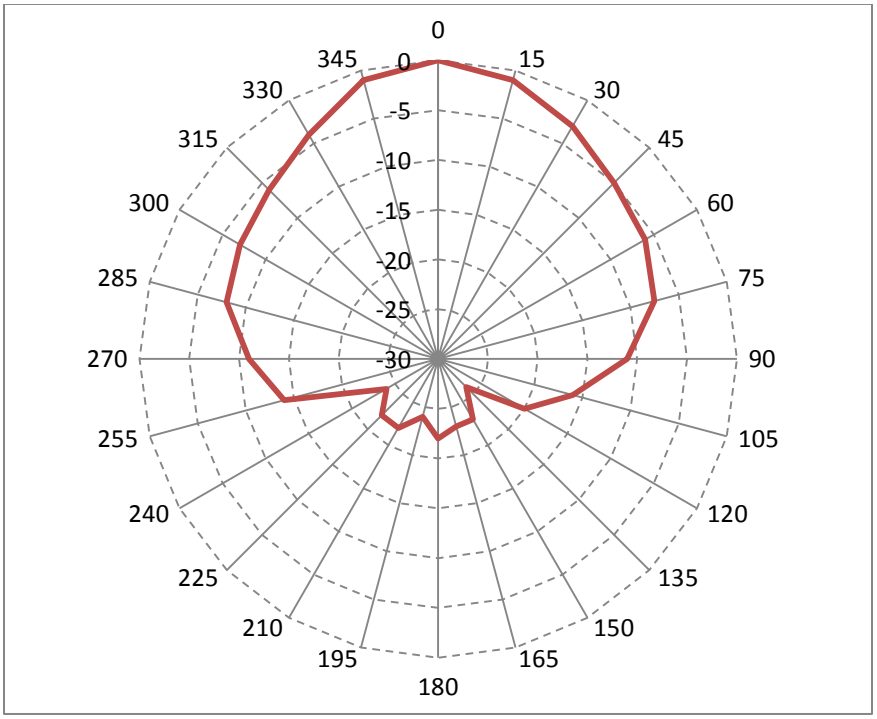

Figure 4.13 90° Bow-Tie Antenna (2.4GHz) Radiation Pattern

The last Bow-Tie antenna that was measured was the 90° Bow-Tie Antenna (5GHz). The S21 parameter was measured and came out to -35.202 dB (Figure 4.14 and 4.15). When the S21 data was put into the Friis Transmission Equation, the gain of the antenna was 1.4466 dBi (Table 4.12).

Table 4.12 *90° Bow-Tie Antenna (5GHz) S21 Measurements and Gain Calculation*

Parameter	Value
Distance (m)	0.6731
λ (m)	0.06
Receiver Antenna Gain (dBi)	6
S21 (dB)	-35.202
Transmitter Antenna Gain (dBi)	1.4466

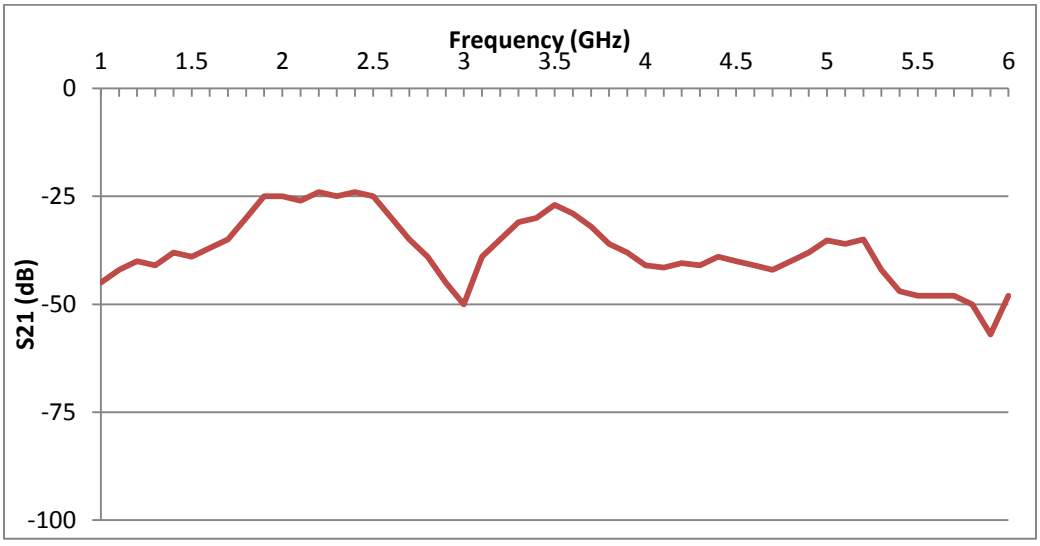

Figure 4.14 S21 Graph - 90° Bow-Tie Antenna (5GHz)

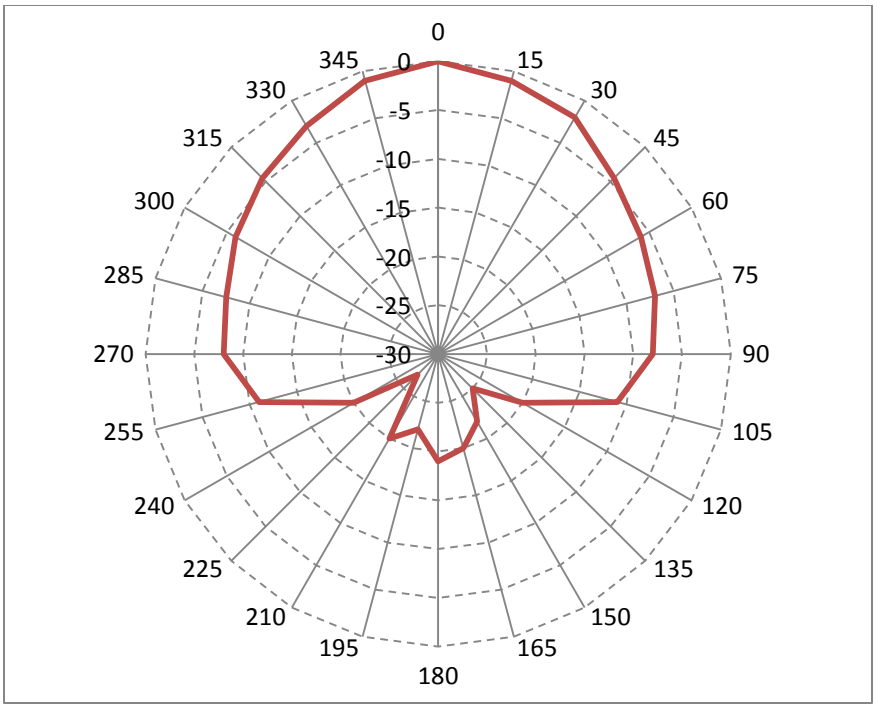

Figure 4.15 90° Bow-Tie Antenna (5GHz) Radiation Pattern

4.2.3 60° Sierpinski Gasket Monopole

The first multiband antenna that had the S21 parameter measured was 60° Sierpinski Gasket Monopole. The S21 levels for the fractal antenna were -30.268 dB at the 2.4GHz band and -36.856 dB at the 5GHz band (Figure 4.16, 4.17, and 4.18). Each S21 value was put into the Friis Transmission Equation and the gains were calculated. At the 2.4GHz band the gain was 0.3458 dBi and at the 5GHz band the gain was 0.1267 dBi (Table 4.13).

Table 4.13 *60° Sierpinski Gasket Monopole S21 Measurements and Gain Calculation*

Parameter	Value
Distance (m)	0.6731
λ 2.4 GHz (m)	0.12491
λ 5 GHz (m)	0.06
Receiver Antenna Gain (dBi)	6
2.4 GHz S21 (dB)	-30.268
5 GHz S21 (dB)7	-36.856
Transmitter Antenna 2.4 GHz Gain (dBi)	0.3458
Transmitter Antenna 5 GHz Gain (dBi)	0.1267

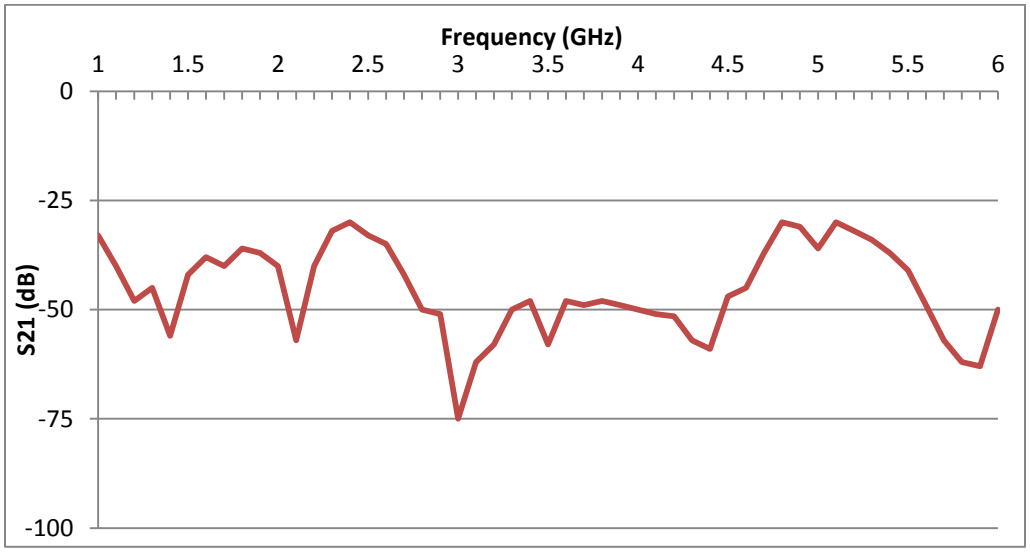

Figure 4.16 S21 Graph - 60° Sierpinski Gasket Monopole

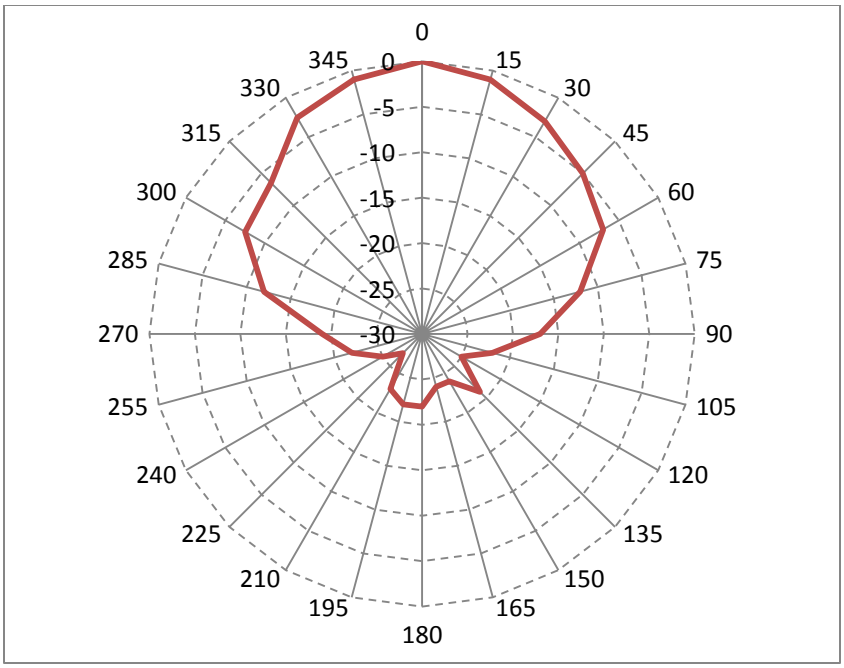

Figure 4.17 60° Sierpinski Gasket Monopole (2.4GHz) Radiation Pattern

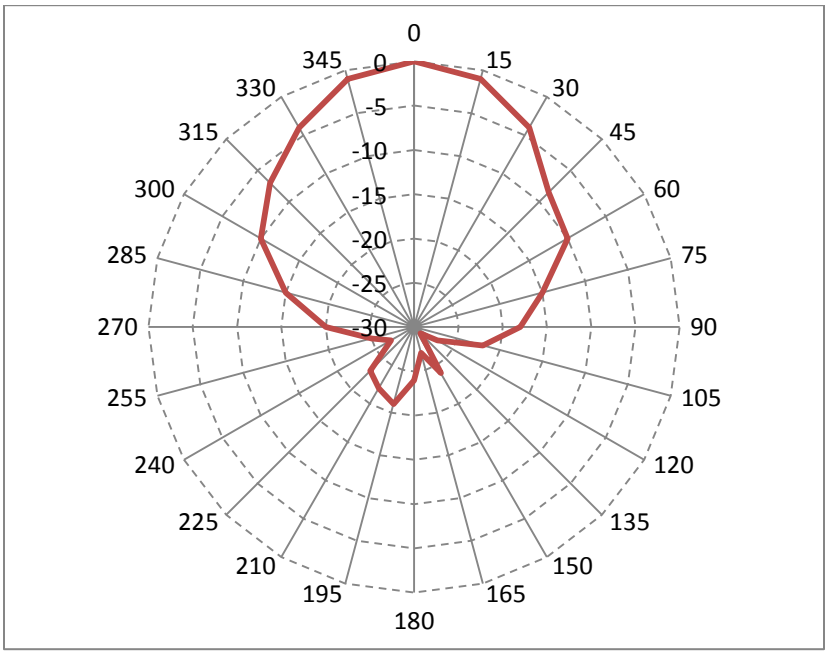

Figure 4.18 60° Sierpinski Gasket Monopole (5GHz) Radiation Pattern

4.2.4 90° Sierpinski Gasket Monopole

The last antenna to be measured was the 90° Sierpinski Gasket Monopole. The measured S21 parameter was -30.442 dB at the 2.4GHz band and -36.206 dB at the 5GHz band (Figure 4.19, 4.20, and 4.21). The two values were inputted into the transmission equation and the gains were 0.1718 dBi at the 2.4GHz band and 0.7767 dBi at the 5GHz band (Table 4.14).

Table 4.14 *90° Sierpinski Gasket Monopole S21 Measurements and Gain Calculation*

Parameter	Value
Distance (m)	0.6731
λ 2.4 GHz (m)	0.12491
λ 5 GHz (m)	0.06
Receiver Antenna Gain (dBi)	6
2.4 GHz S21 (dB)	-30.442
5 GHz S21 (dB)	-36.206
Transmitter Antenna 2.4 GHz Gain (dBi)	0.1718
Transmitter Antenna 5 GHz Gain (dBi)	0.7767

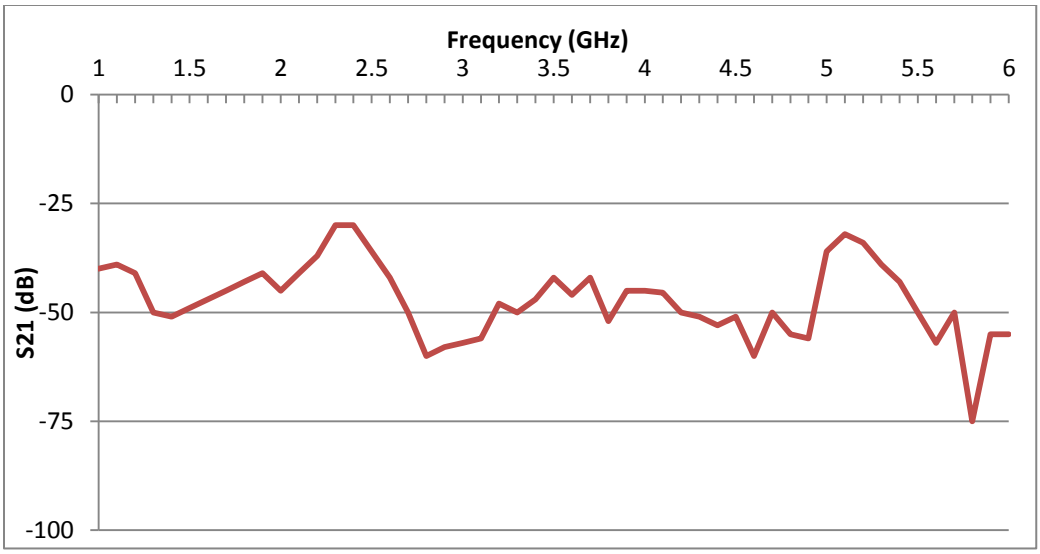

Figure 4.19 S21 Graph - 90° Sierpinski Gasket Monopole

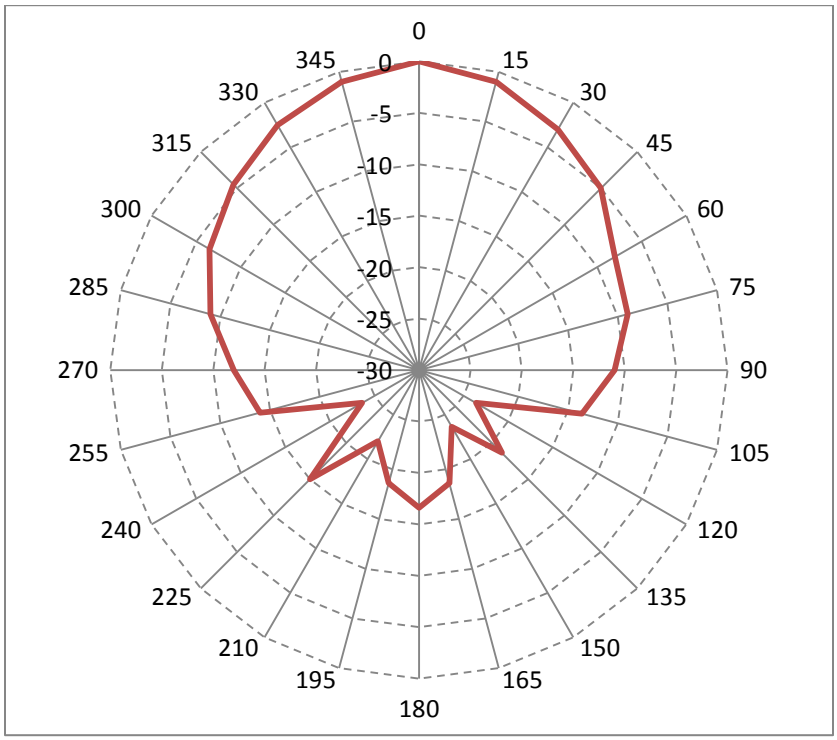

Figure 4.20 90° Sierpinski Gasket Monopole (2.4GHz) Radiation Pattern

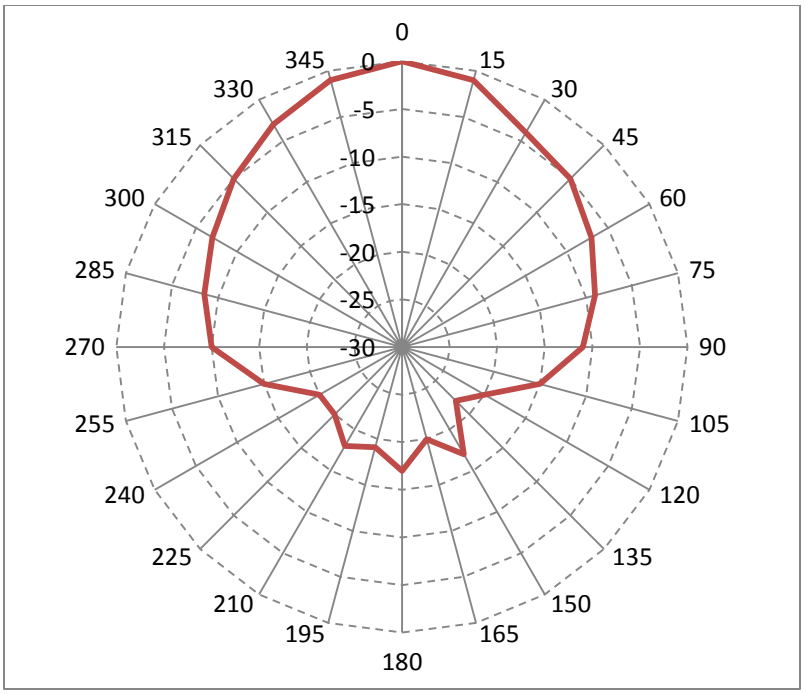

Figure 4.21 90° Sierpinski Gasket Monopole (5GHz) Radiation Pattern

CHAPTER 5. CONCLUSIONS AND FUTURE WORK

When evaluating the performance of each antenna, two parameters need to be observed. The S11 parameter showed the return loss of the antenna which indicates the percentage of power that is being transmitted at each frequency. A lower return loss means more power is being transmitted. The S21 parameter is the forward transmission coefficient of the antenna. By using the Friis Transmission equation, the gain can be calculated. The radiation pattern of the antenna shows the direction at which the antenna is transmitting the signal. After looking at all the variables, some conclusions can be made about the antennas along with some possible explanations on why some performance expectations were not met. The experiments performed in this work were designed to look at how the Sierpinski Gasket Monopole antennas compare to Bow-Tie antennas at the same frequencies and how the flare feed angle performance compared to each other.

5.1 Single Band vs. Multiband Performance Comparison

The measured S11 parameters that were tested partially explained the lack of performance that occurred later with the antennas gain. All four Bow-Tie antennas were expected to have very low return loss. These are single band antennas that should be performing very well at the frequency for which it was designed for. The tests showed

that this hypothesis was correct. Every one of the Bow-Tie antennas transmitted at least 96% of the total signal power.

The Sierpinski Gasket Monopole measured S11 parameters showed a less than expected output. The 5GHz band transmitted at least 92% of the total signal transmission power but the 2.4GHz band only transmitted around 67% of the total signal transmission power. As discussed in chapter 3, each antenna has trade-offs. The single band antenna, such as the bow-tie, can output a single frequency with a high gain. However, the multiband band antenna may have as high of signal gains but it can output multiple frequencies, unlike the single band antenna. There are many questions surrounding the low signal output with the 2.4GHz band on the Sierpinksi Gasket Monopole antenna. The problem might be attributed to a few factors in the design.

The first theory, as explained Chapter 4, is that the 2.4GHz element of the antenna has voids within itself which makes up the 5GHz elements. It is possible that the 5GHz elements are transmitting more power due to a high percentage of the element having copper instead of voids. When looking at the design it can be seen that the 2.4GHz element has only 25% of the entire shape covered in copper while 75% of it is void of copper (Figure 5.1). Compared to the 2.4GHz element, the 5GHz has 56.25% of its shape filled with copper with the other 43.75% void of copper (Figure 5.2). This could have possibly caused the decrease in signal power for the 2.4GHz band.

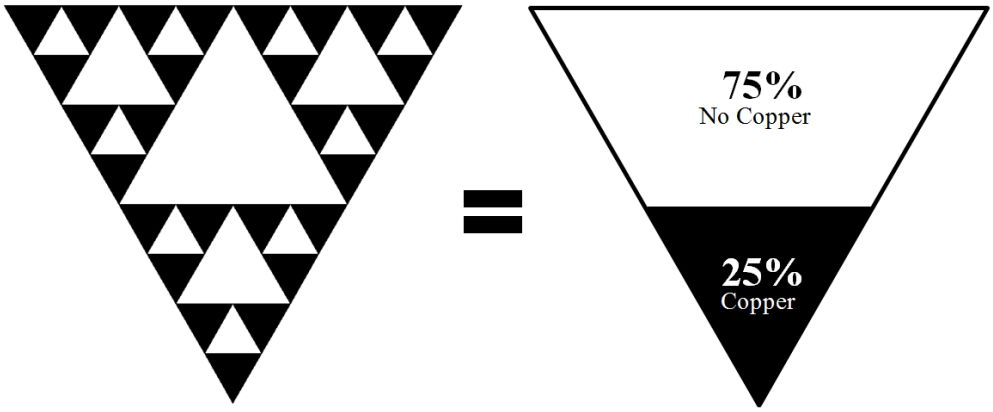

Figure 5.1 Percentage of Copper in the 2.4GHz element of the Gasket Monopoles

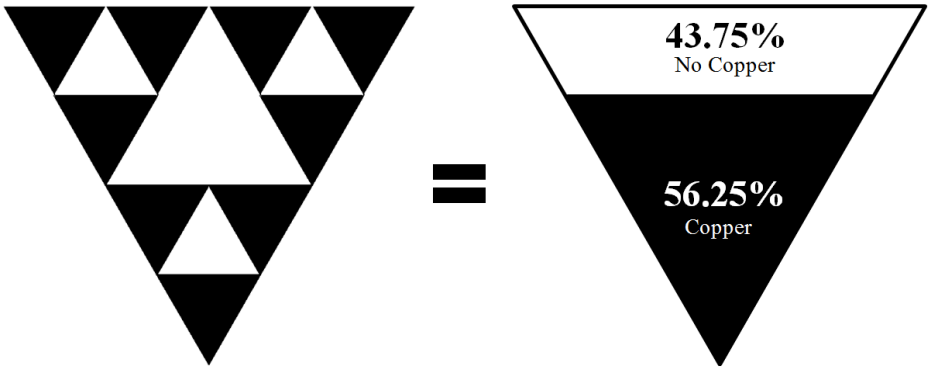

Figure 5.2 Percentage of Copper in the 5GHz element of the Gasket Monopoles

The second theory is that it could be a design error. After the S11 measurements were first performed on the fractal antennas, a second antenna design was simulated with the feed moved to the center of one of the smallest elements on the antenna. The simulation showed no difference in the S11 measurement. The design was also built and tested which reflected what the simulations showed. The next area that was looked at was the distance the antenna was from the edge of the PCB. If it was too close to the edge, the signal could be affected from the electromagnetic fringing field at the edge of the PCB. This design aspect was considered prior to the first boards being built but it had

to be re-visited. The original antennas were designed to be at least 6 times the thickness of the board away from the edge. Simulations were conducted with a larger overall board to see the affect but it showed no differences in transmission power.

The final theory could be how the solder mask on the antenna is affecting the signal. After more research on the topic it was decided that the solder mask most likely did not have an effect on the poor signal transmission. Usually the impedance of the antenna won't be affected by more than 2Ω when the solder mask is less than 4 mils thick (Norfolk, 2006). Manufacturers, like Advanced Circuits, use a 0.5 mil solder mask which should have little influence on the antenna. This also should not have had an effect on the design due to the boards being tweaked in the second (and third) revisions to output closer to the designed frequency which also corrected the impedance accordingly.

Puente's work differed from this project with the size and materials that were used in the experiment (Puente-Baliarda et al., 1998). With Puente's previous work, a CuClad substrate ($\varepsilon_r = 2.5$) was used with a thickness of 1.588mm. This thick substrate with a lower relative permittivity allowed for the same size of the antenna as this experiment but with the ability to output lower frequencies (0.52GHz and 1.74GHz). This can be seen by looking at the designs of both antennas. The second iteration of Puente's antenna outputs a lower frequency (1.74GHz) but is smaller than the 2.4GHz iteration of the antenna from this experiment (Figure 3.1). This reduction in size could have attributed to less error in Puente's experiment. While the dielectric area ratio for the antennas was the same for both experiments, the size of the antenna allowed for more possibilities for errors in this study due to the larger size. A larger antenna length will have more error

build up throughout the system. The smaller antenna will have error but it will not have as much build up throughout the system due to less length to do so.

By reviewing Puente's work, it can be seen that the first iteration does not perform as well as the other iterations in the antenna. In his first work, the S11 data for the first iteration showed the return loss at -10 dB while the second iteration was -14 dB and the third iteration was -24 dB (Table 5.1). This might be a reoccurring problem within the type of antenna that might need to be looked into more in another study.

Table 5.1 *Sierpinski Measurements of Puente's Study (Puente-Baliarda et al., 1998)*

Band	Freq (GHz)	h (cm)	S11 (dB)
1	0.52	8.89	-10
2	1.74	4.45	-14
3	3.51	2.23	-24
4	6.95	1.11	-19
5	13.89	0.55	-20

The S11 measurements that were taken were able to predict the results that came from the S21 measurements and gain calculations. After the initial S11 readings it was expected that the Sierpinski Gasket Monopoles would have a lower gain than the single band antennas. It was just a matter of how low would the gain be. The goal was to have each antenna at least have a gain between 1 – 2 dBi. When the initial gains were calculated between 1 – 1.5 dBi for the Bow-Tie antennas it was predicted that the fractal antennas would probably have gains lower than 1 dBi due to the S11 readings. While the gains were not as good as expected for the Sierpinski Gasket Monopole antennas it still showed that the antennas were working correctly. They were still transmitting a signal above 0 dBi at the correct frequencies.

The gains in this experiment cannot be compared to Puente's experiment due to the fact that gains were not discussed in the previous work. By observing the similarities of the S11 parameters in the previous work it showed very similar performance amongst both studies. The S11 readings in this work showed, as expected, that the single band antennas were always going to have a higher gain due to the fact that they were designed strictly for that one frequency while the Sierpinski Gasket Monopoles had a design trade-off that allowed each antenna to output two frequencies but with less signal gain than the single band antennas. They still outputted signals within 1dBi of the single band frequencies which showed that this antenna design can be an adequate substitute for the two single band elements.

5.2 Flare Feed Comparison

Along with comparing the single band versus multiband performance, the experimental data showed how the feed flare angle affected the antennas performance. During the design process for the Sierpinski Gasket Monopole it was known through research that the impedance would be affected based on the flare angle causing a frequency shift between the 60° and 90° designs. This frequency shift was seen in the initial design for the 90° fractal design. The frequencies were shifted by 150MHz and 200 MHz at the 2.4 GHz and 5GHz band respectively. This was expected based on research conducted in chapters 2 and 3. As explained in chapter 3, the increase of the flare angle changed the impedance of the antenna. To get the correct output frequencies, the overall size was changed, which also changed the impedance.

The other difference between the two Sierpinski Gasket Monopole antennas was the radiation patterns for each frequency band. Like the single band radiation patterns of the 90° design, the Sierpinski Gasket Monopole had a larger radiation pattern than the 60° antennas did. All three 60° antennas had a major drop-off in power after the antenna was turned more than 30° in either way of the control antenna, thus the smaller beam indicated that the 60° antennas were more directional than the 90° antennas. This may have occurred due to the wide shape of the 90° antennas having a wider range to transmit from all angles. The 60° antennas were more compact and might have had less range to transmit the omnidirectional signal. While the flare angle did affect the impedance slightly it was easily fixed by adjusting the size of the overall antenna. With the performances showed in both Sierpinski Gasket monopole antennas it can be concluded that a fractal design can be built for simple multiband applications based on the gain and radiation patterns shown in this work.

5.3 Recommendations for Improving this Study

Here are a few of the recommendations that may offer ways to improve this study.

1. Look into using a control antenna that has better performance at the design frequencies of the study. By doing this it will allow for less work on interpreting the data shown from the S21 VNA readings. In this study, the control antenna was a good wide band antenna but it did not have the best S11 performance at the 2.4GHz and 5GHz frequency bands. Many antennas were looked at for this study and the wide-band Yagi-Uda that was used was by far the best option within our means. The S11 parameters for this antenna can be seen in the appendix.

2. Look into other fractal patterns to see if the same problems arise with the lower frequency band in the experiment. For this study, it was the 2.4GHz frequency band. While the performance was ok and showed that the antenna output at the right frequency there are still questions as to why it was only transmitting 67% of the total signal power. By testing more fractal patterns during the study it might have shown that this problem is common or that it might have been an error or an anomaly in this study for the two fractal patterns.
3. If this study was revisited, I would revise the study to create multiple antennas where each one had one more iteration than the last design. It would start out as a single patch antenna and increase iterations with each design. This could show how the performance changes as more iterations are added to the fractal design.
4. Design the Sierpinski Gasket Monopole antennas with different PCB material and thickness. As described earlier, Puente's experiment was conducted using a CuClad 250 substrate with a thickness of 1.588mm. Next time, it would be interesting to see how the physical size and error of the antennas differ from each other depending on the substrate and thickness of the PCB.

LIST OF REFERENCES

LIST OF REFERENCES

Ali, M., Hayes, G. J., Sadler, R. A., & Hwang, H.-S. (2003). Design of a multiband internal antenna for third generation mobile phone handsets. *IEEE Transactions on Antennas and Propagation*, *51*(7), 1452–1461. doi:10.1109/TAP.2003.812282

Anguera, J., Puente, C., Borja, C., & Soler, J. (2004). Broad-Band Dual-Frequency Microstrip Patch, *52*(1), 66–73.

Bartz, R. (2008). [Photo of Parabolic Antenna]. Retrieved from http://upload.wikimedia.org/wikipedia/commons/4/40/Erdfunkstelle_Raisting_2.jpg

Bentley, W. (1922, November 17). [Photo of snowflake]. Retrieved from http://snowflakebentley.com/WBpopmech.htm

Bevelacqua, P. J. (2011a). Antenna Impedance. *Antenna-Theory.com*. Retrieved from http://www.antenna-theory.com/basics/impedance.php

Bevelacqua, P. J. (2011b). Directivity. *AntennaTheory.com*. Retrieved June 24, 2013, from http://www.antenna-theory.com/basics/directivity.php

Bevelacqua, P. J. (2011c). Radiation Pattern. *Antenna-Theory.com*. Retrieved June 3, 2013, from http://www.antenna-theory.com/basics/radPattern.html

Bevelacqua, P. J. (2011d). [Photo of Antenna Fields]. Retrieved from antenna-theory.com

Bevelacqua, P. J. (2011e). The Dipole Antenna. *Antenna-Theory.com*. Retrieved May 20, 2013, from http://www.antenna-theory.com/antennas/dipole.php

Bevelacqua, P. J. (2011f). Yagi-Uda Antenna. *Antenna-Theory.com*. Retrieved July 14, 2013, from http://www.antenna-theory.com/antennas/travelling/yagi.php

Bevelacqua, P. J. (2011g). [Photo of Patch Antenna]. Retrieved from Antenna-Theory.com

Bevelacqua, P. J. (2011h). Bow Tie Antennas. *Antenna-Theory.com*. Retrieved June 3, 2013, from http://www.antenna-theory.com/antennas/wideband/bowtie.php

Borja, C., & Romeu, J. (2000). Multiband Sierpinski Fractal Patch Antenna. *IEEE Antennas and Propagation Society International Symposium* (Vol. 3, pp. 1708–1711). doi:10.1109/APS.2000.874572

C. Puente, Romeu, J., Pous, R., Garcia, X., & Benitez, F. (1996). Fractal multiband antenna based on the Sierpinski gasket. *Electronics Letters*, *32*(I), 1–2. doi:10.1049/el:19960033

Chen, Z. N., & Chia, M. Y. W. (2001). Impedance Characteristics of EMC Triangular Planar Monopoles. *Electronics Letters*, *37*(21), 1271–1272. doi:10.1049/el:20010866

Chung, K., Kim, J., & Choi, J. (2005). Wideband Microstrip-Fed Monopole Antenna Having Frequency Band-Notch Function. *IEEE Microwave and Wireless Components Letters*, *15*(11), 766–768. doi:10.1109/LMWC.2005.858969

Ciais, P., Staraj, R., Kossiavas, G., & Luxey, C. (2004a). Design of an internal quad-band antenna for mobile phones. *IEEE Microwave and Wireless Components Letters*, *14*(4), 148–150. doi:10.1109/LMWC.2004.825186

Ciais, P., Staraj, R., Kossiavas, G., & Luxey, C. (2004b). Compact internal multiband antenna for mobile phone and WLAN standards. *Electronics Letters*, *40*(15), 3–4. doi:10.1049/el

Coppens, J. (n.d.). [Photo of Helical Antenna]. Retrieved from http://jcoppens.com/ant/helix/calc.en.php

Croswell, W. F., Christiansen, D., Alexander, C. K., & Jurgen, R. (2004). Types of antennas. *Standard Handbook of Electronic Engineering* (Fifth., pp. 18–46). The McGraw-Hill Companies. Retrieved from http://203.158.253.140/media/e-Book/Engineer/Electronic/Standard Handbook of Electronic Engineering/0071462775_ar075.pdf

Davies, S., & Holliday, H. R. (2005). Wideband Antennas – an Historical Perspective. *IEE Symposium* (pp. 1–4). Retrieved from http://www.q-par.com/corporate/marketing/wideband-antennas-an-historical-perspective-article.pdf

Djordjević, A. R., Zajić, A. G., & Ilić, M. M. (2006). Enhancing the Gain of Helical Antennas by Shaping the Ground Conductor. *IEEE Antennas and Propagation Letters*, *5*(1), 138–140. doi:10.1109/LAWP.2006.873946

Fordham. (2012). [Photo of EM Spectrum]. *Students Quarterly Journal*. Retrieved from http://9-4fordham.wikispaces.com/file/view/em_spectrum.jpg/244287321/em_spectrum.jpg

Jaspers, R. (n.d.). [Photo of Helical Antenna]. Retrieved from http://helix.remco.tk/helical_krimpwit1.jpg

Johannesson, K. A., & Mitson, R. B. (1983). [Photo of Transducer Beam Pattern]. *Fisheries Acoustics. A practical Manual for Aquatic Biomass Estimation*.

Jugandi. (2001). [Photo of Yagi-Uda Antenna]. Retrieved from http://en.wikibooks.org/wiki/File:Yagi.gif

Key Global Telecom Indicators for the World Telecommunication Service Sector. (2012).*International Telecommunication Union*. Retrieved December 2, 2013, from http://www.itu.int/ITU-D/ict/statistics/at_glance/KeyTelecom.html

Kishk, A. A. (2009). Fundamentals of Antennas. In Z. N. Chen & K.-M. Luk (Eds.), *Antennas for Base Stations in Wirless Communications* (pp. 1–30). The Mc Graw Hill Companies. Retrieved from http://www.mhprofessional.com/downloads/products/0071612882/0071612882_chap01.pdf

Kohavi, Y., & Davdovich, H. (2006). Topological dimensions , Hausdor dimensions & fractals. *Bar-llan University*, (May), 1–16.

Kraus, J. (1985). Antennas Since Hertz and Marconi. *IEEE Transactions on Antennas and Propagation*, *33*(2), 131–137. doi:10.1109/TAP.1985.1143550

Kraus, J., & Marhefka, R. (2001). Antenna Basics. *Antenna for all Applications* (Third., pp. 11–56). McGraw-Hill. doi:10.1016/B978-075064947-6/50002-2

Krzysztofik, W. J., & Member, S. (2009). Modified Sierpinski Fractal Monopole for ISM-Bands Handset Applications. *Antennas and Propagation, IEEE Transactions on*, *57*(3), 606–615. doi:10.1109/TAP.2009.2013416

Li, D., Zhang, F. S., Zhao, Z. N., Ma, L. T., & Li, X. N. (2012). A CPW-Fed Wideband Koch Snowflake Fractal Monopole For WLAN/WiMAX Applications. *Progress in Electromagnetics Research*, *28*, 143–153. doi:10.2528/PIERC12022106

Lin, Y. de. (1997). [Photo of Bow-tie]. Retrieved from http://ieeexplore.ieee.org/stamp/stamp.jsp?tp=&arnumber=560350

Lythall, H. (n.d.). [Photo of Quarter-wave Dipole]. Retrieved from http://www.sm0vpo.com/antennas/anten5.gif

Maci, S., & Gentili, G. B. (1997). Dual-Frequency Patch Antennas. *IEEE Transactions on Antennas and Propagation*, *39*(6), 13–20. doi:10.1109/74.646798

Matsumori, B. (2011). Reality Check : Is it an antenna evolution or is there more ?, (August). Retrieved from http://www.rcrwireless.com/article/20110830/reality_check/reality-check-is-it-an-antenna-evolution-or-is-there-more/

Matz, K. S. (2003). Nautilus pompilius. Retrieved from http://www.nsf.gov/news/mmg/mmg_disp.jsp?med_id=51901&from=mmg

McMullen, C. (1984). Hausdorff Dimension of General Sierpinski Carpets. *Nagoya Mathematical Journal*, 1–9.

Molinaro, M. (2006). What is Light? Davis, CA: Lawrence Livermore National Laboratory. Retrieved from http://unihedron.com/projects/spectrum/downloads/spectrum_20090210.pdf

Nikolova. (2012). Half Wave Folded Dipole Antennas and Impedance Transformation with Baluns. McMaster University. Retrieved from http://www.ece.mcmaster.ca/faculty/nikolova/antenna_dload/labs/Exercise1-5.pdf

Norfolk, R. (2006). Controlled Impedance. Hallmark Circuits, Inc. Retrieved from http://pcbwizards.com/SDDC/sddc_impedance_mfg_view_jan06.pdf

Orban, B. D., & Moernaut, G. J. K. (n.d.). The Basics of Patch Antennas. *Orban Microwave Products*. Retrieved from http://www.orbanmicrowave.com/The_Basics_Of_Patch_Antennas.pdf

Pantoja, M., Ruiz, F., Bretones, A., Gonzalez-Arbesu, J. M., Martín, R. G., Romeu, J., & Rius, J. M. (2003). GA Design of Wire Pre-Fractal Antennas and Comparison With Other Euclidean Geometries. *IEEE Antennas and Wireless Propagation Letters*, *2*(1), 238–241. doi:10.1109/LAWP.2003.819694

Poole, I. (n.d.). [Photo of Half-wave Folded Dipole]. Retrieved from http://www.radio-electronics.com/images/dipole-folded-01.gif

Puent-Baliarda, C., Romeu, J., & Cardama, A. (2000). The Koch Monopole: A Small Fractal Antenna. *IEEE Transactions on Antennas and Propagation*, *48*(11), 1773–1781. doi:10.1109/8.900236

Puente, C., Navarro, M., Romeu, J., & Pous, R. (1998). Variations on the Fractal Sierpinski Antenna Flare Angle. *Antennas and Propagation Society International Symposium*, *4*, 2340–2343. doi:10.1109/APS.1998.701794

Puente-Baliarda, C., Romeu, J., Pous, R., & Cardama, A. (1998). On the Behavior of the Sierpinski Multiband Fractal Antenna. *Antennas and Propagation, IEEE Transactions on*, *46*(4), 517–524. doi:10.1109/8.664115

Ramsay, J. (1981). Antenna history. *IEEE Communications Magizine*, *5*(19), 4–8. doi:10.1109/MCOM.1981.1090561

Riddle, L. (2014). [Photo of Koch Geometry Sequence]. *Agnes Scott College*. Retrieved from http://ecademy.agnesscott.edu/~lriddle/ifs/ksnow/ksnow.htm

Segalstad, T. V. (1972). [Photo of Half-wave dipole]. Retrieved from http://folk.uio.no/tomvs/la4ln/dipole_en.pdf

Shlager, K. L., Smith, G. S., & Maloney, J. G. (1994). Optimization of Bow-Tie Antennas for Pulse Radiation. *IEEE Transactions on Antenna and Propagation*, *42*(7), 975–982. doi:10.1109/8.299600

Shui, C. R. L. I. N., Wang, W. L., Huang, J. L. U. Y., Jing-huil, Q. I. U., & Jin-xiang, W. (2010). Design and Experiment of a High Gain Axial-Mode Helical Antenna. *IEEE International Conference on Communication Technology*, 522–525. doi:10.1109/ICCT.2010.5688887

Silver, S. (1984). Microwave Antenna Theory and Design, 97–100. Retrieved from http://www.jlab.org/ir/MITSeries/V12.PDF

Sischka, F. (2002). The Basics of S- Parameters. *Characterization Handbook* (pp. 1–20). Durham, NH. Retrieved from http://tesla.unh.edu/courses/ece711/refrense_material/s_parameters/1SparBasics_1.pdf

Technologies, Q. (2010). Spectrum Frequency Chart. Retrieved from http://www.qrctech.com/assets/Frequency-Chart/19Nov201024x36FreqChart.pdf

The Great Soviet Encyclopedia. (1970). [Photo of Half Wave Dipole]. Retrieved from http://encyclopedia2.thefreedictionary.com/Half-Wave+Dipole

Thiele, G. (1969). Analysis of yagi-uda-type antennas. *IEEE Transactions on Antennas and Propagation*, *17*(1), 24–31. doi:10.1109/TAP.1969.1139356

Ultra-wideband antenna. (2005).*Track it System*. Retrieved from http://www.thetrackit.com/library/UWB Defin.pdf

Vinoy, K. . J., Jose, K. A., Varadan, V. . K., & Varadan, V. . V. (2001). Hilbert Curve Fractal Antenna: A Small Resonant Antenna For VHF/UHF Applications. *Microwave and Optical Letters*, *29*(4), 215–219. doi:10.1002/mop.1136

Visser, H. J. (2012). *Antenna Theory and Applications* (1st ed., pp. 1–13). New York City, New York: John Wiley & Sons.

Wentworth, S. (2007a). Transmission Lines. *Applied Electromagnetics: Early Transmission Lines Approach* (First., pp. 31–113). Hoboken, NJ: Wiley.

Wentworth, S. (2007b). Plane Waves. *Applied Electromagnetics: Early Transmission Lines Approach* (First., pp. 320–372). Hoboken, NJ: Wiley.

Wentworth, S. (2007c). Antennas. *Applied Electromagnetics: Early Transmission Lines Approach* (First., pp. 426–540). Hoboken, NJ: Wiley.

Werner, D. H., & Gangul, S. (2003). An Overview' of Fractal Antenna Engineering Research. *Antennas and Propagation Magazine, IEEE*, *45*(I). doi:10.1109/MAP.2003.1189650

Wolff, C. (n.d.). [Photo of 3D radiation pattern]. Retrieved from http://www.radartutorial.eu/06.antennas/pic/parabol3.print.jpg

APPENDICES

Appendix A: VNA S11 Measurements

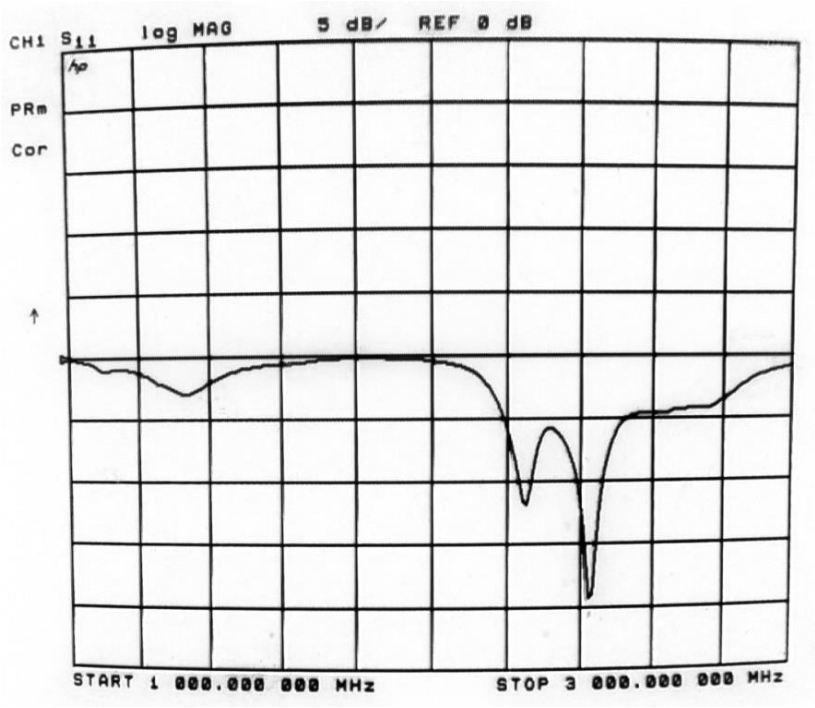

60° Bow-Tie (2.4GHz)

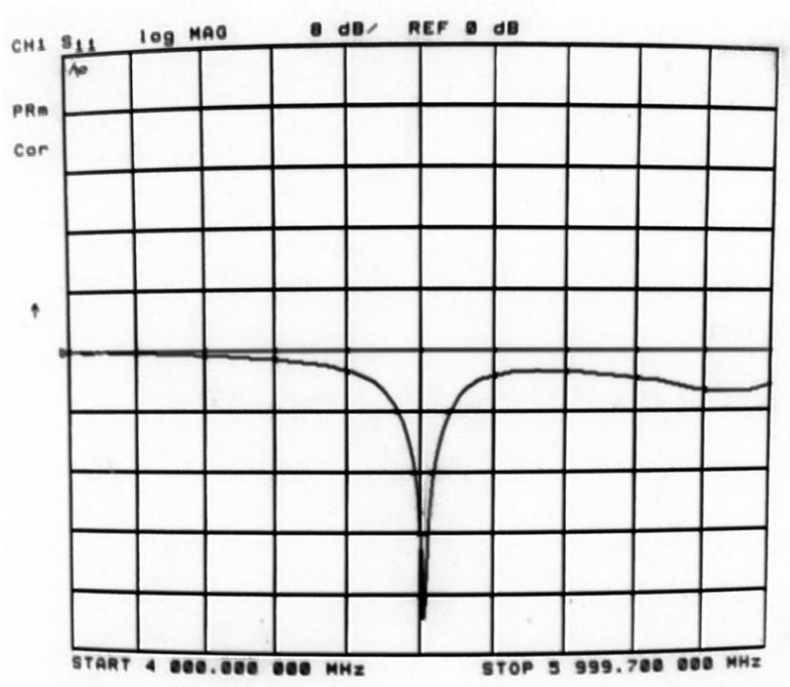

60° Bow-Tie (5GHz)

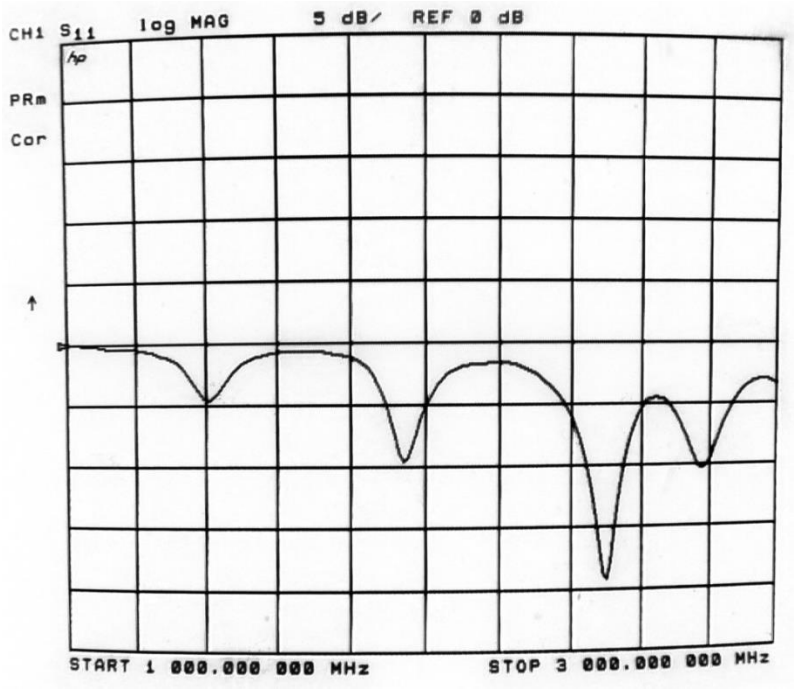

90° Bow-Tie (2.4GHz)

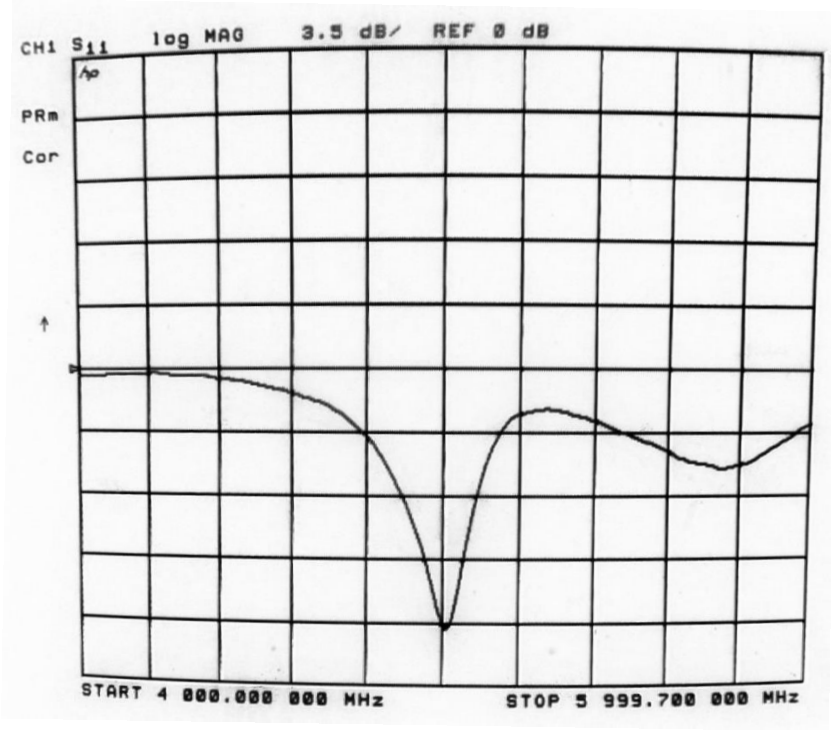

90° Bow-Tie (5GHz)

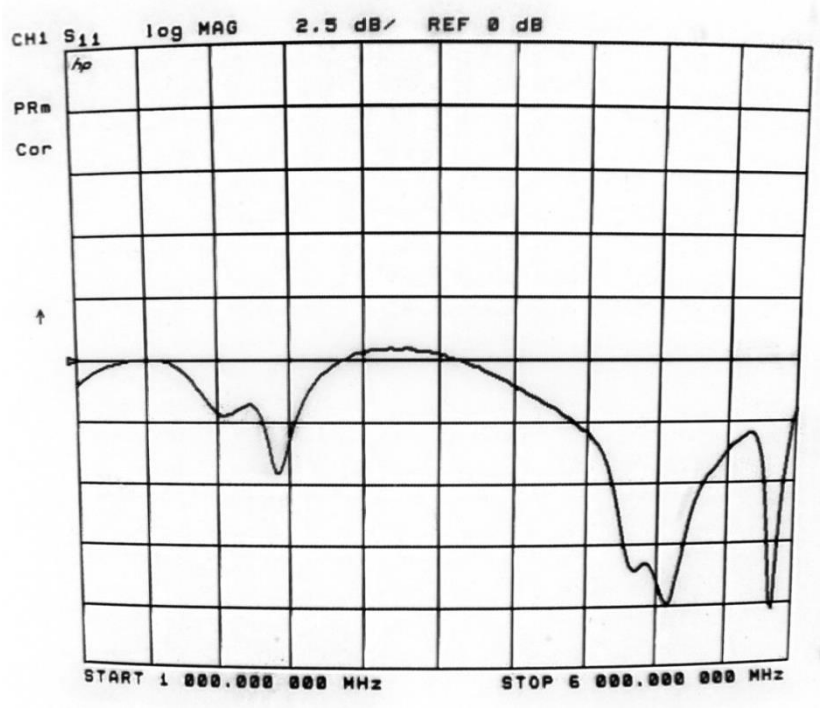

60° Sierpinski Gasket Monopole

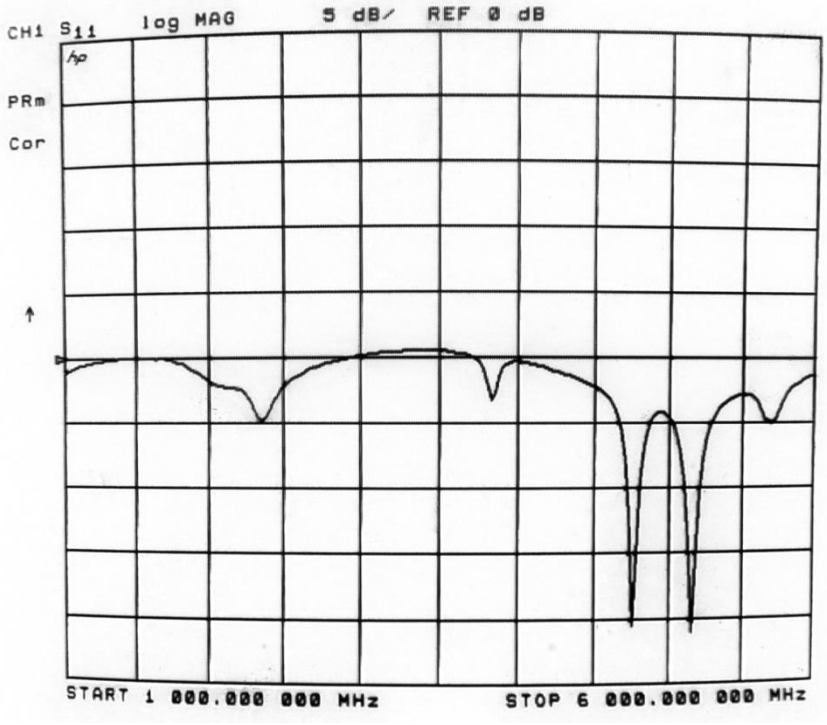

90° Sierpinski Gasket Monopole

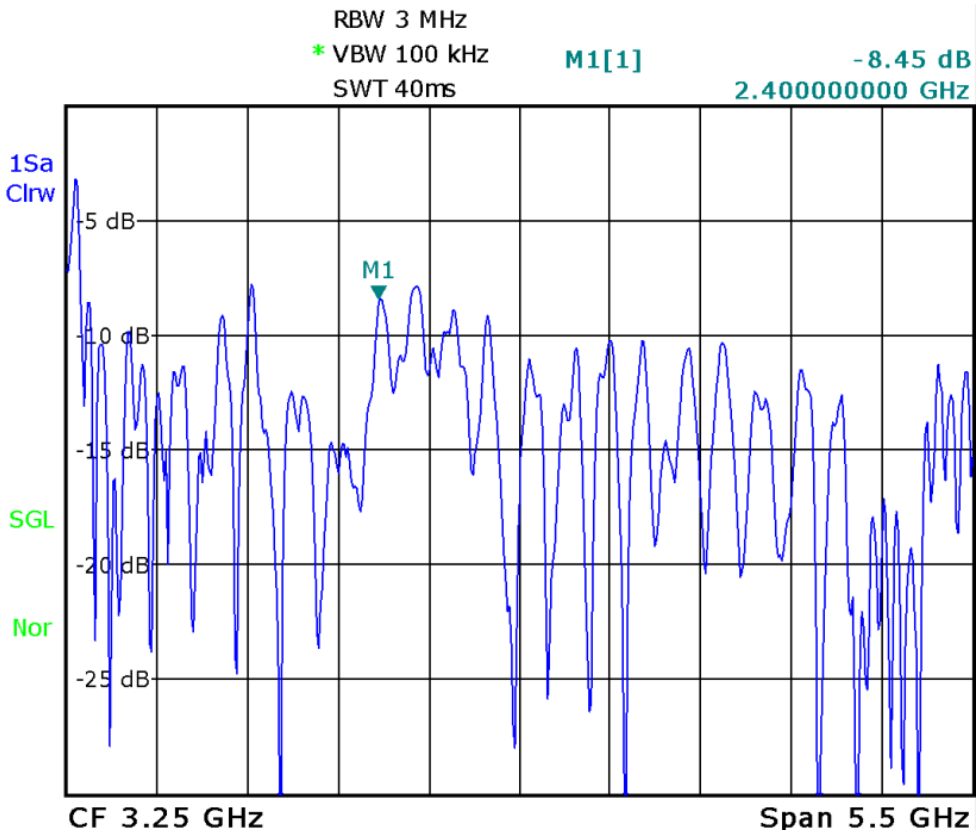

Control Antenna (WA5VJB Yagi)

Appendix B: VNA S21 Measurements

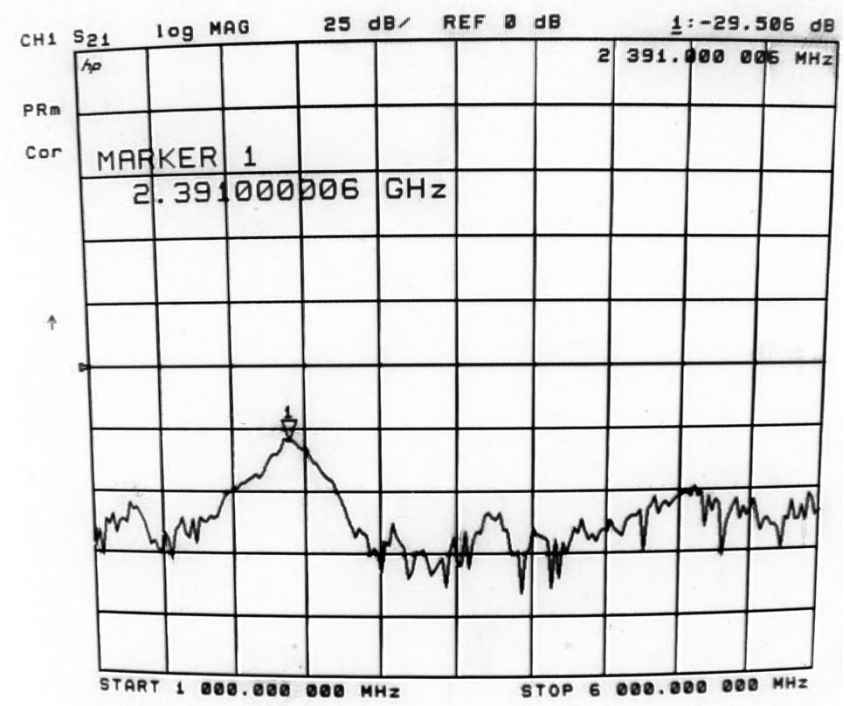

60° Bow-Tie (2.4GHz)

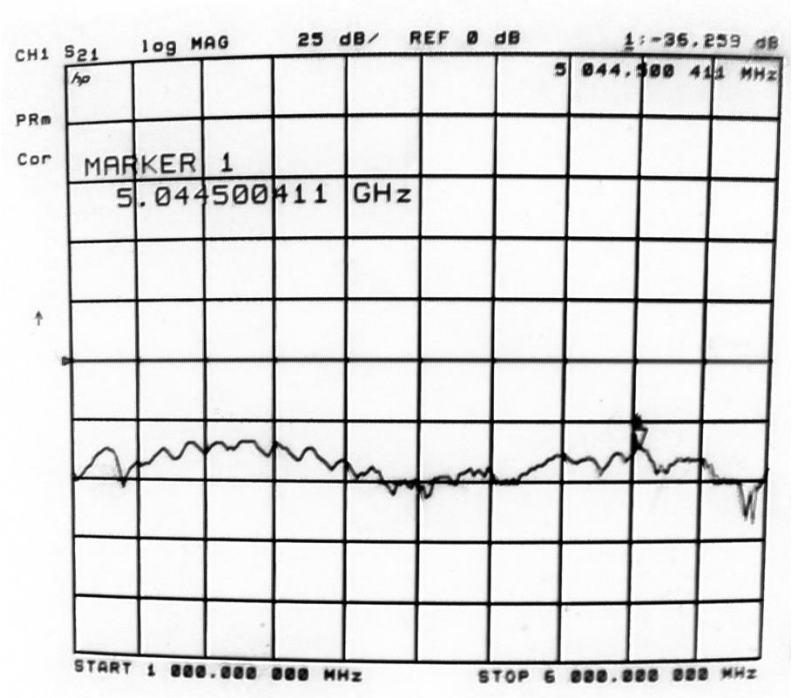

60° Bow-Tie (5GHz)

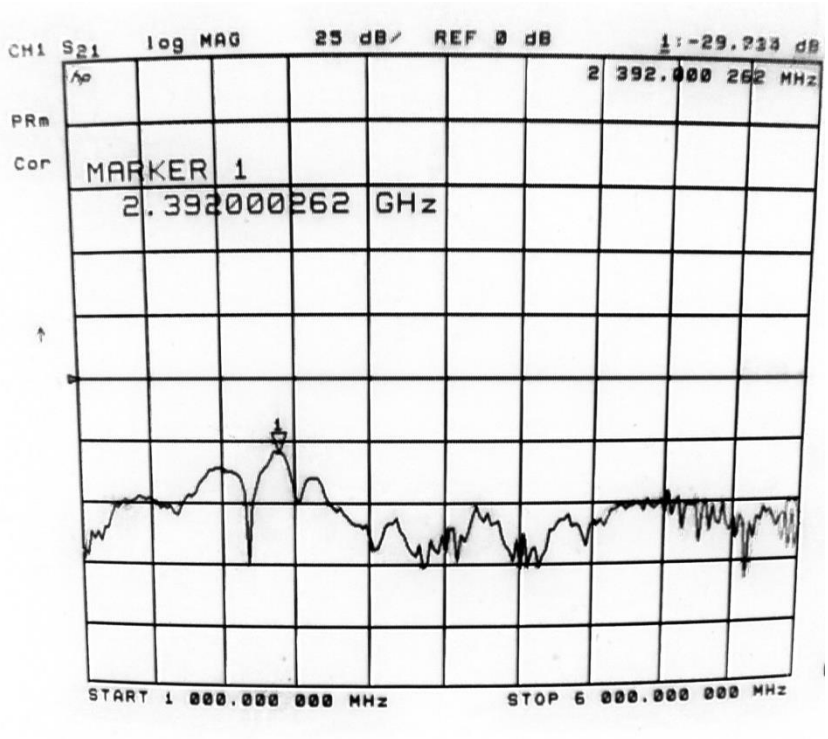

90° Bow-Tie (2.4GHz)

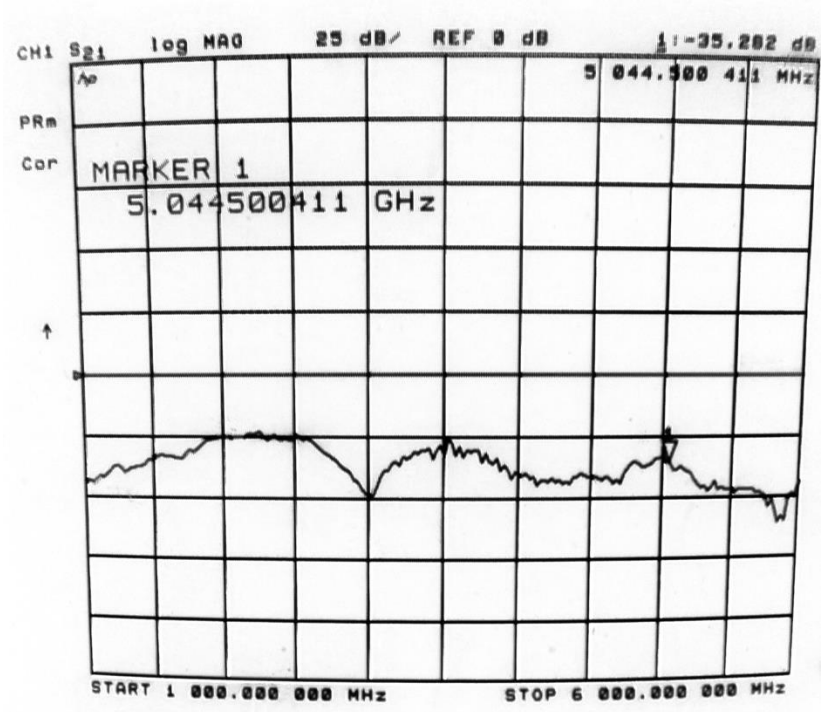

90° Bow-Tie (5GHz)

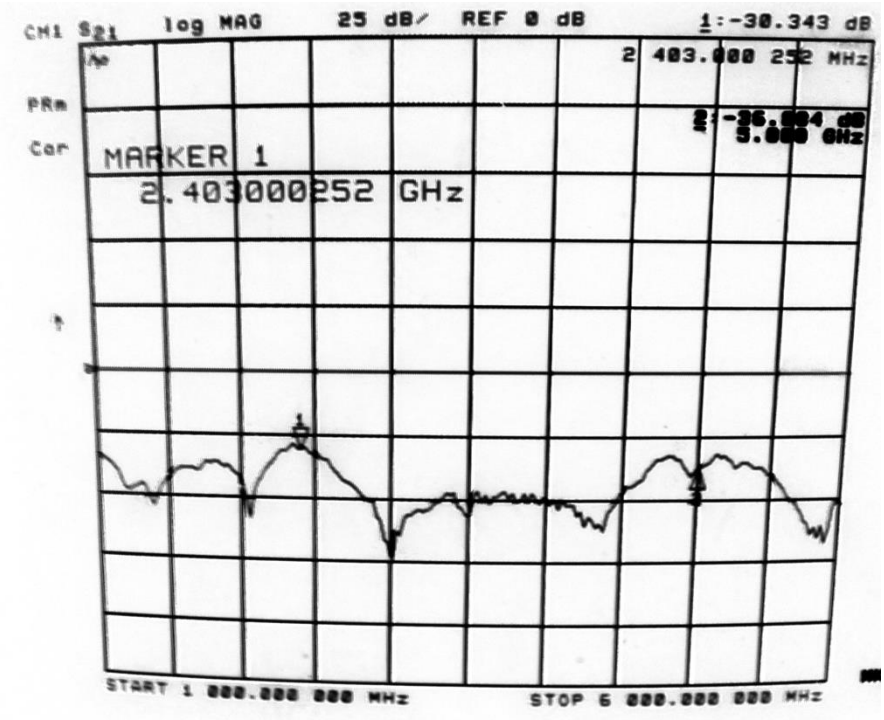

60° Sierpinski Gasket Monopole

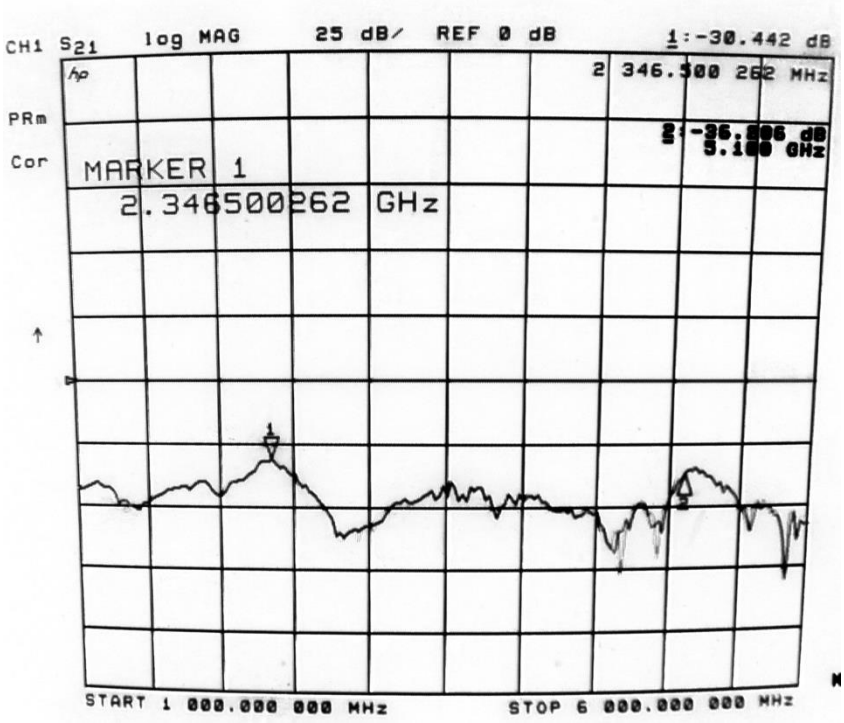

90° Sierpinski Gasket Monopole

Appendix C: Pictures of the Antennas

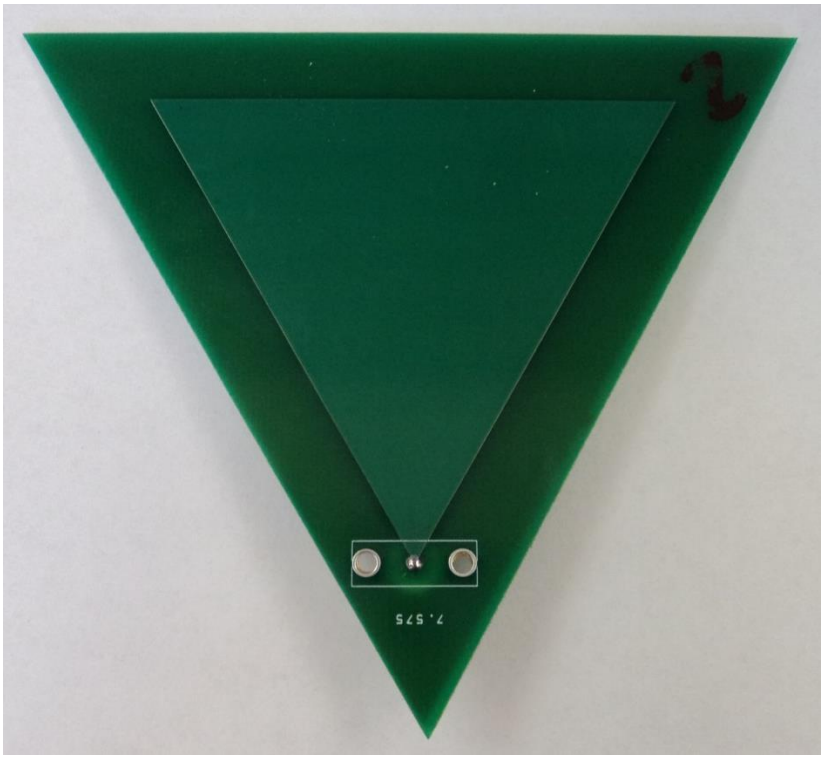

60° Bow-Tie (2.4GHz)

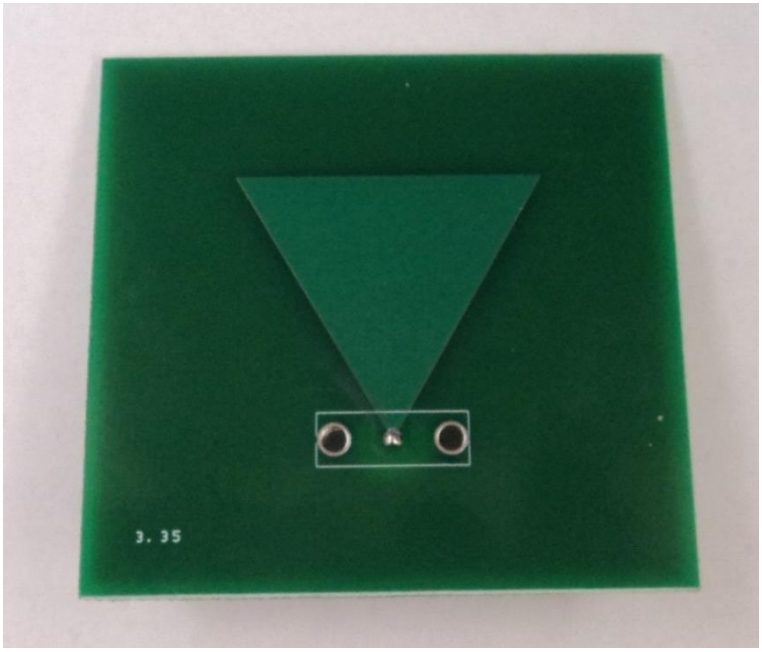

60° Bow-Tie (5GHz)

90° Bow-Tie (2.4GHz)

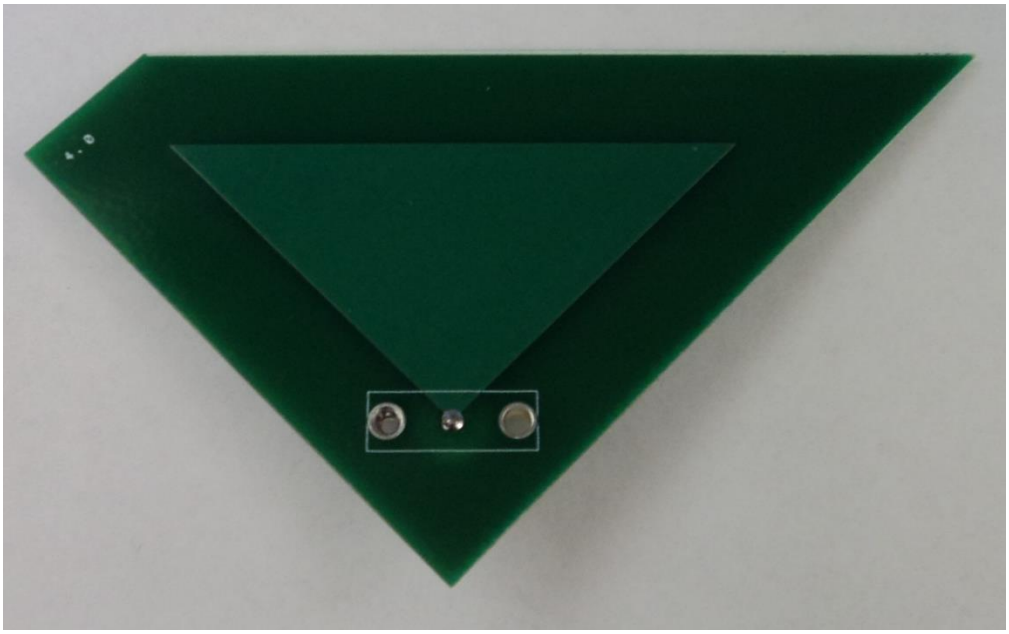

90° Bow-Tie (5GHz)

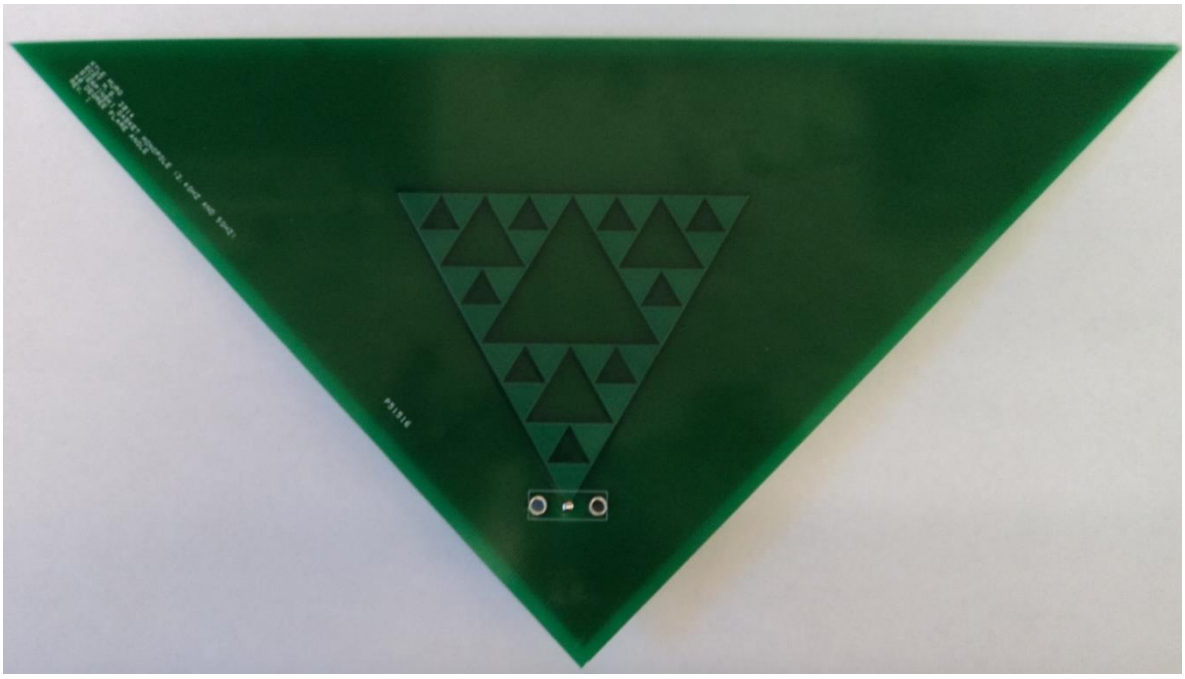

60° Sierpinski Gasket Monopole

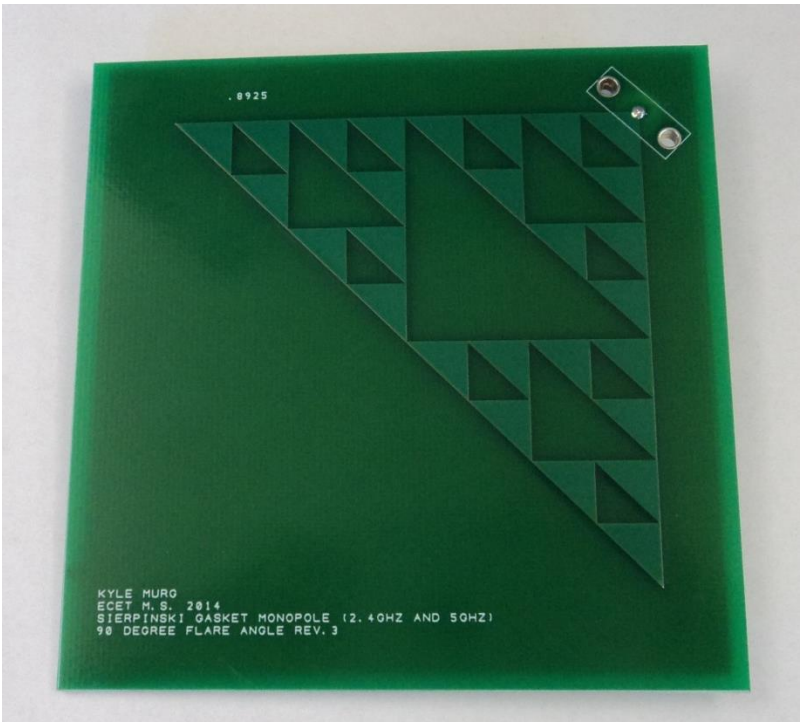

90° Sierpinski Gasket Monopole